Dynamic Modelling and Simulation of Major League Baseball Pitching Biomechanics to Reduce Ulnar Collateral Ligament Injury and Improve Performance

by

Cedric E. Attias

A thesis
presented to the University of Waterloo
in fulfillment of the
thesis requirement for the degree of
Master of Applied Science
in
Mechanical and Mechatronics Engineering

Waterloo, Ontario, Canada, 2025

© Cedric E. Attias 2025

Author's Declaration

I hereby declare that I am the sole author of this thesis. This is a true copy of the thesis, including any required final revisions, as accepted by my examiners.

I understand that my thesis may be made electronically available to the public.

Abstract

Baseball teams of all levels rely on their pitchers to achieve the ultimate goal: win games. This fact is exacerbated in professional baseball, where pitchers are considered the most important members of the team and are compensated as such. Because of this, many efforts are made to maximize the performance of pitchers, without compromising their health. Doing so is no easy task and is often considered a balancing act, where teams want to get the most out of their pitchers, while making sure they are available long-term.

Historically, scientific work in baseball pitching typically constitutes the study of kinematics and kinetics of pitching motions, to extract relevant joint angles, forces, and moments. However, most efforts in this space do not consider elite calibre athletes. In high-level organizations, most research and development work is conducted internally, by sports science and analytics departments, which are often kept confidential, to not give opponents the same competitive advantage that the analyses might produce.

With the modelling, simulation, and computing tools available today, an opportunity exists to conduct a comprehensive analysis of elite baseball pitching biomechanics, that can inform the management and training of these athletes, without the need for physical experimentation that may impart additional strain on the pitcher. In collaboration with a confidential industry partner (a high-level baseball organization), practical strategies to reduce injury risk and improve performance for their pitchers are deduced from in-game kinematic data, shared and anonymized by the researcher partners. This work also provides expertise to the participating team in modelling and simulation, which can contribute to their on-field success and future scientific work.

This is done by employing a series of simulation strategies, the first being an inverse dynamic approach. The shared kinematic data is initially used to track the pitching motion in an inverse kinematic analysis, which will provide estimates of joint angles over time and an animation of the motion. The same data is then used to calibrate the dimensions and joint kinematics of the athletes for the development of a full-body, skeletal model. An inverse dynamic analysis was then performed to estimate the net joint moments responsible for this motion, while also considering the model's reliability at estimating joint angles and net joint dynamics. Particular attention was paid to the throwing arm, namely the shoulder and elbow joints, to understand the etiology of ulnar collateral ligament (UCL) injuries in pitchers.

Next, a predictive forward dynamic simulation was developed. This approach was generated by solving an optimal control problem for the muscle forces and activations that maximize ball speed during a pitch, with constraints on the model's physiology, joint kinematics, and joint kinetics. First, a comprehensive musculoskeletal (MSK) model that is

tuned and scaled to represent a baseball pitcher's dimensions and forcer generating capabilities was developed. Using this model, a series of "what-if" simulations were conducted to explore the influence of variable pitching mechanics on UCL loads, while continuing to prioritize the identification of factors that have the most impact on elbow valgus torques, without compromising performance. Specifically, the predictive simulations were used to identify the pitching motion that minimized UCL loading while maintaining pitching speed. The cost function used involved minimizing actuation effort while achieving a competitive pitch speed. Constraints were imposed on joint angles and speeds, muscle activations, and ball speed to reflect realistic bounds for elite athletes. The final cost function of the optimal control problem rewarded reaching a desired pitch speed threshold, achieving a lead foot speed of zero at ball release (to maintain balance and prevent slipping), and minimizing the actuation of the shoulder rotation actuator (shoulder external rotation), which tends to load the UCL. Results demonstrated how variations in pitching mechanics alter UCL loads. For instance, faster pitches exhibited greater contralateral trunk tilt and higher arm slot, elevating UCL loads, while slower pitches demonstrated greater ipsilateral trunk tilt with a lower arm slot (sidearm), reducing UCL loads.

Throughout all of the simulations, care was made to evaluate the robustness of the model through validation using a series of case studies and comparisons to literature. Using these validated models, findings relating to the variability in pitching strategies were identified. Each pitcher and simulation analyzed employed unique biomechanics to achieve the defined costs, while all producing competitively viable throwing speeds. While performance was prioritized, each set of throwing mechanics posed different levels of threat to the athlete's UCL, indicating that these highly individualized motions can create inconsistent loading patterns within subjects. These findings can be used to develop personalized pitching and conditioning programs aimed at maximizing throwing velocity while reducing injury risk, without the need for strenuous physical testing.

Acknowledgements

I would like to thank Prof. John McPhee for his unwavering support and guidance throughout the supervision of this research.

I would like to thank Dr. Keaton Inkol for his indispensable advice and direction throughout the duration of my studies, in both my undergraduate and graduate studies.

I would like to thank my thesis committee members, Dr. Clark Dickerson and Dr. Stewart McLachlin, for their advice in improving this work.

I would like to acknowledge the Canadian Institute of Health Research - Master's Graduate Scholarship Program, the Canada Research Chairs Program, the Queen Elizabeth II Graduate Scholarship in Science and Technology, and the University of Waterloo's Engineering Excellence Master's Fellowship program for their financial support of this research.

I would like to thank all my colleagues from the Motion Research Group for their uplifting attitude and encouragement over the past two years.

Finally, I would like to thank my family for their steadfast support of my academic journey and for encouraging me to pursue my passions with this research.

Dedication

This is dedicated to my family, friends and all those who have supported me in the pursuit of my passions through education.

Table of Contents

Author's Declaration ii

Abstract iii

Acknowledgements v

Dedication vi

List of Figures xi

List of Tables xiii

1 Introduction 1

1.1 Problem Description and Motivation 2

1.2 Research Goals 3

1.3 Contributions 3

2 Background and Literature Review 5

2.1 Baseball Pitching 5

2.2 Baseball Pitching Kinematics and Kinetics 7

2.2.1 Motion Capture for Inverse Kinematic Analysis 9

2.2.2 Implications of Pitching Biomechanics on Performance 10

2.2.3 Pitching Biomechanics and UCL Injuries . . . 11
2.3 Dynamic Models of Pitching . . . 14
2.3.1 Inverse Dynamic Models . . . 16
2.3.2 Forward Dynamic Models . . . 21
2.4 Areas of Improvement for Muscle-Driven Models . . . 26

3 Inverse Kinematics **29**
3.1 Provided Kinematic Data . . . 29
3.1.1 Data Collection . . . 29
3.1.2 Data Format . . . 31
3.1.3 Data Pre-Processing . . . 32
3.1.4 Pitch Event Determination . . . 33
3.2 Visual3D Skeletal Model . . . 34
3.2.1 Model Description . . . 35
3.2.2 Selected Kinematics and Joint Movement Definitions . . . 38
3.3 Joint Kinematics Extraction Pipeline . . . 39
3.3.1 Visual3D Inverse Kinematics and Angle Calculations . . . 40
3.3.2 Cardan Sequence Selection . . . 40
3.3.3 Visual3D Differentiation Methodology and Joint Velocities . . . 41
3.3.4 Post-Processing and Kinematic Visualization Pipeline . . . 42
3.4 Kinematic Results . . . 42
3.4.1 Joint Trajectories and Velocities . . . 44
3.4.2 Discussion and Comparison of Kinematics Across Pitchers . . . 46

4 Inverse Dynamics **51**
4.1 Revised Visual3D Skeletal Model . . . 51
4.1.1 Model Anthropometrics and Inertial Properties . . . 52
4.1.2 Ball Model and External Forces . . . 53

4.2 Modelling Approach and Implementation . . . 55
4.2.1 Visual3D Inverse Dynamics Tool . . . 56
4.2.2 Extraction Pipeline for Selected Joint Dynamics . . . 56
4.2.3 Post-Processing and Kinetics Visualization . . . 57
4.3 Dynamics Results . . . 60
4.3.1 Net Joint Moments and Forces . . . 61
4.3.2 Discussion and Comparison of Dynamics Across Pitchers . . . 63
4.4 Implications of Dynamics on Injury and Performance . . . 67
4.5 Sensitivity Study 1: Modelling of the Baseball-Hand Interface and Impact of Ball Variations on Joint Kinetics . . . 70
4.5.1 Test Case 1 Results: Ball Positioned Closer to the Thumb . . . 71
4.5.2 Test Case 2 Results: Heavier Ball (32 oz) . . . 71
4.5.3 Test Case 3 Results: Lighter Ball (1 oz) . . . 71
4.5.4 Implications . . . 71
4.6 Sensitivity Study 2: Pitching Cadence . . . 73
4.7 Model Evaluation for Inverse Kinematics and Dynamics . . . 75

5 Forward Dynamics **80**
5.1 OpenSim Musculoskeletal Model and Revisions . . . 81
5.2 Post-Processing and UCL Loading Calculations . . . 84
5.3 Optimal Control of the Pitching Motion . . . 87
5.4 Case Studies . . . 89
5.4.1 Case 1: Average MLB Fastball . . . 89
5.4.2 Case 2: Excessively Fast Throw . . . 90
5.4.3 Case 3: Minimizing the Valgus Load . . . 90
5.5 Results and Discussion . . . 92
5.5.1 Validation of Predictive Simulations . . . 93
5.5.2 Varus-Valgus Torque Balance at the Elbow: UCL Loading . . . 99

5.5.3 Muscle Behaviours . . . 99
5.5.4 Simulated Kinematics . . . 102
5.6 Limitations of Forward Dynamic Work . . . 104

6 Conclusions **106**
6.1 Project Summary . . . 106
6.1.1 Inverse Kinematics . . . 107
6.1.2 Inverse Dynamics . . . 107
6.1.3 Forward Dynamics . . . 108
6.2 Recommendations . . . 109
6.3 Future Research Opportunities . . . 110

References **113**

Appendices **122**

A Selected Angular Kinematics and Joint Movement Definitions for Inverse Kinematic Analysis **123**

B Inverse Kinematic Results of Interest **125**

C Inverse Dynamic Results of Interest **131**

D Forward Dynamic Model Degrees of Freedom and Ranges of Motion **138**

E Muscle Behaviour During Forward Dynamic Simulations **140**

List of Figures

2.1 6 phases of a baseball pitch 7
2.2 Visualization of elbow forces and torques during pitching 12
2.3 UCL anatomy during pitching 13
2.4 Full body pitching model, with muscles, by Buffi et al. 23
2.5 Simulation framework and sensitivity study flow chart by Buffi et al. . . . 25

3.1 Sample KinaTrax in game camera system 30
3.2 markerless segment orientation and position measurement by KinaTrax . . 31
3.3 Visual3d skeletal model of pitcher 1 36
3.4 Visual3D animation of the pitching events for pitcher 1 38
3.5 Sample kinematic visualization of shoulder rotation 43

4.1 Revised Visual3D model with the addition of the baseball 54
4.2 Visualization of the movements associated with the extracted kinetics during inverse dynamic analysis 58
4.3 Sample kinetic visualization of the throwing elbow varus-valgus moment in Pitcher 4 59
4.4 Sample kinetic visualization of the throwing elbow varus-valgus moment during the cadence study 74

5.1 Base and revised OpenSim musculoskeletal model 85
5.2 Contact sphere definition for lead foot 86

5.3 Simulated pose of the forward dynamic model at ball release for all case studies 92
5.4 UCL load across the case studies 94
5.5 Muscle forces for simulated case studies 95
5.6 Comparison of arm kinematics between experimental and simulated joint trajectories 96
5.7 Peak UCL load vs. ball speed 100

E.1 Muscle activations of the 93 MPH simulation. 141

List of Tables

3.1 Kinematic metrics for five pitchers across three key phases of the pitching motion. 45

3.2 Comparison of mean kinematic values across studies 49

4.1 Post lead foot contact mean peak kinetic values for five pitchers. 61

4.2 Post lead foot contact mean peak kinetic values for pitcher dynamics. . . . 65

5.1 Segment scaling factors for the OpenSim scaling tool 83

5.2 Sensitivity study results while varying cost function weights 98

5.3 Peak muscle activations during simulation 101

A.1 Joint definitions and degrees of freedom for inverse kinematic analysis . . . 124

D.1 Musculoskeletal parameters for the OpenSim forward dynamic model . . . 139

Chapter 1

Introduction

Baseball, often dubbed "America's pastime," has captured the hearts of millions across the globe with its rich history, strategic complexity, and cultural significance. As one of the most popular sports in the United States, it boasts a dedicated fan base and a professional league that commands substantial media attention and financial investment. According to Major League Baseball (MLB), the league draws tens of millions of spectators each season, both in-stadium and through various broadcasting platforms [1].

Moreover, the league generated over US $11 billion in 2023, with the average revenue per team surpassing US $370 million [1]. In addition to the high revenue generated by the league, the MLB is home to some of the highest-paid athletes in the world. Notably, in 2024, the top three highest-paid athletes in the sport were pitchers, with an average salary of about US $55 million per year [1]. The widespread popularity of the sport underscores the importance of maintaining the health and performance of its athletes, particularly pitchers, who play a pivotal role in the game's outcome, and command close to half of a team's payroll [2, 3].

Amid the excitement and competitive spirit that drives baseball lies a significant challenge: the prevalence of injuries among pitchers, particularly those necessitating Tommy John surgery, which involves the reconstruction of the UCL in the elbow [4]. From 2000 to 2011, a mean 16 UCL tears per year occurred in MLB, but from 2011 to 2014, this number increased to 26 per season [4]. Today, this procedure has become alarmingly common, even trickling down to amateur pitchers, classifying the injury into epidemic proportions, affecting not only the longevity of pitchers' careers but also their overall performance and the financial dynamics of teams [4, 5].

1.1 Problem Description and Motivation

In 2023, nearly half of the 64 of the hardest fastball throwers that season underwent UCL reconstruction surgery [6]. Studies have shown that fatigue, weight, age, and valgus torques contribute to the onset of the injury; however, higher pitch velocity is the most predictive factor of UCL injuries in MLB pitchers [5]. Moreover, as the calibre of amateur baseball increases, 23-31% of youth baseball players have also succumbed to UCL injuries, which may be attributed to excessive training [5]. The competitive spirit and desire to win has pushed these athletes to the brink of their capabilities, jeopardizing the health of their throwing arm. This indicates a dire need for efforts to be made to understand and prevent this debilitating injury from occurring at all levels. From the team's perspective, a winning at all costs mentality takes precedent, to increase revenue and remain relevant. From the athlete's and sport's perspective, longevity and health are essential to a fulfilling career and growth of the game through youth development.

As the demands on these athletes continue to escalate, there is a pressing need for innovative approaches to predict the onset and reduce the prevalence of these injuries, without compromising on performance. Historically, most work in this area consists of biomechanical evaluations of elite pitching mechanics [7–10]. These studies are particularly considerate of the kinematics and kinetics that contribute to the onset of the injury and are essential to understanding its etiology. However, while these studies are useful for identifying the underlying mechanics that make an elite pitcher and why they might get hurt, they are not as strong at foreseeing potential injury risk. While these studies excel at evaluating established and measurable mechanics, they lack the ability to evaluate how variations in the mechanics impact the pitcher's health, which can be addressed through predictive modelling.

The absence of more proactive techniques for UCL injury predictions points to the opportunity for contribution to the sports science and medical communities. A major barrier in predictive UCL injury research relates to the conventional experimentation required for such analyses. Elite pitchers are often subjected to predefined pitch counts, that are put in place to prevent any additional strains or load on a pitchers' joints. This is why predictive modelling is a promising alternative. By simulating various scenarios through forward dynamic simulations, researchers can assess the effects of different pitching techniques on joints, without risking athlete well-being. However, challenges persist, notably in the complexity of forward dynamic modelling, which requires sophisticated computational techniques and comprehensive sets of biomechanical data to create accurate models. The models used in this study rely on assumptions that introduce limitations. Segmental properties and joint mechanics were estimated from generic templates, which may not

capture individual variability. Muscles were modelled using simplified Hill-type representations that overlook complex behaviours like tendon compliance and recruitment dynamics. Joint constraints were idealized, and external forces, such as ground reaction forces, were applied under assumptions of rigid contact. Neural control was simulated via optimization, assuming cost functions that do not accurately reflect true motor strategies. These models are also highly sensitive to parameter errors, computationally intensive, and difficult to validate across full motion trajectories. For these reasons, only a few publications on the topic exist, such as those by Buffi et al. [11] and van der Pijl [12].

As will be discussed in Chapter 2, some predictive models have been published in the literature, but have room for improvement. More notably, a validated forward dynamic pitcher model that predicts novel, yet biomechanically plausible, pitching motions of professional pitchers during a game and includes a detailed set of throwing hand, arm and shoulder muscle-tendon and ligament complexes, has yet to be published.

1.2 Research Goals

The goal of this thesis was to develop a state-of-the-art forward dynamic model, that is scaled and tuned to replicate the throwing mechanics of an elite pitcher during a game. Simulations of this model will permit exploration into the influence of mechanical changes on joint torques and UCL loads, to identify factors that have the most impact on UCL loading and elbow valgus torque. The model will aim to increase pitching velocity, while constraining injury inducing joint and muscle dynamics, by computing the optimal controls of muscle forces and activation firing patterns. This will be done by first assessing the kinematics and kinetics of elite pitchers, as these analyses will inform the design of the forward dynamic model, while providing novel insight into UCL injury etiology in an elite population.

1.3 Contributions

This research was made possible through collaboration with a Major League Baseball (MLB) organization, with whom a player confidentiality agreement was signed. As part of the agreement, the team has provided anonymized motion capture (kinematic) data of the pitching motions collected from in-game appearances. In exchange, all relevant publications, kinematic, inverse dynamic, and forward dynamic models outlined in this research are being provided to the team. Confidential information is protected by a mutual

non-disclosure agreement, and ethics approval was received from the University of Waterloo and the MLB to use externally collected data.

Contributions:

- A first of its kind muscle and actuator driven forward dynamic model that simulates elite pitching motions, by optimizing the controls of muscle and torque generators, without solely relying on tracking kinematic inputs.
- Predictive, yet biomechanically plausible, pitching motions that are novel and unique as a result of their optimization criteria.
- A novel full-body musculoskeletal model that is scaled and tuned to match the capabilities and dimensions of elite baseball pitchers, including the relevant muscles of the throwing hand, arm and shoulder, as they relate to UCL loading characteristics.
- The use of optimal control in addition to muscle dynamics, versus the previous work of Hubbard (no muscles) [13], Buffi (computed muscle controls, not optimal control) [11], and can der Pijl (static optimization, not optimal control) [12].
- Kinematic and kinetic analysis of professional MLB pitchers, where most previous work has assessed amateurs.
- Insight as to how throwing kinematics and kinetics contribute to UCL injuries.
- Insight as to how throwing kinematics and kinetics contribute to ball velocity generation.

Chapter 2

Background and Literature Review

Prior to describing the research undertaken, it is essential to review the background of the subject. To begin, a general overview of the baseball pitch will be discussed from a non-scientific view to introduce the relevant terminology and concepts to the audience. This will transition into a kinematic description of the throwing mechanics, implications of such mechanics on performance, the etiology of the ulnar collateral ligament injury (UCL) in pitchers, and the methodology of measuring throwing kinematics using motion capture (MoCap) technology. Next, and more relevantly, a critical review of the most up-to-date publicly available models in baseball pitching will be presented. This will include several publications that describe inverse and forward dynamic models. For brevity, only the most relevant works, with regards to this research, will be reviewed here.

2.1 Baseball Pitching

The baseball pitch is one of the most dynamic movements in all of sports. In baseball, a pitcher will take the mound in a defensive setting, where their primary goal is to prevent the offensive team from scoring, by delivering the ball to the catcher to make it difficult for the batter to hit effectively. A pitcher wants the batter to be out in a few ways, including throwing a strike, where either the batter swings at the ball and misses, the batter hits foul (with some exceptions), or if the batter does not swing but the umpire deems it to have passed through the strike zone. The strike zone is an imaginary box over home plate, extending from the midpoint between the batter's shoulders and the top of their waist down to an area beneath the kneecap. If the ball passes through this zone and the batter does not swing, the umpire calls a strike. Accumulating three strikes results in a strikeout,

meaning the batter is out and the turn at bat ends. An out can also occur if the batter hits the ball into fair play territory, and the ball is either caught prior to landing, or if the defensive team catches the batter before they reach any of the plates in play, after the ball contacts the ground. Ultimately, a pitcher is responsible for ensuring the opposing team does not have the ability to hit the ball, and potentially score, prior to three outs occurring.

A pitcher utilizes a variety of throws, each with unique characteristics and strategic purposes. The fastball, known for its velocity, aims to overpower batters with speed. In contrast, the curveball features a significant downward and lateral break, designed to deceive the batter with its unexpected trajectory. The slider, combining speed and break, serves as a middle ground between a fastball and a curveball, often used to induce weak contact or swings and misses. Additionally, the changeup is a slower pitch that mimics the fastball's arm action, intended to disrupt the batter's timing. Each type of pitch requires specific mechanics and grips, highlighting the complexity and skill involved in effective pitching. Understanding these different throws and their applications is essential for optimizing pitching strategies and enhancing player performance while mitigating injury risks. This research will focus on the most dynamic and stress-inducing throw, the fastball.

Although pitching is a highly dynamic, continuous motion, it can be separated into a series of 6 phases to better understand the kinetic chain, each of which is separated by some notable events [7]. The detailed kinematics of the movement will be discussed in section 2.2, but in general, the 6 phases of the pitching motion are the wind-up, stride, arm cocking, arm acceleration, arm deceleration, and follow-through, which are separated by the events, maximum knee height, lead foot contact (LFC), maximum external shoulder rotation (MER), release, and maximum internal rotation (MIR), respectively [7]. The result of this sequence is the generation of immense ball speed, with violent joint velocities that produce high rates of injury. See a detailed visual of the phases of the motion in Fig. 2.1.

Great variation exists in the kinematics and temporal variables prior to LFC, namely the windup and stride phases. In general, the duration of the most dynamic portion of a pitch (arm cocking to MER) is less than 1.7 seconds, with a majority of the time being occupied during the arm cocking phase (approximately 1.5 seconds), and a volatile 0.145 seconds between LFC to ball-release [8, 15]. The time prior to the arm cocking and throughout the follow-through phase is very pitcher-dependent and are less relevant due to their relatively effortless mechanics. As such, this research will ignore those portions, especially since they have less implications on UCL injuries.

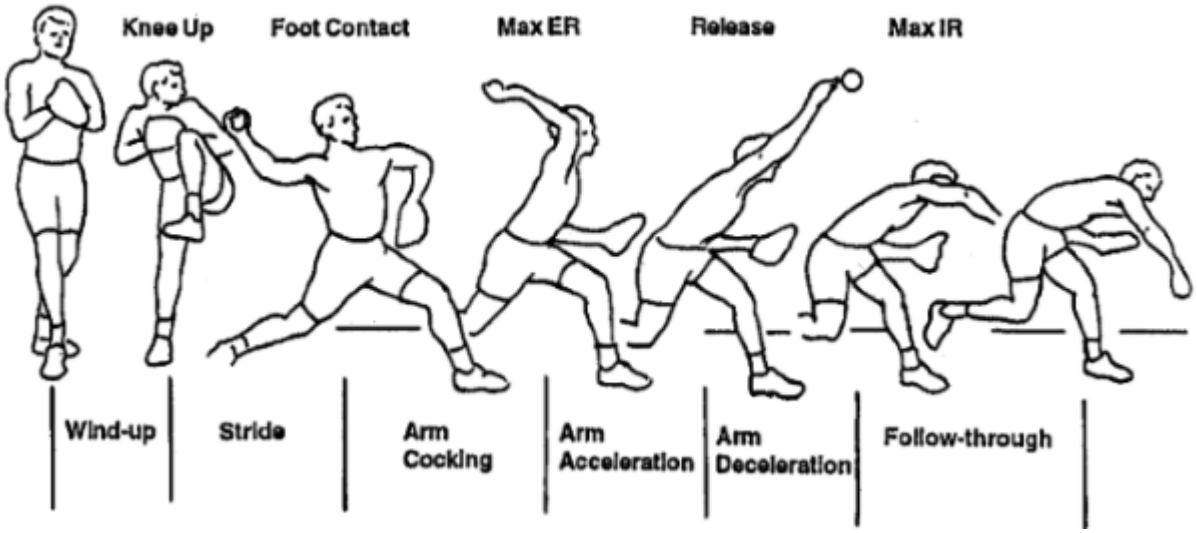


Figure 2.1: The six phases of baseball pitching. The name of the phases are marked at the bottom, while the events separating each phase in the sequence is noted at the top. Each image represents an instance in the motion. Taken with permission from [14].

2.2 Baseball Pitching Kinematics and Kinetics

In this section, a more detailed outline of pitching kinematics/kinetics is presented. The implications of these on biomechanics is also commented on from an injury and performance perspective. To finish, techniques in MoCap are introduced, which are the primary methods of collecting kinematic data in baseball pitching. An understanding of the mechanics of the pitching motion and the association of the movement to injury is essential to developing accurate models and simulation of pitchers. For reference, kinematics are the branch of biomechanics that describes pure motion of the body without consideration of the forces acting on or producing the movement [16]. As an extension, the area of biomechanics that deals with all internal and external forces and moments that are responsible for producing a motion is called kinetics [16]. While the kinematics are useful in identifying the mechanics of pitching and making correlations to performance, the inverse dynamics identified via kinetic analyses are pertinent to injury etiology.

The baseball pitch begins with the windup. This starts when the pitcher initiates the first motion and ends with the maximum knee lift off of the stride leg [7]. The pitcher starts with weight evenly distributed on both feet. The pitcher initiates the motion by pushing off with the leg on the same side as the pitching arm [8]. This movement shifts

the centre of gravity forward. As the lead leg lifts off, the pitcher's arms flex forward, the stance leg and trunk rotate approximately 90°, and the lead hip and knee flex. The stance foot pivots to be parallel with the rubber while the lead leg is lifted, and the lead side (left side for a right-handed thrower) faces the target [7]. Forces in the upper extremity are low, thus shoulder and elbow injuries are rare during this phase [7].

Shortly afterwards, during the stride phase, the pitcher strides the lead leg (left leg for a right-handed thrower) towards the target while separating the hands, swinging them down, apart, and up [7]. Weight shifts from the contralateral leg to the ipsilateral leg (pivot leg), which slightly flexes at the knee to lower the center of gravity [8]. The pitcher's throwing shoulder undergoes abduction, extension, and internal rotation. This coordination is crucial for optimal timing in later phases [7]. The throwing shoulder is abducted to around 9°, the elbow is flexed 90°, and the shoulder is slightly internally rotated [7]. As the stride leg swings forward, the pivot leg extends forcefully, propelling the body towards the plate [8]. The hips and pelvis rotate forward, followed by the trunk [8]. At LFC, the stride length should be about 80% of body height, and the lead knee should be flexed at around 45° [7]. The pelvis should twist and open to the target, with the shoulder about 15° extended [7]. This movement does not generate any notable forces in the throwing arm [7].

Beginning at LFC, and ending at MER, the arm cocking-phase involves the pelvis and upper trunk rotating to face the target while the throwing arm cocks back [7]. The non-throwing arm tucks near the trunk to decrease inertia and increase upper trunk rotational velocity [7]. Proper timing of pelvis and upper trunk rotation is critical for energy transfer to the throwing arm. The phase ends with the throwing shoulder in MER at up to 180°, where the forearm is perpendicular to the trunk, and the palm faces up [7]. The range of MER is far beyond those seen in an average human and puts the shoulder and elbow in a very compromising position, where muscles and ligaments are excessively stretched. Although this position is vital for generating ball speed, it also poses a high injury risk due to the generation of valgus torques at the elbow [7]. Peak elbow valgus torques can exceed 100 N·m, which for comparison, is about equivalent to holding a 25 kg mass in the thrower's hand at the instant of MER [7].

From this dangerous position, the athlete accelerates the arm forward, achieving elbow extension velocity exceeding 2400°/s and shoulder internal rotation velocity of about 7500°/s [7]. This rapid elbow extension spans from a flexed position (about 90-120°) to almost full extension (25°) at the point of ball release (BR) [8]. These motions are the fastest recorded joint rotations documented in sports, which explains the risk for injury [7]. Forces exceeding 1100 N are also produced at the shoulder and elbow to resist dislocation of these joints, with tensions on ligaments and muscles potentially leading to tears after many repetitions [7]. At this point, the lead knee is flexed, and the lagging knee is extending,

transferring energy from the pelvis to the ball. The trunk is tilted forward and to the side, and the throwing shoulder is abducted over 90° [7]. Right before BR, the wrist begins to flex from an extended position to neutral and pronation of the forearm reaches about 90° at release, where this phase ends [8].

Immediately after release, significant deceleration forces are generated, particularly by the posterior shoulder muscles and the biceps, marking the initiation of the deceleration and follow-through phases [8]. The shoulder moves into horizontal flexion and internal rotation, and the throwing elbow rebounds, flexing to about 45°, leaving the forearm pronated [8]. The shoulder and elbow continue to decelerate, as the body catches up with the arm's motion [7, 8]. The arm horizontally adducts in lead of the chest, and the trunk continues to tilt forward while the pitcher's lead leg moves into a position to stabilize the body and the back leg swings forward, in front of the body [7, 8]. Proper deceleration and follow-through mechanics are essential to dissipate the energy generated during throwing and prevent further forces in the throwing shoulder and elbow [7].

2.2.1 Motion Capture for Inverse Kinematic Analysis

MoCap is a common tool used in biomechanics studies of all movements, especially in baseball pitching [17]. A majority of the work done in baseball biomechanics relies on the collection of kinematic data using MoCap for subsequent analysis. Most work in this field has been conducted in laboratories with 3-dimensional (3D) marker-based MoCap systems [17]. A limitation of marker-based systems is that they cannot be used in-game, and could influence the throwing mechanics while attached, making the research less translatable to in-game applications. More recently, marker-less MoCap technology has become commercially available and has been adopted by most MLB teams for research and development endeavours for use in-game and in-training sessions [17]. In fact, a survey of MLB teams by the American Baseball Biomechanics Society found that 70% of MLB clubs used 3D marker-less systems as of 2021, with more promise of growth [17]. The data collected for this research used a marker-less system, and all analyses are based on in-game data.

Marker-based MoCap systems rely on a series of cameras or optoelectronic sensors in a controlled lab-setting to track the 3D trajectories of reflective markers strategically placed on anatomical landmarks [18]. The results of the data collection are coordinates of the various markers, which can be used to determine the orientation and motion of a particular body segment in space, otherwise known as kinematics [18]. Marker-less systems offer an interesting alternative to marker-based systems, and are fully-automatic and non-invasive [18]. Using a series of synchronized cameras, these systems rely on deep learning-based software (pose estimation algorithms) to describe human posture, and segmental

orientation, for each individual image or frame within a video [19]. Both approaches ultimately result in a set of coordinates associated with points on the body that can be used to track motion.

2.2.2 Implications of Pitching Biomechanics on Performance

For a pitcher to be considered elite, the athlete needs to consistently produce high ball velocity. By outputting extreme ball speeds, a pitcher can increase the likelihood of throwing a strike, since the increased ball speed may elude the batter more easily, improving the thrower's performance. This is particularly evident in a fastball throw, which relies on ball speed over movement and is the pitch of interest in this research. One way to predict a pitcher's ability to throw effectively is through the analysis of the kinetic chain [15].

The kinetic chain can be considered as the relationship between a movement's kinematics and temporal joint sequencing patterns [20]. During a pitch, the chain manifests as an interaction of body segments, in a sequential pattern from the ground up, and from more proximal segments to distal ones [20]. The chain terminates at the end-effector, which in pitching is the ball-hand complex [20]. Studies have shown that seamless sequencing of the kinetic chain can lead to an increase in the velocity of the terminal segment, which would ultimately produce greater ball velocities at release [15, 20, 21]. A pitcher's ability to generate ball velocity is very much related to the activation and deactivation times of the muscles of the throwing arm, which will become apparent during the forward dynamic analysis component of this research, in Chapter 5 [22]. From a physiological perspective, if the delay between proximal and distal joint sequencing is premature, the throw may be completed sooner, leaving less time for contraction of the proximal muscle [22]. This may result in decreased torque generation or generation over a smaller range of motion (ROM), reducing the work done by the muscles on the ball [22]. The lack of torque generation ultimately reduces the velocity production capabilities of the pitcher, hampering their in-game fastball performance and ability to throw strikes with this pitch [22].

Despite the variation within pitchers' throwing biomechanics, there are some key factors that may indicate greater ball velocity generation capabilities by elite pitchers [15]. Kinetically, a study by Stodden et al. showed that elbow flexion torque, shoulder proximal force, and elbow proximal force production abilities were significantly correlated to increased ball velocity [15]. The ability to produce these forces relates to temporal and kinematic parameters present during a pitch [15]. Specifically, an increased time to maximum shoulder horizontal adduction and decreased time to maximum shoulder internal rotation significantly contribute to ball speed [15]. Furthermore, decreased shoulder horizontal adduction

at LFC, decreased shoulder abduction during arm acceleration, and increased forward trunk tilt at BR have also been shown to be major contributors to throwing performance [15].

The increased proximal force at both the shoulder and the elbow is directly related to the increase in the rotational velocities of the pelvis and upper torso [15]. Moreover, as a result of the kinematic and temporal pitching parameters, as an individual threw faster, pelvis and upper torso angular velocities increase and shown an increased forward tilt of the trunk [15]. The kinematic behaviour of the trunk in faster pitchers induces a lag effect on the throwing arm, putting them in a position to generate a larger ROM of shoulder horizontal abduction at LFC [15]. The resultant shoulder action suggests that the distance the ball travelled from LFC to BR was greater in elite pitchers [15]. Regarding the temporal variables, a quicker time to maximum shoulder horizontal adduction and maximum shoulder internal rotation contributes to throwing speed, since they allow for a swifter internal rotation, mimicking the action of a slingshot [15]. Overall, the ability of elite pitchers to create violent dynamics at the shoulder and elbow, as well as high velocities and extensive ranges of motion in the trunk and upper extremities lead to increased throwing velocity. This supports the notion in literature stating that a greater range of motion enables greater torque generation capabilities [15, 22]. Ultimately, increases in pitching velocity are due to a more effective transfer of momentum in the kinetic chain and suggests that pitchers should focus on consistent mechanics and joint flexibility to maximize fastball speeds.

2.2.3 Pitching Biomechanics and UCL Injuries

The mechanisms of UCL injuries are complex and have been extensively studied, but vary between different pieces of literature [5, 23–25]. However, the primary channel of the injury in elite pitchers involves the excessive valgus loading on the UCL during the pitching motion [23, 24]. The peak valgus torques are present at the end of the arm cocking phase/beginning of the arm acceleration phase of a pitch, where greater loading is generally correlated to higher pitch velocity in MLB pitchers [5]. During this pitching phase, the elbow is subjected to an external valgus torque, while the shoulder rotates externally, imparting a massive tensile force on the medial side of the elbow. The UCL plays an essential role in resisting this external valgus torque, by applying a counteracting and stabilizing varus load, but like all soft tissue, has its limits [20, 24]. This is visualized in Fig. 2.2 [25].

In-vitro studies conducted on cadavers have stated that the UCL would rupture after an ultimate external valgus torque of 34 N·m was applied to the proximal end of the ligamentous insertion [24]. However, in-game data suggests that MLB pitchers may experience

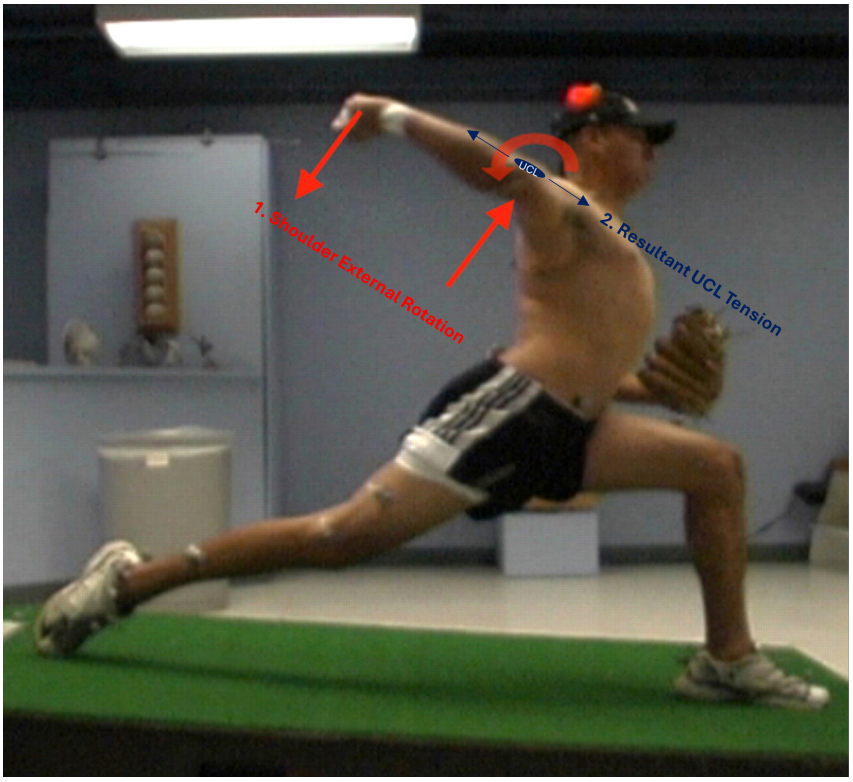


Figure 2.2: Visualized valgus torque and tensile force on the medial elbow during the late arm cocking-early arm acceleration phase of baseball pitches. As the shoulder externally rotates (red), the hand-ball complex moves downwards and away from the torso, while the elbow is driven upwards. This creates resultant tensile loads at the medial elbow (blue), stretching the UCL. Adapted from [25].

peak valgus torques in the range of 40 to 120 N·m [24]. This would imply that a pitcher would routinely injure the UCL, for almost all throws, which is not the case. This can be explained by the fact that the injury thresholds reported were extracted from experiments on the isolated ligament and do not consider the stabilizing behaviour of the surrounding structures, such as the joint capsule, other ligaments and even muscles that span the elbow joint. A recent study has even shown that the musculature in the elbow alone produces a maximal counteracting varus torque of 71 N·m, contributing to the stabilization of the elbow [26]. The complex anatomy and structural contribution of the elbow joint make predicting UCL injuries difficult [24,26]. Coupling this with the variability induced by fatigue, weight, age, and pitch counts makes predicting UCL injuries unrealistic [5]. The anatomy

of the UCL is shown in Fig. 2.3, and highlights the 3 bands that make up the UCL [27]. In this research, the anterior band of the UCL is considered in the greatest detail since this band is most commonly reconstructed during Tommy John surgery in pitchers [4].

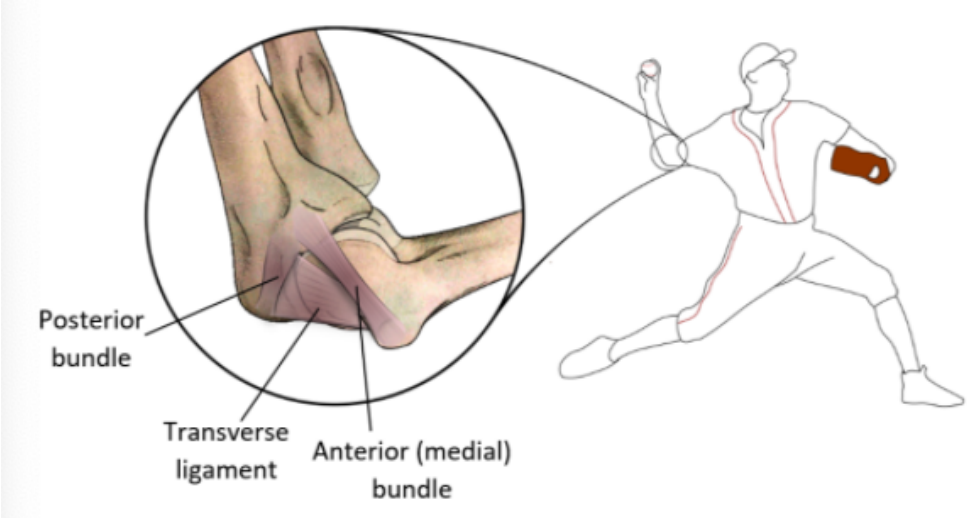


Figure 2.3: UCL anatomy during pitching. Taken with permission from from [27].

The extreme valgus torques applied to the elbow are a product of the extreme laxity in shoulder ROM, present in elite pitchers [28]. For example, pitchers achieve between 150-180° of external shoulder rotation during the late arm cocking-early arm acceleration phase of the pitch, with between 70-90° of elbow flexion [28]. The values of MER in pitchers far exceed those of the average population, and are learned through years of repetitive dislocation of the shoulder joint capsule [28]. This laxity allows the hand-ball complex to lag severely behind the trunk, allowing more torque generation over a greater distance, but also imparts massive loads on the shoulder and elbow [15, 22, 28].

From a pitching biomechanics perspective, there are a series of variables in sequential body motion that are correlated with increased elbow valgus torques [25]. The essential conditions to increased valgus loads are the range of MER, increased elbow extension angle at the instance of peak valgus load, increased elbow extension angle at BR, timing of maximum elbow flexion, onset of trunk rotation before BR and elbow valgus loading rate [25]. Although the effect of large ranges of MER have been discussed, the elbow extension angle throughout the most dynamic portion of the pitch also heavily contributes to UCL strain. Between arm acceleration and BR, where the valgus loads are the highest, a more extended elbow induces a greater bending moment, compared to a flexed elbow, as

the throwing arm lags behind the trunk due to the arm's inertia. Nonetheless, pitchers are taught to extend the elbow during the throw, despite the detrimental loading effects, since extension generates increased velocities [25]. These larger velocities are a product of the increased centrifugal force present during a pitching action with greater elbow extension [25]. Temporal parameters of the trunk are also indicators of increased elbow valgus loads. Pitchers who rotate their trunk to square up to the batter later in the pitching cycle generally have decreased elbow valgus loads [25]. Specifically, initiation of trunk rotation prior to LFC produces excessive valgus loads.

Interestingly, sidearm pitchers are more susceptible than traditional overhand pitchers to larger elbow valgus torques, as a result of their lower shoulder abduction angles [25]. Similar to the effect of elbow extension on valgus torques, the lower arm slot found in sidearm pitchers increases the amount of lag in the throwing arm, relative to the trunk, inducing a greater bending moment at the elbow [25]. Sidearm pitchers also tend to have earlier trunk rotations than overhand throwers, also contributing to greater elbow valgus magnitudes [25]. Various pitching styles have different arm slot positions at BR. Arm slot is traditionally defined as the frontal plane position of the throwing arm during the ball delivery, relative to the ground, particularly relevant to shoulder abduction [25]. However, as discussed later, measuring the arm slot relative to the torso is a more informative metric.

2.3 Dynamic Models of Pitching

Modelling and simulation of baseball pitching is a pursuit that reaches a multitude of disciplines from biomechanics and biology to multi-body dynamics and numerical optimization. The highly dynamic nature of the baseball pitch and its repeatability make it an interesting motion to model, but also highly complex. In this section, a number of published pitching models will be presented to provide sufficient context and background regarding the current state of the art in this area. The chapter will conclude by highlighting potential areas of improvement in published models, to be adopted in this research. Prior to detailing the components of previously developed models, it is important to understand the various simulation strategies that are commonly used to study the kinematics and kinetics of a pitching motion. In addition to assessing joint angles and speeds using inverse kinematics, there are two additional approaches that will be used in this research: inverse dynamics and forward dynamics. Both rely on multi-body dynamics and classical equations of motion, which provide a relationship between motion and forces.

The inverse dynamic problem is one where the goal is to reconstruct the internal forces and moments from known movements (kinematics) and external forces [29]. Some typical

outputs of such models in a biomechanical application would be internal joint forces or net joint torques acting on the body during a movement. It is important to note that only net forces and torques are extractable from this simulation platform, since there is no consideration for contributions from soft tissues or other biological components such as muscles and ligaments. This is because this method does not differentiate between contributions from individual muscles, ligaments, or soft tissues. All it tells you is the combined effect, since muscle forces are not calculated using the purely mechanical Newton-Euler equations used in inverse dynamics. Some common examples of external forces would be gravity acting on the body and ground reaction forces (GRF). As such, it is important to design an inverse dynamic model with accuracy compared to the subject it aims to replicate, since any outputs would be approximations of net dynamics. For musculoskeletal (MSK) inverse dynamic models, an accurate model will consist of detailed anthropometrics and inertial properties, including segment mass, segment length, segment centre of mass (COM) location, and principal moments of inertia [29]. The major disadvantage of inverse dynamics studies is that they are not predictive and approximate net joint kinetics, making it difficult to identify individual contributors to forces and torques [30]. Inverse dynamic simulations will be discussed in greater detail in Chapter 4. Ultimately, inverse dynamics is a very useful tool for correlating motion to net dynamics during locomotion.

The forward dynamics problem consists of the calculation of motion from known internal muscle forces and moments [29, 30]. A benefit of forward dynamic models is that an assessment can be made into individual muscle and ligament contribution to a net joint force or torque, which is useful when assessing injuries such as those found in baseball pitchers. Nonetheless, this approach is complex, since it is difficult to control movement by adjusting joint moments and forces. This problem is especially evident when dealing with a full-body model, with over a dozen segments, or for a highly dynamic movement, like a baseball pitch. It is also difficult to predict the change in other forces, such as the GRF, or a change of acceleration of a centre of mass, based on known forces.

Forward dynamic simulations require numerical integration of the differential equations of motion of the system, which takes a considerable amount of time, especially when an optimization framework is outlined within the simulation [30]. Optimization is required since the human MSK system is underdetermined, meaning that there are more muscles than degrees of freedom (DOF) in the body [30]. As such, there exists an infinite amount of solutions of muscle forces and recruitment of muscles for a given motion [30]. To address this, optimization or optimal control can be used to constrain the problem and identify a suitable solution. A suitable solution in this case would mean the production of a realistic motion under a set of specified outcomes. These specified outcomes in the human body would be treated as cost functions in an optimization problem and could include the

minimization of metabolic energy expenditure, minimizing joint reaction forces, or even maximizing segment velocities for a desired movement [30]. Despite its immense benefits, there are no direct non-invasive ways to validate predicted muscle forces or determine if the optimized solution is global, further complicating this type of analysis [30]. Regardless of the complexity associated with forward dynamic analysis, it is a powerful tool that is particularly useful in identifying individual muscle contributions. Moreover, it is predictive and can simulate hypothetical scenarios and assess the resultant impacts on the body, without the need for physical testing. This will be discussed in detail in Chapter 5.

2.3.1 Inverse Dynamic Models

Two-Segment Model

The first identified inverse dynamic analysis comes from a pair of articles developed by Feltner et al., which provides a detailed mathematical methodology of a two-segment model, with particular applications to baseball pitching [21, 31]. The article focuses on understanding the three-dimensional interactions in a two-segment kinetic chain of the throwing arm and aims to elucidate the mechanics behind the motion of body segments. Using an inverse dynamic analysis on the developed model, the authors determined the effects of the shoulder and elbow joint torques on the angular accelerations of the arm segments during baseball pitching [21]. The main point of interest in this article is the development of the system model, but most of the article discusses the mathematical formulations used to solve the inverse dynamic problem. The simplified system under study consists of only the throwing arm of a baseball pitcher, divided into two segments: the upper arm and the distal segment (which includes the forearm, hand, and baseball).

The article continues by describing the use of Newton-Euler equations to describe the motion of each segment. The equations break up the motion into linear and angular components, considering both accelerations and moments of inertia for each segment. The model decomposes the angular accelerations into components associated with joint torques and those dependent on the motions of other segments (motion-dependent terms). These terms include components due to the gravitational force acting on the segments, contributions from the joint forces and torques at the shoulder and elbow, and kinematic interaction parameters reflecting the interactions between the angular and linear motions of the segments. With a set of kinematic data, the authors relied on inverse dynamics to connect the arm's motion during a pitch to kinetic outputs. From this study, the authors concluded that the violent external rotation of the upper arm is primarily driven by the sequential

activity of the horizontal adduction and abduction moments at the shoulder [31]. Moreover, the transition from stopping the external rotation to initiating internal rotation of the upper arm is largely due to the internal rotation proximal joint torque at the shoulder. Next, it was shown that the resistive varus joint torque at the elbow is closely associated with the internal rotation joint torque at the shoulder. This varus torque plays a critical role in maintaining the stability of the elbow joint during the upper arm's movement to MER and its subsequent MIR before the ball is released. Finally, the data suggested that the rapid extension of the elbow prior to BR is primarily a result of the counterclockwise moment of the trunk during the pitch, rather than the direct actions of the elbow extension moment.

Three-Segment Model

A separate study conducted by Matsuo et al., in 2006, also leveraged an inverse dynamic analysis on baseball pitching to assess the influence of shoulder abduction and lateral trunk tilt on peak elbow torques [32]. This was done through simulations and regression analyses. Understanding these dynamics is crucial for developing strategies to minimize injury risks during pitching. The developed model builds upon previous work by using a three-link model of the throwing arm, composed of the hand with the ball, the forearm, and the upper arm before the instant of BR. An identical model, without the ball, was created to simulate the dynamics of the throw after the instance of BR. This model is novel in the sense that it simulates both pre-release and post-release phases of the pitching motion. 33 healthy college baseball pitchers (24 right-handed, 9 left-handed) were collected for this study and fit with reflective markers to capture motion data with four infrared cameras. Each pitcher threw 5 to 8 fastballs, and motion data was collected.

Using the kinematic data from the pitchers, combined with a Newton-Euler inverse dynamic method, the joint forces and torques were extracted from a series of hypothetical simulations. The simulations were conducted on the three-link model, using detailed segment inertial parameters that were based on the participant's body weight and segment lengths. Each simulation leveraged the general kinematics of the subject, but with 7 altered angles for lateral trunk tilt (-20° to 40°) and 6 angles of shoulder abduction (70° to 120°) at the instance of BR. Each of the edited trunk angles was applied with each of the different shoulder angles, for a total of 42 simulations for each pitcher. A two-way analysis of variance (ANOVA) was then conducted to analyze the combined effects of shoulder abduction and lateral trunk tilt on elbow torque. For each lateral trunk tilt angle, a one-way ANOVA was used to assess the specific impact of shoulder abduction. Regression analyses, including simple, second-order, and multiple regression models, were also performed

to explore the relationships between these variables and elbow torque.

The key findings of this study were that there was a significant interaction between shoulder abduction and lateral trunk tilt on elbow valgus torque. As lateral trunk tilt increased contralaterally, the shoulder abduction angle that minimized peak elbow valgus torque decreased. For ipsilateral trunk tilt conditions (-20°, -10°, 0°), higher shoulder abduction angles tended to show less elbow valgus torque. At -20° trunk tilt, the minimum peak elbow valgus torque was observed at 120° shoulder abduction, but this was not statistically significant. At -10° and 0° trunk tilt, peak valgus torque was minimal at 110° shoulder abduction (66.0 ± 31 N·m and 62.1 ± 14.4 N·m, respectively) and significantly smaller than at 70° and 80° shoulder abduction. Moreover, at 10° contralateral trunk tilt, peak valgus torque was minimal at 100° shoulder abduction and significantly different from 70°, 80°, and 120° shoulder abduction conditions. Finally, at 20° and 30° contralateral trunk tilt, peak valgus torque yielded a minimum at 90° shoulder abduction. The study demonstrated that both shoulder abduction and lateral trunk tilt significantly influence peak elbow valgus torque during pitching. The optimal shoulder abduction angle to minimize elbow varus torque decreases as the trunk tilts more to the contralateral side. These findings suggest that shoulder abduction and lateral trunk tilt are important considerations for minimizing elbow injury risks in baseball pitchers.

Inverse Dynamics and Induced Acceleration Analysis

Although it is not traditional inverse dynamics, the combined use of inverse dynamics and Induced Acceleration Analysis (IAA) in literature are related to model building, and provide some necessary context. Two notable publications by Naito et al. and Alderink et al. are of particular interest, since they leverage inverse dynamics and IAA, for an upper-body and full-body model respectively [33, 34]. It is important to note that unlike the previously defined throwing arm models, the models in this section will rely on the use of GRF, in addition to segmental gravitational forces, as key external forces being applied to the model. This provides additional context for the subsequent analysis, making the extracted dynamics more accurate.

IAA is highlighted as a more effective method for examining how joint kinematics are produced by various torque components. IAA can provide information about how individual muscle contributions accelerate joints in a link-segment model, as a function of segment pose. The theoretical model accounts for both instantaneous angular accelerations induced by a joint torque at that instant, the cumulative effect of angular accelerations induced by the entire joint torque, gravity torque history until that instant (which is pose dependent),

as well as velocity-dependent torques at all joints [34]. Traditional inverse dynamic approaches are related to the concept that complex systems cannot be explained by simply deconstructing the system into parts. Nonetheless, traditional inverse dynamics is still a very useful tool for gaining a general understanding of the kinetics involved in the baseball pitch. Moreover, although IAA does have its benefits in identifying respective contributions to torques from external forces, velocities, and accelerations, it is not as effective in identifying internal muscle contributions as a forward dynamic approach, which will be discussed in section 2.3.3 [33, 34]. Inverse dynamics relates to IAA, since the equations of motion that govern IAA rely on the inverse dynamics extracted from kinematics as an input. However, since ball velocity is of greater interest in baseball than acceleration, an integration of the induced acceleration results is typically conducted in baseball research. The integration of IAA is called induced velocity analysis (IVA), and was used in both of the referenced publications.

Upper-Body Model

Naito et al. developed an upper-body model to identify the detailed mechanisms that maximize throwing arm endpoint velocity [33]. More specifically, the study aims to identify how maximum throwing velocity is determined by non-muscular passive torques, including gyroscopic and centrifugal effects, particularly in the upper body. The model leverages IAA and IVA, to address the shortcomings of traditional inverse dynamics. For this study, male collegiate baseball pitchers, all right-handed, participated and threw at least five maximum-effort pitches, with the fastest pitch selected for analysis. A three-dimensional MoCap system tracked their movements, capturing the positions of reflective markers placed on various body parts, in addition to force plates built into the mound to collect GRF. More notably, the throwing system was modelled as an eight-segment linked system with 20 DOF, involving the trunk, thorax, bilateral upper arms, forearms and hands. The study defined specific joint rotations and calculated joint angles using the Euler angle convention.

Kinematic variables were obtained from the positional data, and joint torques were calculated via traditional inverse dynamics, with the addition of the GRF. IAA on the model's joints was then used to decompose joint angular accelerations into components related to muscular torques, gyroscopic moments, Coriolis and centrifugal forces, trunk linear acceleration, gravity, and external forces. Subsequent integration using IVA found that the three key joint motions involved in generating angular acceleration and subsequent ball velocities through internal rotation of the shoulder were thorax rotation, elbow extension, and wrist flexion. These were based on their ability to develop large passive motion-dependent effects and muscular torque effects at the shoulder. In particular, the

centrifugal force-induced elbow extension motion was the greatest contributor among individual joint contributions. The study also found that a compensatory mechanism was achieved by the negative and positive contributions of the muscular torque components, further highlighting the importance of IAA and IVA in determining the dynamic coupling mechanisms in a baseball throw.

Full-Body Model

Similarly, Alderink et al., used IVA to investigate which joints made the largest contribution to the velocity of a pitched ball, but on a full-body scale [34]. The experimental data collection process was similar to Naito et al., so the modelling and key finding are more notable here [33]. A 14-segment biomechanical model, which included feet, legs, thighs, pelvis, a combined thorax-abdomen-head, upper arms, forearms, and hands was implemented in Visual3D software. The hip and shoulder joints were given 3 DOF as spherical joints. The elbows and ankles were modelled as two DOF universal joints, where the elbow allowed flexion/extension and forearm pronation/supination, while the ankle allowed dorsi/plantar flexion and inversion/eversion. The knees and wrists were modelled as revolute joints allowing flexion/extension. The pelvis served as the root segment and was given 6 DOF, to rotate and translate in all directions relative to the ground.

Using equations of motion to extract the accelerations of the joints induced by the inverse dynamic forces acting on the body, a dynamic coupling analysis was completed to identify individual contributions of torques. Joint torques were turned on one at a time in the IAA equations of motion, to determine forward acceleration imparted on the ball by that torque. Forward acceleration due to gravity was determined by setting all torques to zero and activating gravity. Velocity-dependent effects were determined by setting all torques and gravity to zero and driving the model using all the joint velocities from an inverse kinematic analysis. The induced velocity of the ball was obtained by integrating the induced acceleration results, where the IAA equations of motion relied on the decoupled parameters described. The model-generated induced velocity of the ball was validated against ball velocity obtained from a radar gun during data collection. The study found that velocity-induced torques at the shoulder prior to BR and the elbow during the cocking phase contributed to pitching velocity by 31.0% and 18.1%, respectively. The centripetal and Coriolis effects from the upper arm and forearm velocities made the largest contribution to ball velocity where they generated around 57.8% to total velocity. Finally, the lower extremities, pelvis and, trunk made the least direct contribution to pitched ball velocity, but were not negligible.

2.3.2 Forward Dynamic Models

As previously described, a forward dynamic analysis is challenging, making its use in literature scarce for a movement as dynamic as baseball pitching. However, it is the state-of the art simulation method to identify individual contributions of soft tissue to motions. The predictive and optimal control based methodology associated with the forward dynamic problem justifies the undertaking of such a challenge, since it is immensely beneficial in simulating a variety of hypotheticals.

Two forward dynamic approaches of particular interest in this research are torque-driven and muscle-driven. A torque-driven forward dynamic simulation uses torque generators to represent and apply a net effect of all muscles acting across a joint [35]. To achieve realistic joint kinematics and activation dynamics, models typically use separate agonist and antagonist torque generators, for each DOF in a joint, which permits co-contraction. Studies using torque-driven models prioritize net joint torques rather than the role of individual muscles. On the other hand, muscle-driven models consider the effect of each muscle torque individually using a muscle–tendon complex representation that is built into the model [35]. The benefit of such a model is also its biggest drawback, since the selection of realistic muscle parameters to accurately model the tissue is difficult, and current muscle models are insufficient in generating highly dynamic motions, such as a pitch. Nonetheless, the advantage of gaining insight into soft tissue behaviour during motion is crucial to simulating injury scenarios, making it an invaluable component of this research.

Torque-Driven Model

The most notable torque-driven forward dynamic model of a baseball pitcher was developed by Fujii and Hubbard in 2002 [13]. In this study, a simulation and optimization procedure was designed to identify the relationship between optimized pitching mechanics and muscular strength. Their model consisted of 3 segments in additiom to the torso, which were the upper arm, lower arm and hand. Each segment is assigned a local coordinate system to track movements accurately. The shoulder joint was given three DOF, the elbow joint has two DOF, including pronation/supination, the wrist joint had one DOF, with ulnar/radial flexion omitted and the ball was fixed to the middle finger.

The model implemented 6 bilateral torque generators at each of the joints at the shoulders, elbows and wrists. The actuators were designed with the characteristics of Hill-type muscle models to replicate realistic torque-angle and torque-angular velocity behaviours. The generators were given a passive torque component, and was proportional to the squared angular deviation when joint angles exceed certain thresholds. There were also constraint

torques implemented at the joints, to ensure the DOF are maintained, particularly at the elbow joint. Finally, the movement inducing, or active torques were modelled to simulate muscular inputs and are a product of maximum isometric torque, normalized active state, and functions of joint angle and angular velocity. The active torque component is modelled to reflect Hill-type muscle characteristics, capturing the dynamic interplay between muscle activation, joint angles, and velocities. The model was also given anthropometric and inertial data from various sources of literature, not from professional atheltes. The torque generators are sometime referred to as muscle torque generators (MTG) [30].

The objective function of the forward dynamic model was to optimize for maximal release velocity while penalizing joint loading with negative terms. Different simulation strategies were implemented to assess the trade-offs between performance and injury by adjusting the weighting coefficients. For instance, conditions 1 through 5 progressively increased the emphasis on minimizing joint loads and the effects on velocity were noted.

The optimized pitching motion closely resembled a measured pitching motion from a Japanese varsity level pitcher. It was shown that reducing joint loads while maintaining throwing speed relied on precise coordination of generator activation patterns. The release velocity in the optimized simulations was slightly less than the measured ball velocity from experimentation due to simplifications in the model, such as fixing the ball in the hand rather than allowing it to roll to the fingertips. The weighting coefficient for joint loads were also shown to have a strong influence on the results. As this coefficient grew, the motion becomes more similar to actual measured pitches, indicating a tendency for the body to naturally attempt to minimize loads.

Muscle-Driven Model

Arguably, the most notable and impactful research in modern pitching biomechanics modelling and simulation came from Buffi et al. in 2015 [11]. They used a forward dynamic muscle-driven model to compute the soft tissue contributions to the stabilizing elbow varus load during baseball pitching. The article presents a sophisticated 3D model designed to analyze the biomechanical contributions to the elbow varus moment during baseball pitching, and serves as a key resource for this research. The generic, whole-body model implemented in this study was made in OpenSim and included 12 segments, 30 DOF, and was designed to represent the anthropometry of a 50^{th} percentile young-adult male. Notably, a DOF for the varus-valgus motion at the elbow was included. The original model came from an open-source whole-body model designed to simulate lower-extremity tasks, but the right arm was updated since the study was interested in right-handed throwers with particular focus on the elbow joint. This included the insertion of a baseball, modelled as a spherical mass,

which coincided with the middle finger of the throwing hand. The model of the throwing arm included 6 kinematic DOF: three at the shoulder (adduction, flexion, and rotation), two at the elbow (flexion and varus), and one at the forearm (pronation). A visual of the model can be seen in Fig. 2.6, which also includes a depiction of the varus-valgus joint movements.

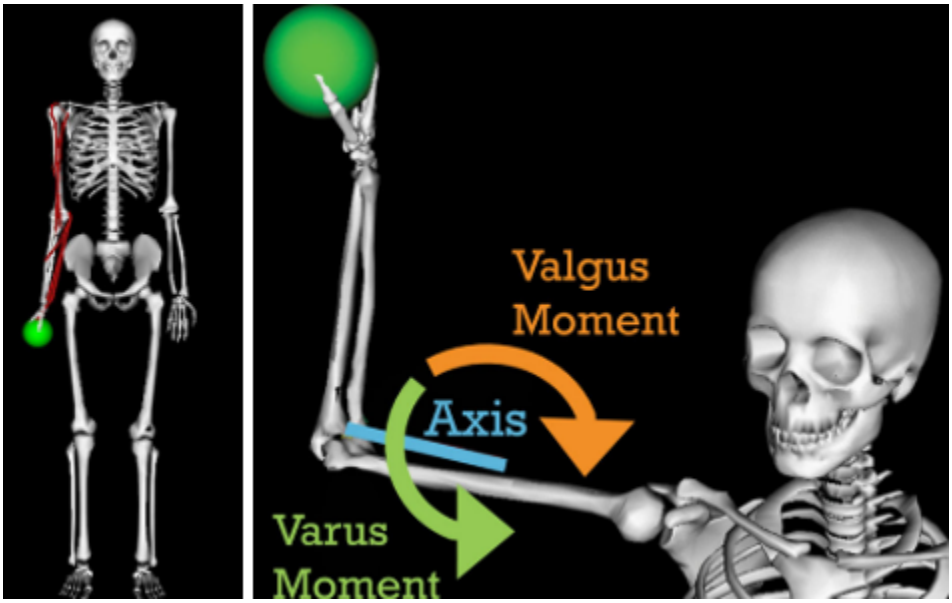


Figure 2.4: (Left) Full body MSK pitching model by Buffi et al. The green sphere is the baseball and is welded to the right hand. It also includes 14 muscles of the right arm. (Right) Definitions of the varus–valgus reactionary moments and their axis of rotation. Taken with permission from from [11].

The model included 14 muscle–tendon actuators, representing the medial elbow musculature, capable of generating elbow varus moments. The actuators were implemented to replicate the coordinates of the muscle origins and insertions. Moreover, the intermediate muscle points and the geometries of muscle wrappings were found from open-source upper-limb models. The actuators were defined as Hill-type muscle–tendon models. These muscles were supplemented by reserve actuators, which were activated when the muscles could not generate enough force to track the inputted kinematics. These actuators also drove the motion of the non-muscle driven joints. Modern muscle models were not strong enough to drive a motion as dynamic as a baseball pitch, which undergoes extreme joint velocities, forces, and torques. As such, reserve actuators are often included in forward dynamic models to support the motion. Three pre-processing steps were applied to the

model, which were scaling to match the height and mass of subjects, inverse kinematics to extract joint angles from marker trajectories, and residual reduction via mass distribution tuning to ensure that the model was dynamically consistent with the recorded GRF. Data was collected as outlined by Alderink et al. to serve as inputs into the forward dynamic model [34].

After the pre-processing steps, a forward dynamic simulation and sensitivity study were conducted to calculate muscle forces and moments. From the results of each simulation, the elbow joint compression force and the valgus UCL loads were computed externally. The sensitivity study evaluated the loading of the elbow structures from muscles that varied in performance, or activation, levels. This was done by changing the musculotendon force-generating parameters in the model's actuator set and the muscle excitation constraints. A total of 4 simulations were conducted during the sensitivity analysis. For each actuator and excitation constrained simulation, a forward dynamic simulation was produced using an algorithm known as computed muscle control (CMC) [11]. The pitching motion was assessed only at the arm cocking and acceleration phases, since these phases produce the highest risk of injury. CMC works to calculate actuator control signals to produce each forward simulation of the motion. This algorithm relies on the outputs of the pre-processing steps, GRF, actuator sets, and excitation constraints to drive the forward dynamic simulation. At each time step, CMC solves a static optimization (SO) problem that calculates the control signals for the actuators to generate the desired joint accelerations, based on the inputted kinematics. The computed control signals at each time step minimize the error between the modelled joint accelerations and the desired joint accelerations, extracted from the input joint angles. A flow chart of the forward dynamic analysis can be seen in Fig. 2.7

The simulations showed that the medial elbow musculature produces a large, stabilizing, and resistive varus elbow moment, to protect the elbow joint during the violent pitching motion. During peak valgus loading, between the arm cocking and acceleration phases, the triceps generated large varus moments. The researchers also noted that a significant varus moment was generated by the flexor digitorum superficialis, but occurred later in the motion, well after the peak valgus torques. Overall, it is seen that the flexor-pronator muscles of the forearm have the capacity to generate considerable protective elbow forces. The sensitivity studies showed that increasing the muscle–tendon force output, through alteration of muscle excitation or strength/power parameters in the actuator models, decreased the load on the UCL. With enough sufficient hypothetical improvement to the actuator sets, the UCL load could even be effectively eliminated. This is a very notable revelation, indicating that strength and muscular training can be used in baseball pitchers to support the elbow joint and reduce injuries.

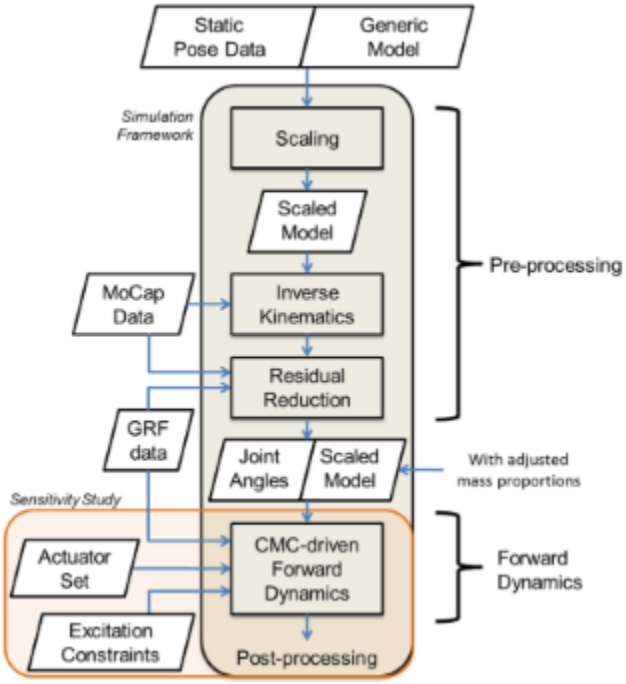


Figure 2.5: A flow chart outlining the simulation framework and sensitivity study for the forward dynamic analysis of baseball pitchers, by Buffi et al. Taken with permission from [11].

Others have attempted to build upon the work of Buffi et al., namely van der Pijl, in his 2022 Masters thesis, out of the Delft University of Technology [12]. Similar to Buffi et al., van der Pijl's thesis presents a MSK modelling approach to understanding the load distribution on the UCL during baseball pitching, focusing on how various muscles contribute to countering the external valgus torque applied at the elbow. The OpenSim model, based on the Delft Shoulder and Elbow Model, integrates elbow and wrist muscles to predict force dynamics during pitching motions. Interestingly, this model also added a varus-valgus DOF at the elbow. The study employed inverse dynamics and SO techniques in OpenSim to simulate ten baseball pitches, recording muscle moments and joint loads across two conditions; with and without wrist motion. This method allowed the identification of muscle contributions to stabilizing the UCL, showing that certain muscles, notably the flexor digitorum superficialis, generate substantial internal varus moments during wrist-included simulations [12]. The main difference between the two works are the OpenSim algorithms used to simulate the model with Buffi using CMC and van der Pijl employing SO.

SO in OpenSim is a computational method used to estimate muscle forces and activations required to perform a motion, based on kinematic and kinetic data. This technique minimizes the sum of squared muscle activations at each time point, optimizing muscle contributions without simulating complex muscle dynamics or time-dependent changes. This allows for efficient analysis by treating each time step independently, rather than integrating over time. Some of the drawbacks of SO include the fact that muscle dynamics are not included, so the MSK model may get very fast oscillations in muscle loads (which are all independent of each other), leading to discontinuities in signals.

Analysis of the MSK simulations revealed the extent to which each muscle counters the external valgus torque. The findings indicate that while the UCL contributes 31% of the countering moment in wrist-included simulations, the osseous articulation (or joint compression force-induced moment) provides the majority of stability (59%). In contrast, when the wrist motion is excluded, the UCL load increases significantly, bearing 48% of the countering moment. This comparison underscores the importance of the osseous articulation and specific muscle groups, like the flexor carpi radialis, in minimizing UCL load. Such results support the idea that training programs emphasizing wrist extension and selective muscle activation may reduce the risk of UCL injury [12].

2.4 Areas of Improvement for Muscle-Driven Models

Given that this research is particularly interested in developing muscle-driven predictive models, only such models will be evaluated for areas of improvement. The key areas of improvement of the models mentioned in this chapter would be the use of a more accurate set of anthropometric, inertial, and musculotendon actuator parameters for MLB-type athletes. Moreover, this is the first work to use optimal control in addition to muscle dynamics, versus the previous work of Hubbard (no muscles) [13], Buffi (computed muscle controls, not optimal control) [11], and can der Pijl (static optimization, not optimal control) [12]. Most studies discussed relied on data from high-school or collegiate players, but professionals have more developed bodies and throw harder, making efforts to research these sorts of subjects very fruitful. An attempt to address these shortcoming will be done in this research.

Regarding forward dynamic analysis, most of the improvements that can be made come from an adjustment of parameters in muscle-driven approaches. In the work by Buffi et al. and van der Pijl, standard models with generic subjects were used [11]. Despite efforts to scale the models, the actuator sets were generally also defined using models representing the average male population. The abilities of elite pitchers exceed the abilities of most human

beings, and this will be reflected by updating the actuator sets used for muscle-driven forward dynamic models in this work.

Moreover, Buffi et al.'s work uses CMC to assess joint loading characteristics under a variety of actuator conditions, but in no way is this considered an 'optimal' throw, due to its reliance on kinematic data as input. This is also true for van der Pijl's model, which uses SO. This technique is highly dependent on kinematic and kinetic input data, which is used to estimate muscle forces and activations required to perform a motion. Optimal control and optimization techniques can be used to produce an ideal pitching motion, which maximizes throwing velocity, while also penalizing loading patterns. Although this was done by Fuji and Hubbard, the use of a torque-driven model meant that there was no consideration for the effect of optimal pitching mechanics on soft tissues, like the UCL or muscles, marking an opportunity for novelty that will be explored in this thesis [13].

Additionally, and arguably the most notable area of improvement for the muscle-driven models of Buffi et al. and van der Pijl, was the addition of varus-valgus DOF at the elbow, which were also actuated. Physiologically, there are no muscles that actively actuate the varus-valgus DOF at the elbow joint, nor is this DOF directly controllable. This was included to allow a torque balance of the elbow, permitting a simpler calculation of the UCL load, which will be presented in Chapter 5. However, literature suggests that the varus-valgus torque and DOF are primarily attributed to an undeseired reaction to the external rotation of the shoulder, which loads the medial elbow [20, 24, 28]. The forward dynamic model in this thesis will use the degree of shoulder rotation, which acts along the same axis of rotation of as the varus-valgus DOF in Buffi et al.'s model, to calculate the load on the UCL, instead of relying on an additional varus-valgus DOF.

Finally, another limitation in Buffi et al.'s work, is the absence of some key muscles, which were somewhat addressed by van der Pijl's model [11,12]. Buffi et al. omitted lateral elbow muscles and palmaris longus, in addition to many of the shoulder stabilizers [11]. It would be beneficial to expand on the anatomy of the throwing extremity, which is no easy task considering the fact that there are 52 muscles in the upper extremity and shoulder. Nonetheless, an effort will be made in this thesis to include additional throwing arm muscles, to see the effect they have on preserving the UCL, especially at the shoulder and elbow.

Overall, while Buffi et al.'s work was a huge step in forward dynamic modelling of baseball pitching, it is not entirely accurate to say that their work was predictive or even a forward dynamic approach, since it relied on kinematic/kinetic data as an input for tracking. The CMC algorithm used in Buffi et al. aims to fit muscle and actuator activation to generate joint trajectories that are dynamically consistent with an input of kinematic

data, which in this case, came from the inverse kinematic pre-processing step. Similarly, van der Pijl's simulations, which use SO, can not be called predictive, since this technique is highly dependent on kinematic and kinetic input data as well, which is used to estimate muscle forces and activations required to perform a motion. This implies that their work constituted an inverse dynamics problem, where motion was used to determine forces, but on a muscular/actuator level, versus a net joint level.

This thesis will use a novel technique to optimize the pitching motion, which will rely more on constraints and cost-function selection, than kinematic/kinetic inputs, in order to truly make a predictive model, providing insight into pitching mechanics that may go beyond what we expect from a traditional throw. Additionally, this research uses both optimal controls and muscle dynamics, making it unique compared to previous publication in this space [11–13].

Chapter 3

Inverse Kinematics

Prior to diving into the more detailed modelling work conducted in the inverse dynamic and forward dynamic chapters, an understanding of the general kinematics involved in a baseball pitch is necessary. Moreover, the kinematic data will serve as inputs into the other two modelling approaches. In this chapter, an overview of the kinematic data collection, format, pre-processing, skeletal modelling, and post-processing/data analysis will be discussed. Recall that inverse kinematics uses MoCap technology to track coordinates on the subject that can be used to replicate the collected motion virtually. The output of the kinematic analysis are the joint angles and velocities throughout the duration of the motion, and is a useful tool in assessing the implications of biomechanics on performance and injury.

3.1 Provided Kinematic Data

3.1.1 Data Collection

Recall that this research was conducted with a confidential organization in the MLB, who shared kinematic data with the Motion Research Group at the University of Waterloo. The data collected came from in game play of these pitchers, and only fastball throws were considered. Kinematic data of the fastball throws from 5 right-handed starting pitchers was collected throughout all the home games played during the 2022/2023 season (81 games). In total, data from 162 fastball pitches were shared, where pitchers one through five had 43, 27, 29, 39, and 24 unique throws, respectively. This was done using a KinaTrax

markerless MoCap system (KinaTrax, FLA, USA), which collects data at sampling rates of 300 Hz [36]. The KinaTrax system consists of a series of 8-16 high-speed Emergent Vision cameras (Emergent Vision Technologies Inc, BC, CAN), set up above and around the edges of the baseball field, with a central focal point at the pitching mound. A sample of the data collection system can be seen in Fig. 3.1.

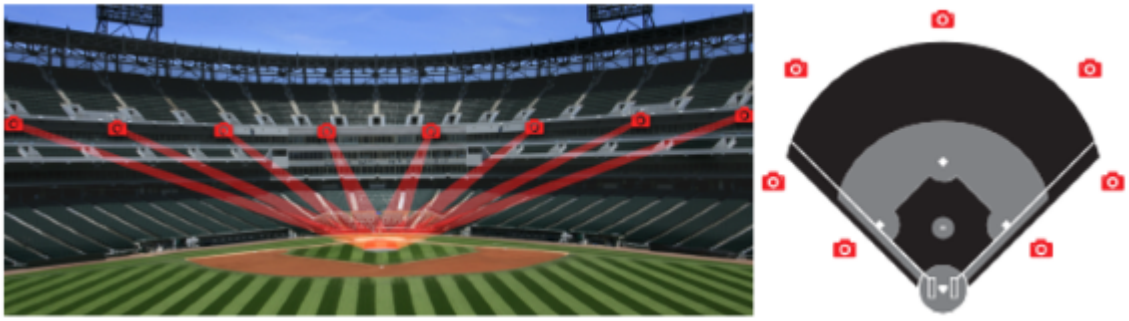


Figure 3.1: Sample in-game data collection and camera configuration utilized by the KinaTrax markerless MoCap system. Taken with permission from [36].

The KinaTrax system leverages markerless MoCap algorithms to track 25 points, corresponding to landmarks on the athlete's body, which ultimately outputs kinematic data on 16 segments. The KinaTrax algorithm automatically converts the landmark data to segment position and orientation, which will be discussed in detail in section 3.1.2. Ultimately, the kinematic data produces motion information for the head, neck, spine, pelvis and bilateral upper arms, forearms, hands, thighs, shins and feet, as seen in Fig. 3.2. This data was used to calculate joint angles and velocities incurred by the pitching motion. All the kinematic and dynamic analyses done in the next few chapters was done for a given pitcher, meaning that each reported metric was pitcher-specific. The results were compared across pitchers. There are some potential limitation is markerless MoCap systems. Accuracy can be compromised by factors such as camera resolution, occlusions, lighting conditions, and clothing, leading to errors in joint localization and segment tracking. Unlike marker-based systems, which rely on physical markers for precise anatomical calibration, markerless systems often infer joint centres from computer vision estimations, which may reduce reliability—especially during rapid or complex movements. Additionally, soft tissue artifacts cannot be easily distinguished from true joint motion.



Figure 3.2: Visualization of the markerless segment tracking capabilities of the KinaTrax system. Taken with permission from [36].

3.1.2 Data Format

Prior to being shared, the data was anonymized by representatives at KinaTrax to maintain confidentiality and protect the athletes' and participating organization's privacy. All 162 pitches were shared as a .csv file containing coordinates of body segments. The files contained the global transformation matrix for each tracked segment where every row of data corresponds to a video frame. The number of frames varied in each trial, since initiation and ending of MoCap was done manually, making the capture duration inconsistent. This was addressed in the pre-processing of the data. The global transformation matrix was formatted as a 4x4 3D rigid transformation matrix, provided in column-wise ordering. A rigid transformation matrix is composed of a standard 3x3 rotation matrix with an appended 3x1 translation vector as a fourth column. To make the matrix symmetrical, a 1x3 perspective transformation and 1x1 scaling vector is added to the fourth row, with all zero entries for the transformation columns and a 1 for the scaling column, indicating that no scaling or perspective transformation of the data is undergone. A sample rigid transfor-

mation matrix is shown in equation 3.1, where the top-left is the 3x3 rotation matrix (R), the top-right is the 3x1 translation vector (t), and the bottom row is the 1x3 perspective transformation and 1x1 scaling vector (0001).

$$\mathbf{T} = \begin{bmatrix} \mathbf{R} & \mathbf{t} \\ \mathbf{0}^{\mathsf{T}} & 1 \end{bmatrix} = \begin{bmatrix} r_{11} & r_{12} & r_{13} & t_x \\ r_{21} & r_{22} & r_{23} & t_y \\ r_{31} & r_{32} & r_{33} & t_z \\ 0 & 0 & 0 & 1 \end{bmatrix} \tag{3.1}$$

Besides reporting kinematics on the 16 segments, the data was organized to also have a hierarchical structure that used coordinates to provide further information about the articulation of different segment coordinates to form joints. It was structured so that a parent entry (joints) had child entries (segments). Parent segments with more than one child segment have zero-translation child segments termed 'Joint' segments. For example the 'Hips' joint has three child segments called 'JointSpine', 'JointLeftThigh', and 'JointRightThigh' each of which have segment lengths of zero. Moreover, the head end effector, has an orientation identical to the trunk. A total of 6 joints are used in the KinaTrax definition and although the joint coordinates were not used explicitly, this structure is useful for visualizing the data. In total, each kinematic dataset had 417 columns, pertaining to each entry of the rigid transformation matrix, for each segment and joint defined.

3.1.3 Data Pre-Processing

All of the pre and post-processing steps were conducted in MATLAB 2023b (The MathWorks, Inc, MA, USA) and the kinematic and dynamic work was mostly done in Visual3D (V3D) (HAS-Motion, ON, CAN). The kinematic data was first filtered to account for any extreme frequencies that made the data noisy. A fourth-order low-pass Butterworth filter with cutoff frequency of 10 Hz was used, as is the standard for highly dynamic human motion [37]. The *filtfilt* function was used for filtering as it performs zero-phase digital filtering by processing the input data in both the forward and reverse directions [38].

Next, the filtered kinematic data had to be resampled, since each set contained a different number of time steps, due to variation in the start and end time of the MoCap session. This was also done in MATLAB, and was based on various temporal milestones in the entire pitching motion. The determination of the pitching events will be discussed in detail in section 3.1.4, but in short, 10ms prior to maximum lead knee height and 10ms after BR was selected as a suitable duration to report kinematics and dynamics, since this encapsulates the crucial parts of the motion and is fairly standard in the literature

[8,39]. Taking data prior or after this capture sequence produced too much variation in the data, skewing the means and standard deviations of the reported analysis. The mechanics before and after times were also very pitcher-dependant and did not depict any important behaviours. Using V3D, the pitch events for each trial were extracted and identified in MATLAB, where all the data 10ms prior to maximum lead knee height and 10ms after BR was cropped out.

After that, the trial with the most number of remaining frames was marked, and the maximum number of frames was saved. This was done to take an up-sampling (interpolation) approach, instead of a down-sampling one, which could have omitted some interesting behaviours, due to the data lost with a down-sampling approach. All trials for a given pitcher were then resampled to contain the same number of frames as the trial with the greatest number of frames. The *resmaple* function was used in MATLAB, which interpolated the data to the new fixed rate (maximum number of frames identified) [38]. For each pitcher, the output of the pre-processing steps was a set of filtered, cropped, and resampled kinematics, which contained the same number of frames.

Resampling ensures temporal alignment across trials, which is critical for downstream comparisons and time-series analyses. However, this interpolation-based up-sampling can also introduce potential artifacts and smoothing effects that may not reflect true behaviour, especially during high-velocity motions such as pitching. Moreover, it assumes that the dynamics between sampled points follow a smooth progression, which may not be valid for all signals. As such, care was taken to interpret interpolated features in the context of the original sampling resolution and signal content.

3.1.4 Pitch Event Determination

Determining the crucial temporal events in the pitching sequence was essential to encapsulating the most important mechanics and visualizing the data. The selected steps were largely related to the pitching events seen in Fig. 2.1, and were also requested by the collaborating industry partner. The four crucial milestones were the time of maximum lead knee height during the windup, lead foot contact LFC during arm cocking, MER of the throwing shoulder during arm acceleration and finally, BR.

The V3D software was imperative to identifying each event, since it provided spatial data in addition to the kinematic data. To identify peak lead knee height, the instance of maximum vertical potion at the distal end of the leading thigh segment (knee) was noted for each trial and each pitcher. Next, the instance of LFC was noted as the time where the proximal end of the leading foot segment (heel) reached a vertical position of

zero, indicating that the heel had struck the ground. The instance of throwing shoulder MER, was determined using the built in inverse kinematic capabilities of the software, to be discussed in section 3.3.1, where the event was identified as the time of the peak value of shoulder external rotation. Finally, the moment of BR was a little more tricky to calculate, since the baseball is not part of the measured segment kinematics. To address this, a standard procedure used by the collaborating partner, as recommended by KinaTrax, was selected. The instance of BR for each trial was measured as 3 frames prior to the instance of peak throwing hand speed. More specifically, the instance was selected as 3 frames prior to the moment at which the distal hand segment (finger-tips) reach their peak speed.

Ultimately, these events were identified for each pitcher and trial, and was used to assist in the pre-processing of the data. The mean and standard deviation of the pitch event timings, for a respective pitcher, across all of their trials, was also calculated, and reported alongside the plots of the pitching kinematics, to provide more context into the timing of the joint trajectories. This was implemented in MATLAB as outlined in section 3.3.4.

3.2 Visual3D Skeletal Model

There is collaboration between Has-Motion, the developers of V3D, and KinaTrax, where KinaTrax developed an algorithm that integrates the MoCap data from their systems to automatically build a V3D skeletal model. The models built are unique to the subjects' innate geometry present in the collected data. As such, for the inverse kinematic and inverse dynamic research conducted in this thesis, the pre-developed skeletal model in V3D is used. The model making algorithm creates a unique model for each set of pitching data, and is pitcher-specific, meaning that all 5 subjects assessed in this thesis each had unique model geometries and parameters. Due to the research confidentiality agreements, pitcher-specific anthropometrics were not provided, meaning that many model parameters were consistent between subjects, but could not be validated. The detailed geometry, inertial properties, and anthropometrics of the model are not relevant to a kinematic analysis, and is more pertinent to the kinetic analysis, so those parameters will be discussed in section 4.1. Instead, this section will discuss the V3D modelling overview, methodology, and key definitions as they relate to an inverse kinematic analysis. Notably, the V3D software is used to extract joint trajectories and velocities, enabling an increased understanding on the mechanics of these elite pitchers.

3.2.1 Model Description

The V3D model consists of 15 different segments, including the head, combined thorax-abdomen, pelvis and bilateral hands, forearms, upper arms, thighs shanks, and feet. In V3D, segments are described as a rigid object defined geometrically by a local coordinate system (LCS) and a length [40]. The software assumes that the LCS is capable of moving in space, so there is an assumption that a sensor that tracks motion data is attached to the segment to follow this movement. As is the case in this research, the MoCap system tracks the position and orientation of the segments and V3D computes the pose (position and orientation) of the segment from the transformation between marker coordinates, segment coordinates, and joint constraints [40]. These segments are explicitly linked through the specification of inverse kinematic constraints, which will be discussed later in this section.

As it pertains to the KinaTrax system, its markerless nature implies that there are no body-fixed sensors to implicitly track the pose of the various segments. Instead, for these types of systems, V3D uses an algorithm to handle the rotation matrices needed to automatically build models, which for the dataset provided, was developed by KinaTrax [40]. In order to associate a model with a motion, a defined static trial and motion trial need to be imported. A static trial is a recording made with the subject stationary, and is useful for model building, while a motion trial is a recording of the subject moving through a prescribed sequence, which is the pitching motion in this case. Since the KinaTrax data is collected from in game play, there is no opportunity for the collection of a static trial. To address this, the algorithm developed by KinaTrax uses pose estimation and computer vision techniques to associate segments on the subject to digitized coordinates, relating to anatomical landmarks on the subject. These landmarks are then used to automatically build and scale the model, as if markers were placed on the pitcher. Using the segment data collected from markerless systems, the average location of all markers are determined using all frames of data, to predict accurate segment poses, since the markers needed to define the segments from a static calibration trial are unavailable.

A visualization of the skeletal model developed for pitcher 1 can be seen in Fig. 3.3, and includes important details such as joint definitions, model centre of mass (COM), and segment LCS. Note that the selection of LCS orientations and origins are made at the discretion of the model's creator, but generally follow the standards outlined by the International Society of Biomechanics, which is not the case in KinaTrax LCS definitions [41]. Note that Fig. 3.3 also denotes the neutral position of the model. This is essential when interpreting the kinematics in Appendix B and the results in section 3.4. Note that the starting position follows classic anatomical position, with the exception being that the shoulder neutral position is in 90 degrees of abduction.

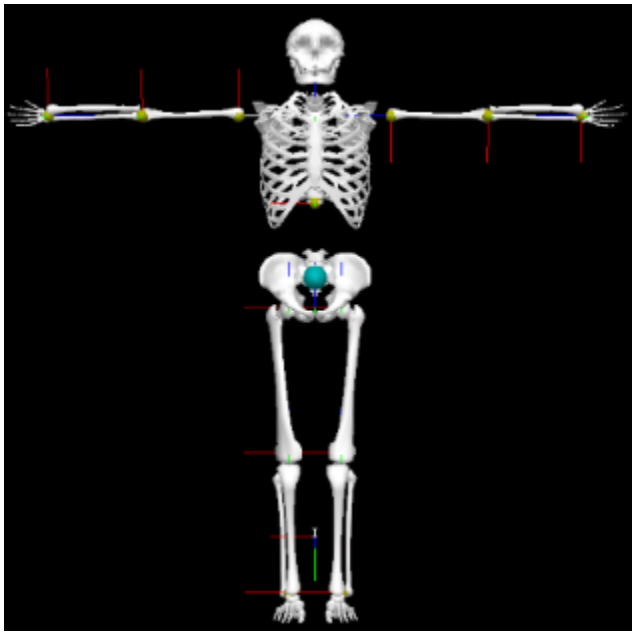


Figure 3.3: Visual3D model of pitcher 1, including all 15 segments. The red, green and blue lines protruding from a segment represent the x, y and z axes of the local coordinate systems, respectively. The yellow spheres represent joint definitions, based on the articulation of segments, but not all of them are visible, due to the segment geometries. In Visual3D, the origin of the local coordinate system is at the proximal end of the segment. The large blue sphere by the pelvis indicates the model's centre of mass.

In V3D, if two segments are in a close enough proximity (the distal end of one segment and the proximal end of another segment), they are linked and defined as a joint [40]. The proximity is defined by a joint radius model input, which by default is 0.95 cm, but was later changed for the inverse dynamic model, to 1.1 cm, which will be explained in section 4.1. The joint does not constrain the segments, but is a bookkeeping tool that keeps track of which segments have equal and opposite joint reaction forces and moments [40]. In this model, the joints included are those of the neck, pelvis-spine complex, and bilateral shoulder, elbow, wrist, hip, knee, and ankle joints. Notably, many joints contribute to the motion of the trunk relative to the pelvis, but has been simplified in this model. The term trunk will be used to refer to the collection of joints that permit this movement. Moreover, for the shoulder kinematics, contributions of the scapulothoracic joint is not considered and the clavicle, shoulder, trunk and scapula complex were lumped together into a single shoulder joint, as these are considered complex joints to model. This is a key V3D model

limitation. The definitions of the LCS in the model are important, as they indicate the direction of positive joint movements. Moreover the LCS help inform the definition of transformation matrices, which are used in conjunction with Euler sequences to extract joint kinematics. This will be discussed in detail in section 3.3.1.

An essential component of the model segment and joint definitions are the inverse kinematic constraints that govern the movement of the bodies. These constraints can be added between segments that restrict the relative motion between them [40]. Each of the 15 segments are constrained, relative to a parent segment, which relate to the permitted DOF. The pelvis is the only segment that has a complete 6 DOF, that permits rotation and translation in all 3 directions, relative to the ground. The remaining 14 segments are not permitted to translate freely, and are given 3 DOF, which are rotations relative to their parent segment. Even if a joint does not have 3 DOF in real life, like the elbow joints, this will be reflected in the kinematics as an insignificant amount of motion about that axes. Furthermore, there may also be discrepancies between defined axes and anatomical axes in addition to anatomical axes that can change throughout a motion, which can be accounted for by providing additional DOF than required. The reason it is not zero is because of limitations to MoCap, which always have some degree of marker tracking error. In general the parent segments are the more proximal adjacent segment. For example, the hands are only permitted to rotate against the forearms, where their translation is constrained to follow that of the forearms as well. Moreover, the upper arms have the thorax as the parent segment, which articulate at the shoulder joint, and the thighs have the pelvis as the parent segment, articulating at the hip joint. More notably, the thorax has the pelvis as the parent segment, articulating at the combined trunk joint. The pelvis is free to rotate and translate freely, with the ground frame as the parent segment. The pelvis is the root segment, meaning that all segments translate relative to the pelvis.

With the model segments, joints, inverse kinematic constraints, and LCS defined, the motion trials, captured from in game play, can be applied to the static trial model, through a link model routine [40]. The connection between the model and the movement trials comes from the digitized markers contained in the static trial model, where identical markers exist in both the static and motion trial. The output is an animation of the skeletal model, that replicates the movements captured by the MoCap systems. An example of an animation can be seen in Fig. 3.4. The completion of the model enables the use of inverse kinematic theories to extract relevant kinematic information.

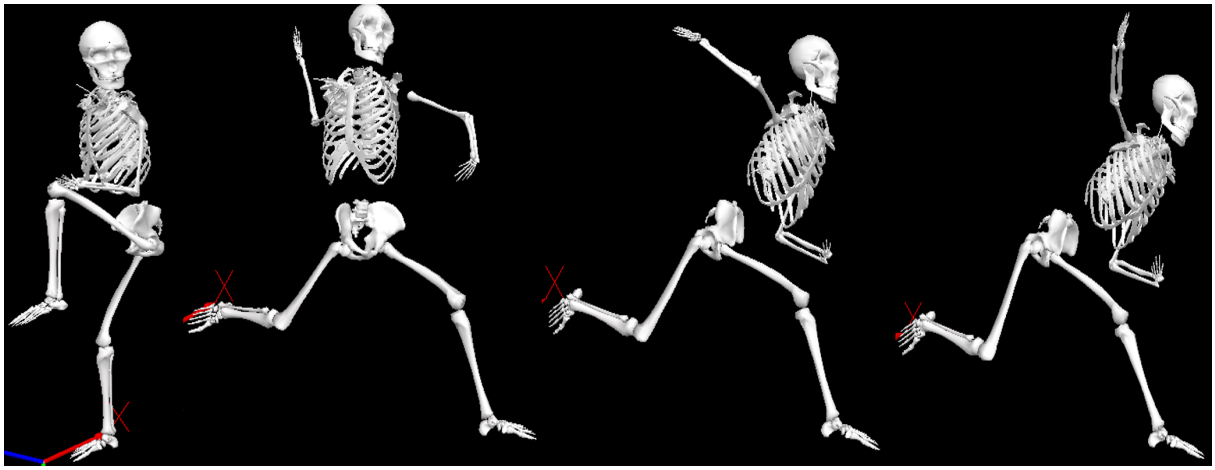


Figure 3.4: Visual3D animation of pitch number 1 of pitcher 1 throughout the four pitching events outlined in section 3.1.4. Each captured frame represents a sequence of the pitching events, extracted from a complete animation. From left to right, the events are the instance of peak lead knee height, LFC, maximum throwing shoulder external rotation, and ball release.

3.2.2 Selected Kinematics and Joint Movement Definitions

The LCS of each defined segment originated at the proximal end of the segment. These LCS were important for extracting the kinematics, as their orientations were used in the transformation matrices that yielded joint angles and velocities, in addition defining the positive directions of agonist and antagonist movements. Using the right-hand rule convention, a positive rotation was defined. For each LCS, a DOF could be assigned, which permits rotation about that axis. For example, in reference to Fig. 3.3, the x-axis (red) is protruding upwards (or superior) from the right wrist joint. Using the right-hand convention, the right thumb would point upwards in parallel with the x-axis, while the remaining fingers would curl inwards, towards the forearm. Thus, the positive action of the wrist correlating the motion of the hand towards the forearm would be wrist flexion. Right wrist flexion is considered to be a positive agonist rotation of the hand relative to the forearm, leaving wrist extension as the antagonist movement. This simple analysis was conducted for each axis, pertaining to all relevant DOF across all joints in the body.

One piece of novelty in this thesis is the number of kinematic variables studied. In previously referenced kinematic studies, an emphasis on shoulder and elbow kinematics is made, since these mostly contribute to ball velocity but also have the highest instances of

injury as well [14, 39]. However, considering the contributions of the trunk may provide some additional context and insight into performance indicators and injury risk in these athletes. As such, a diverse set of joint movements were investigated, for a total of 18 pairs of agonist and antagonist joint movements. A detailed account of the investigated kinematics, including the joints, segments, DOF, axis of rotation and, positive agonist/negative antagonist movements are summarized in Appendix A. These are based on the definitions of the LCS as seen in Fig. 3.3. Due to restrictions in content, only a select number of joint analyses were presented in this thesis.

3.3 Joint Kinematics Extraction Pipeline

With the model fully defined, a pipeline to extract the desired joint kinematics was established. In V3D a pipeline is a set of commands that are processed in sequence, which is particularly useful in cases like this, when large sets of data need to be analyzed in succession [40]. With 162 pitches to analyze across the 5 pitchers, the use of the pipeline functionality in V3D greatly increased productivity for both the inverse kinematic and subsequent inverse dynamic analyses. The pipeline was set up so that for a given pitcher, all collected pitches would be opened, and a loop would read each of the files pertaining to a given pitch. Then a subroutine called 'Compute Model Based Data' was used to extract joint angles and joint velocities. This subroutine computes a desired signal using a model's segments, kinematic, and kinetic data. It is reliant on the inverse kinematic chain that is outlined by the inverse kinematic constraints. This chain governs the motion of the model, by defining the relative motion between the segments, and this pipeline was run for all pitchers.

In V3D, an inverse kinematic analysis is the process of determining the parameters of a jointed flexible object (the kinematic chain defined by the kinematic constraints) in order to achieve a desired pose. The solution is dependent on the choice of hierarchical model because the task is to identify an articulated figure consisting of a set of rigid segments connected with joints. As such, there may be an infinite number of joint angle combinations to predict the pose at each time step, so the inverse kinematic analysis problem is solved as a global optimization problem, which computes the pose of a model that best matches the MoCap data in terms of a global criterion [40].

3.3.1 Visual3D Inverse Kinematics and Angle Calculations

To extract each joint angle, the angle was named, and a joint angle calculation was specified. Next the parent and child segments were specified, where the joint angle was taken as the angle between the distal segment (child) with respect to the proximal segment (parent). Finally, the XYZ Cardan sequence was selected to transform relative segment orientations to joint angles.

In V3D, a Joint Angle is the transformation between two coordinate systems that is described by a rotation matrix [40]. The rotation matrix in this case is a Cardan sequence, also known as an Euler angle, which defines an order of rotations, following the right-hand rule convention. This sequence refers to a specific order of rotations about the axes of a coordinate system that is attached to a moving body. These rotations are used to describe the orientation of the body in three-dimensional space. All representations of the transformation are equivalent but the interpretation of the joint angle relative to the anatomy varies with the description. This research used the XYZ Cardan sequence (body-fixed 1-2-3 Euler angles), which generally pertains to flexion/extension (X), abduction/adduction (Y) and axial rotation (Z) of joints.

To calculate joint angles, V3D uses the pose of each segment that spans that joint, with the LCS definitions of the model. The data provided by the collaborators consisted of segment transformation matrices. V3D extracts the rotational matrix components of adjacent segments that span the desired joint, and uses matrix operations to relate the orientation of one segment to another, which is called a rotation matrix. With the relative orientation of the two segments spanning a joint known, it can decompose the relative rotation matrices into joint angles using the selected Cardan sequence. This process was used for all specified joint angles and conducted on each pitch for a given pitcher. The output of this process is a series of joint angles (with angles along x, y and, z axes) at each time step, which when considered altogether, provides the joint trajectories over the duration of the pitch. The pipeline ended by exporting all the joint angles and velocities, which will be covered in section 3.3.3, into MATLAB compatible files for post-processing and reporting.

3.3.2 Cardan Sequence Selection

Choosing the correct Cardan sequence to describe joint angles is crucial for accurately representing the orientation and motion of body segments. The choice depends on the specific joint and the type of movement being analyzed. Ultimately, this research relied on the use

of an XYZ rotation, as the X rotation corresponds to flexion-extension movements, which is present in all joint kinematics being studied (See Appendix A). However, joints with many DOF, like the knee and hip, may be problematic under the XYZ Cardan sequence, since they experience a significant rotation along all axes. This is particularly true in baseball, where the shoulder undergoes significant rotation and abduction, in addition to flexion.

As such, a sensitivity study was conducted on the kinematic outputs of the shoulder, using a series of different Cardan sequences. The sequences examined were XYZ, ZYX and YXZ. The joint velocities and angles were extracted from the shoulder using each of these Cardan sequences and the trajectories and magnitudes were compared to one another. Interestingly, the YXZ Cardan sequence produced unphysical shoulder joint trajectories and was discounted. When comparing the XYZ and ZYX Cardan sequences, both shared very similar trajectories and angular magnitudes. However, the ZYX sequence displayed peak velocity magnitudes of internal and external rotation about 13% smaller than the XYZ sequence results. This discrepancy may be attributed to the rotation order in the ZYX sequence, which projects angular velocity components differently than XYZ, resulting in a reduced contribution to the internal/external rotation axis during shoulder motion. Upon comparing the results to literature, it was clear that the reported magnitudes for the XYZ sequence were closer to previous studies, compared to the ZYX sequence, and as such, the XYZ Cardan sequence was selected for the shoulder [39]. This also maintained consistency throughout the inverse kinematic analysis, since all joint kinematics were extracted using this XYZ Cardan sequence.

3.3.3 Visual3D Differentiation Methodology and Joint Velocities

Similar to the joint angle calculations, joint velocity kinematics used a virtually identical pipeline, including the XYZ Cardan sequence, the only difference being that a joint velocity calculation was specified. To calculate joint angular velocities, V3D using a second-order finite difference algorithm based on a central difference method [40]. This algorithm is a numerical method that approximates the derivative of position data with respect to time. In layman terms, given a set of position data at discrete time intervals, the velocity can be approximated by the difference in position divided by the difference in time. This is done at each time step, beginning at the second frame, to produce a time series of velocity. This process is also used to calculate the second derivative of joint angles, angular accelerations, which are important in the inverse dynamic analysis in Chapter 4.

The only velocity kinematics reported in this research are that of the throwing shoulder and elbow, where the rotational velocity of the shoulder and the flexion/extension angular

velocities of the elbow are considered, since these have the largest implications on UCL injuries [25, 39].

3.3.4 Post-Processing and Kinematic Visualization Pipeline

With the joint angles and angular velocities extracted from V3D, they were uploaded into MATLAB, for post-processing and visualization. The kinematics were already filtered, trimmed, and resampled in the pre-processing steps, meaning that each dataset had the same number of frames, so visualization was the next step. For each pitcher, an independent analysis was done. Each joint angle or velocity kinematic measure for all pitches for a given pitcher were concatenated and the mean and standard deviation at each time step of the selected measure was found. The output was a matrix consisting of the mean joint angle or velocity and its associated time step, which was then plotted in MATLAB.

The time steps were then normalized to a percentage of the total motion time, which as mentioned in section 3.1.3, was approximately 10 ms prior to maximum lead knee height and 10 ms post BR. The standard deviations were reported to show the within-pitcher variation in throwing mechanics. The pitch event timings, which had means and deviations also calculated in the same way, were also normalized as a percentage of the total motion, and vertical lines representing their mean occurrence for a given pitcher were added to the plots. The standard deviations of the temporal pitch event sequences were also reported. Positive agonist and negative antagonist movements were also highlighted in the figure title. An example of the format used to visualize the kinematics can be seen in Fig. 3.5.

3.4 Kinematic Results

This section will review the results of the inverse kinematic analysis, and discuss some of the major observations. Notably, kinematic variations between the 5 pitchers will be discussed and compared to literature, in addition to investigating contributions of the trunk to throwing velocity. This chapter will end by highlighting some of the kinematic factors that may contribute to increased performance or injury risk in the subjects analyzed. Due to difficulties in validating the raw KinaTrax motion data, and associated MSK model in V3D (see section 4.7), an effort will be made to compare similarities and differences across the five pitchers, as opposed to looking at trajectories and magnitudes independently. This approach will aim to eliminate any bias that may be present in the model by assessing the

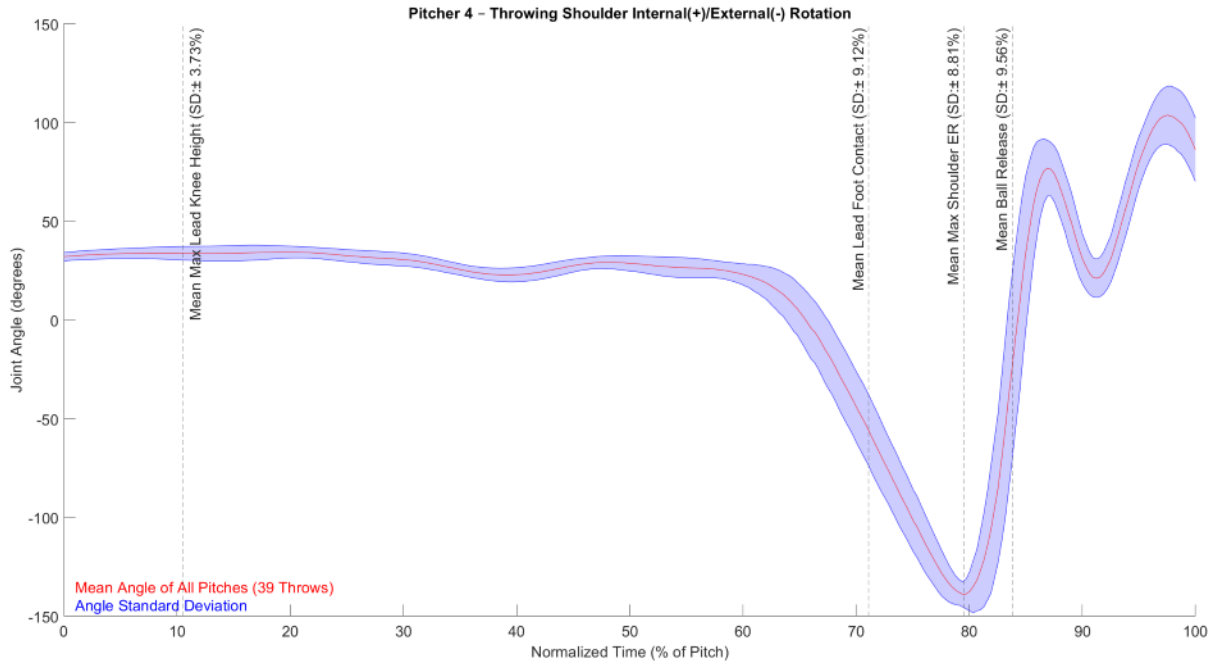


Figure 3.5: An example of the formatting used to display the kinematics collected. In this figure, throwing shoulder internal/external rotation, around 10ms prior to peak lead knee height and 10ms post ball release, is shown for pitcher . The time was normalized as a percentage of the total time. The red line represents the mean value of the kinematic parameter over time, while the blue line and shading represents the standard deviation at that time step. Pitch events are also noted as vertical lines, which includes their standard deviations as well.

results of each pitcher against the other pitchers, who will have the same hypothetical model errors present in their results. However, in order to demonstrate the efficacy of the model, it is also necessary to compare the absolute kinematic values to experiments conducted in literature, so there will be some comments on this as well.

As a reminder, this study extracted a total of 18 pairs of agonist and antagonist joint movements during the inverse kinematic study, but will not be elaborating on all of these for the sake of brevity. As such, the kinematics that will be emphasized here are related to those of the throwing (right) shoulder, elbow and trunk. These were selected since they are correlated with throwing velocity and can also provide insight into potential injury risks for the UCL. The selected kinematics were the throwing shoulder abduction/adduction and internal/external rotation angles, throwing elbow flexion/extension angles and velocities,

and trunk ipsilateral/contralateral tilt plus anterior/posterior tilt angles. Joint kinematic trajectories for all five pitchers is attached in Appendix B. Furthermore, an emphasis on the portions of the pitch between LFC and BR will be made, as this is the most dynamic portion of the pitch.

3.4.1 Joint Trajectories and Velocities

Table 3.1 highlights the joint kinematics of interest across all 5 pitchers from Appendix B, during key and highly dynamic phases of the pitch. Differences across pitchers indicate the variability in pitching mechanics and the significance of differences in magnitudes across pitchers and motions varies by DOF and ROM.

The progression of trunk contralateral tilt followed a consistent trend across all pitchers, with a decline from contralateral dominance at LFC toward a neutral or ipsilateral position at BR. For instance, Pitcher 1 displayed a sharp decline from 15° at LFC to -5° at BR, indicating a pronounced stabilization phase. In contrast, Pitcher 2 exhibited a more subdued trajectory, with contralateral tilt starting at 12° and gradually transitioning to 0° at BR, reflecting a conservative trunk stabilization strategy. Pitcher 4's trajectory mirrored that of Pitcher 1, albeit with a more abrupt shift to ipsilateral tilt, suggesting an aggressive rotational strategy.

Trunk posterior tilt similarly transitioned from a slight posterior lean at LFC to an anterior tilt at BR, reflecting trunk engagement strategies to drive energy transfer. Pitcher 1 progressed from 5° of posterior tilt at LFC to 13° of anterior tilt at BR, representing efficient kinetic chain utilization. In contrast, Pitcher 5 maintained a more upright trunk throughout, with anterior tilt peaking at only 8° by BR, potentially indicating a biomechanical preference for reduced trunk involvement or an adaptation to mitigate lumbar stress.

Shoulder adduction followed a consistent pattern, increasing from LFC to MER before transitioning to abduction at BR. Pitcher 3 displayed the largest range, shifting from -60° at LFC to -75° at BR, highlighting a robust loading and unloading phase. Conversely, Pitcher 5 exhibited a smaller range, moving from -58° to -70°, suggesting a less aggressive adduction-abduction dynamic. This could reflect differences in arm slot mechanics or shoulder flexibility.

As defined, shoulder external rotation peaked consistently at the MER across all pitchers, aligning well with the timing of energy storage during the cocking phase. Pitcher 1 achieved a peak external rotation of -160°, reflecting excellent shoulder flexibility and potential for high velocity. However, this extreme range may impose increased stress on

Table 3.1: Kinematic metrics for five pitchers across three key phases of the pitching motion: LFC, MER, and BR. Positive values indicate the primary direction of movement, while negative values indicate antagonist motion.

Pitcher	Kinematics	Lead Foot Contact	Maximum External Rotation	Ball Release
1	Trunk Contralateral Tilt (+)	15°	3°	-5°
	Trunk Posterior Tilt (+)	5°	15°	13°
	Shoulder Adduction (+)	-60°	-65°	-75°
	Shoulder Internal Rotation (+)	-120°	-150°	-75°
	Elbow Flexion (+)	110°	90°	40°
	Elbow Flexion Velocity (+)	400°/s	10°/s	-1000°/s
2	Trunk Contralateral Tilt (+)	10°	6°	5°
	Trunk Posterior Tilt (+)	5°	13°	12°
	Shoulder Adduction (+)	-50°	-30°	-40°
	Shoulder Internal Rotation (+)	-75°	-125°	-25°
	Elbow Flexion (+)	80°	110°	100°
	Elbow Flexion Velocity (+)	-250°/s	-300°/s	-1250°/s
3	Trunk Contralateral Tilt (+)	20°	10°	3°
	Trunk Posterior Tilt (+)	-4°	-1°	10°
	Shoulder Adduction (+)	-66°	-60°	-58°
	Shoulder Internal Rotation (+)	-100°	-140°	-75°
	Elbow Flexion (+)	40°	72°	80°
	Elbow Flexion Velocity (+)	25°/s	-1100°/s	-1400°/s
4	Trunk Contralateral Tilt (+)	5°	7°	13°
	Trunk Posterior Tilt (+)	-3°	-2°	5°
	Shoulder Adduction (+)	-60°	-63°	-70°
	Shoulder Internal Rotation (+)	-55°	-145°	-35°
	Elbow Flexion (+)	100°	118°	116°
	Elbow Flexion Velocity (+)	-200°/s	-1100°/s	-1200°/s
5	Trunk Contralateral Tilt (+)	15°	18°	12°
	Trunk Posterior Tilt (+)	2°	5°	9°
	Shoulder Adduction (+)	-45°	-52°	-68°
	Shoulder Internal Rotation (+)	-100°	-145°	-70°
	Elbow Flexion (+)	85°	95°	90°
	Elbow Flexion Velocity (+)	-100°/s	-350°/s	-1350°/s

the shoulder joint. Pitcher 2, by contrast, reached a more modest peak of -150°, indicating a more conservative external rotation strategy. The transition from external to internal rotation occurred rapidly between MER and BR for all pitchers, with Pitcher 4 showing the fastest shift, from -165° to -75°, emphasizing explosive rotational mechanics which could lead to faster ball speeds. Ball speeds for a given set of pitching data were not provided, meaning that commentary on the impacts of the mechanics on pitching performance are difficult to make

The elbow consistently progressed from flexion at LFC to extension at BR, with the

peak extension velocity occurring just before BR across all pitchers. For example, Pitcher 3 transitioned from 110° at LFC to 35° at BR, with a sharp acceleration in extension velocity near BR, indicative of a quick energy release phase. Pitcher 5, in comparison, moved more gradually, reducing flexion from 108° at LFC to 40° at BR, suggesting a smoother and potentially less stressful motion, likely at the cost of faster ball speeds.

Interestingly, Pitcher 4 displayed the most abrupt change in flexion, decreasing from 115° at LFC to 30° at BR. This aggressive transition might contribute to higher ball velocity but also increases stress on the UCL. In contrast, Pitcher 2 maintained the most gradual elbow flexion-extension trajectory, reflecting a controlled and potentially injury-mitigating motion.

Across all pitchers, a few trends were universally observed. The elbow transitioned from flexion to extension between MER and BR, with peak extension velocity closely preceding BR. Trunk contralateral tilt progressed from contralateral dominance at LFC toward neutral or ipsilateral tilt at BR, a hallmark of coordinated trunk stabilization. These trends highlight the biomechanical uniformity required for effective pitching mechanics.

Key outliers provide further insights. Pitcher 1 displayed the largest external rotation and contralateral tilt magnitudes, emphasizing a high-speed strategy but potentially increasing joint stress. Pitcher 5, by contrast, maintained a more upright trunk and smaller shoulder adduction range, reflecting a biomechanical adaptation for efficiency over maximal torque. Pitcher 4's abrupt elbow and shoulder transitions underline an aggressive energy transfer strategy, possibly prioritizing velocity over longevity.

3.4.2 Discussion and Comparison of Kinematics Across Pitchers

The kinematic analysis of the five pitchers reveals key insights into the mechanics of elite-level pitching. These findings not only highlight the unique kinematics of each pitcher, but also emphasize the validity of the pitch phase extraction algorithm. Furthermore, it provides a detailed understanding of individual variability and repeatability.

One notable outlier in the data is Pitcher 2, whose kinematic trajectories exhibit irregularities likely attributed to tracking errors. This may result from a tucked arm position during the delivery, complicating the segmentation and tracking of the arm and trunk by the MoCap system. Such challenges are particularly evident in the shoulder and elbow trajectories, where deviations from expected patterns arise. Interestingly, the data for Pitcher 2's external rotation trajectory suggests two distinct instances of MER, as seen in Appendix B, Fig. B.2. While such errors highlight limitations in tracking tucked or

occluded segments, they also underscore the robustness of the data across other pitchers, where MER was consistently observed without such issues.

A critical observation across all pitchers is the alignment of the MER phase with the peak magnitude of shoulder external rotation. The pre and post processing of the raw data could have potentially led to misalignment between the key pitching phases identified from the raw joint angles and the final processed plots. Specifically, when up-sompling the data, the data quality may have been compromised. This consistency is reassuring when considering the validity of the pitch phase extraction algorithm. Peak external rotation is a biomechanical marker for the transition from energy storage to energy transfer in the pitching motion, and its synchronization with the MER phase underscores the reliability of phase identification. This alignment reduces concerns of temporal misclassification, strengthening the algorithm's applicability in future studies. Moreover, the temporal alignment of MER with other kinematic events, such as the peak in elbow flexion velocity and the initiation of trunk stabilization, further validates the extracted pitch phases. These consistent patterns reinforce the utility of the algorithm in analyzing pitching biomechanics at a high level of temporal precision.

The trajectories of kinematic variables reveal several similarities and differences across pitchers. Consistent trends include: the progression of trunk contralateral tilt, which decreases steadily from LFC to MER and neutrality near BR, the transition from shoulder external rotation at MER to rapid internal rotation approaching BR, and the shift from elbow flexion at LFC to extension at BR, with peak extension velocity occurring immediately before release. These results follow a similar trajectory to those outlined by Fleisig et al. [7] and Pappas et al. [8].

Despite these similarities, individual differences highlight unique mechanics. Pitcher 3 exhibits the highest contralateral tilt at LFC (20°), reflecting a pronounced lateral trunk strategy for torque generation, while Pitcher 4 maintains a more conservative tilt throughout. Additionally, the range of shoulder adduction varies significantly, with Pitcher 1 displaying the largest change (-60° to -75°) and Pitcher 5 the smallest (-45° to -68°). These differences suggest variation in arm slots and influences of the trunk, which may influence pitch type and velocity.

The tight standard deviations observed across most kinematic variables highlight the exceptional repeatability of elite-level pitchers. This consistency underscores their ability to execute precise, repeatable mechanics, a hallmark of high performance. For example, the trunk and shoulder kinematics exhibited minimal variability, suggesting refined motor control and mechanical efficiency. However, greater variability was noted in wrist flexion and forearm pronation/supination (not shown), which are difficult to track. This could

stem tracking errors in the MoCap systems. Despite this variability, the broader kinematic repeatability is consistent with findings from previous studies, which emphasize the high level of mechanical precision required for elite pitching [7, 8].

The abduction angles measured in this study provide a detailed view of arm slot variations across pitchers, emphasizing how trunk and shoulder mechanics interact to shape individual pitching styles. As a reminder, the model defines the shoulder's neutral position as 90° of abduction relative to the torso, rather than the ground. This approach, consistent with the conventions of V3D software, highlights the interplay between shoulder and trunk mechanics. Traditionally, arm slot is measured with respect to the ground, but this completely ignores the effect of the trunk to the slot. By considering the torso as the reference frame, the analysis captures how trunk contralateral tilt influences arm slot adjustments during the pitch, particularly at BR. In this convention, -90° represents the neutral anatomical position, while values less than -90° reflect slight arm adduction relative to the neutral position, and values greater than -90° indicate increased abduction.

For example, Pitcher 1, with an adduction angle of -75° at BR, exhibits a slightly adducted arm relative to the neutral position. This suggests a more sidearm throw, consistent with a delivery style prioritizing velocity. The ipsilateral trunk tilt of 5° at release supports this strategy, indicating a stable trunk position that aligns the arm slot for optimized energy transfer. This combination of slightly adducted arm and minimal ipsilateral tilt suggests a more sidearm delivery.

The traditional interpretation of shoulder abduction angles in isolation can lead to an oversimplified classification of pitching deliveries, which in this study, would suggest that all pitchers employ a sidearm delivery. However, animated visual inspection of the throws reveals that only Pitcher 1 demonstrates a trend towards a sidearm arm slot, which can be attributed to limited trunk involvement (ipsilateral tilt at BR). In contrast, Pitchers 2 through 5 exhibit varying degrees of contralateral trunk tilt at BR, which influences the orientation of the throwing arm, explaining why they all have overhead deliveries. This trunk contribution alters the effective arm slot, resulting in deliveries that are more overhead than their shoulder abduction angles alone would indicate. For example, Pitcher 4, despite exhibiting the smallest shoulder abduction angle at BR, demonstrates the greatest degree of contralateral trunk tilt. This combination, when visualized dynamically, results in a distinctly overhead arm slot. These observations underscore the critical interplay between shoulder abduction and trunk mechanics in shaping arm slot, highlighting the adaptability of pitchers to optimize their mechanics for individual styles and pitch demands. Such dynamic adjustments facilitate efficient energy transfer and the achievement of desired pitch profiles. These findings underscore the importance of redefining the concept of arm slot to encompass both proximal (trunk) and distal (shoulder) mechanics, rather than relying

solely on shoulder abduction relative to the ground, as previously published by Escamilla et al. [42]. A more integrative framework for defining arm slot is essential to accurately capture the biomechanical complexity of pitching. This refined perspective not only enhances the understanding of pitching mechanics but also provides valuable insights for optimizing performance and mitigating injury risk.

To assess the validity of the inverse kinematic MSK model and the subsequent results, it is necessary to evaluate the kinematics against experimental data in literature. Most publications list a mean value across all of their participants, so the same is done here and shown in Table 3.2. The kinematic values presented in this study reveal distinct trends in trunk tilt, shoulder kinematics, and elbow mechanics across the critical phases of the pitching motion. These values are compared against established findings in the literature, particularly those reported by Fortenbaugh et al. [43] and Fleisig et al. [44].

Table 3.2: Comparison of Mean Kinematic Values Across Studies

Kinematics	**Phase**	**This Study (Mean)**	**Fortenbaugh et al.**	**Fleisig et al.**
Trunk Contralateral Tilt (+)	Foot Contact	13°	10°	6°
	Max Ext. Rotation	8.8°	–	–
	Ball Release	5.6°	36°	25°
Trunk Posterior Tilt (+)	Foot Contact	1°	–	–
	Max Ext. Rotation	6°	–	–
	Ball Release	9.8°	26°	34°
Shoulder Adduction (+)	Foot Contact	-56.2°	-90	-96°
	Max Ext. Rotation	-54°	–	–
	Ball Release	-62.2°	-90°	- 88 °
Shoulder Internal Rotation (+)	Foot Contact	-90°	-68°	-53°
	Max Ext. Rotation	-141°	-180°	-174 °
	Ball Release	-56°	–	–
Elbow Flexion (+)	Foot Contact	83°	–	78°
	Max Ext. Rotation	97°	–	101 °
	Ball Release	85.2°	90°	–
Elbow Flexion Velocity (+)	Foot Contact	-25°/s	–	–
	Max Ext. Rotation	-568°/s	–	–
	Ball Release	-1240°/s	-2210°	-2480°/s

The current study reports mean trunk contralateral tilt values of 13°, 8.8°, and 5.6° at LFC, MER, and BR, respectively. These values are not entirely consistent with those reported by Fortenbaugh et al. [43], who highlighted the importance of trunk tilt at BR, identifying an optimal tilt of approximately 36° for high-velocity pitches at release. The discrepancy in magnitude, particularly at BR, may be attributed to differences in pitching level, as this study involves professional pitchers, while Fortenbaugh et al. analyzed collegiate athletes. Moreover, differences in the experimental procedures and methods could

also explain the differences.

Mean shoulder adduction in this study was measured at -56.2°, -54°, and -62.2° across the three phases was compare with Fleisig et al. [44], who reported adduction values near -90° at LFC and BR. The negative values indicate that the shoulder was abducted. Shoulder internal rotation was recorded at -90°, -141°, and -56° during LFC, MER, and BR, respectively. These values are somewhat comparable to Fleisig et al.'s findings, particularly during MER, where the reported external rotation exceeded 174° for collegiate pitchers during MER. Differences may persist due to differences in data collection, MoCap sensor errors, and modelling decisions.

Mean elbow flexion values in this study increased from 83° at LFC to 97° at MER before decreasing slightly to 85.2° at BR. These trends align with Fleisig et al. [44], who observed similar flexion profiles in collegiate pitchers, with maximum values occurring near MER. Notably, elbow extension velocity reached an average of 1240°/s at BR in this study, lower than the velocities of 2480°/s reported by Fleisig et al. This discrepancy may be due to differences in motion capture sampling frequency, the level of athletic performance in the participant pool, and the order of numerical differentiation and filtering procedures applied to joint angle data. Given the sensitivity of angular velocity calculations to noise and frame rate, particularly near ball release, conservative filtering or lower sample rates may misestimate true peak extension velocities.

Overall, the trends observed in this study are not entirely cohesive with those reported by Fortenbaugh et al. [43] and Fleisig et al. [44]. The magnitudes of the kinematic variables, particularly trunk tilt and elbow flexion velocity, differ significantly. While the magnitudes differed greatly for those particular studies, the trends in table 3.2 as the pitching phases of interest progress (LFC to MER to BR) were quite comparable across kinematic motions. These differences may largely be attributed to differences in skill in the sample populations. Additionally, variations in modelling methodology and instrumentation may contribute to the observed discrepancies, in addition to different modelling decisions. For example, in this study, each model was scaled to the proportions of an MLB starting pitcher, but that may not be reflective of the actual sample population, since that data was not provided, resulting in inconsistencies in the model and kinematics inputs. Future studies should aim to include a more diverse sample to better contextualize kinematic differences across skill levels and pitching phases. With this in mind, the weak alignment with literature indicated a need for more work to evaluate and validate the models and results from V3D, which will be further investigated in section 4.7.

Chapter 4

Inverse Dynamics

This chapter investigated the inverse dynamics of the skeletal model outlined in the inverse kinematics chapter (see Chapter 3). The net forces and torques experienced by the pitching subjects during their fastball throws were discussed, specifically at the elbow and shoulder. To do so, the model was first revised to represent the subject's proportions and overall dynamics. This included the addition of a ball model and kinematic constraints that govern the model's movements. Special attention was made to the external forces present in the skeletal model, and the use of the top-down inverse dynamic methodology. Post-processing of the results produced plots of joint forces and moments throughout the pitching motion and pitcher-specific conclusions were made. These insights were used to assess potential causes of injury at the joints of interest, in addition to explaining how velocity was generated through throwing kinetics. Finally, two sensitivity studies were completed to assess the validity and accuracy of the inverse dynamic model. The first evaluated the modified hand-ball complex, where the ball was added, providing additional outlook on the implications of gripping techniques and the use of weighted balls on joint forces. The second investigated the effects on speeding up and slowing down the pitching kinematics, by a fixed rate, to assess the impacts on the measured kinetics, providing further insight into the model's behaviour.

4.1 Revised Visual3D Skeletal Model

The goal of inverse dynamics is to reconstruct the internal forces and moments of a motion from known movement and external forces [29]. Moreover, it is important to design an inverse dynamic model with parameters specific to the subject it aims to replicate.

An accurate model requires realistic anthropometric and mass properties, to ensure that the model is dynamically-consistent with all external forces. When inconsistencies between model properties, kinematics, and external forces are present, an inverse dynamics analysis will produce unphysical kinetics. The reliance on external forces in an inverse dynamic analysis means that outputted net joint kinetics are very sensitive to the segment inertial definitions. For the skeletal inverse dynamic models used in this research, an accurate model consists of detailed anthropometrics and inertial properties, including segment masses, segment lengths, segment COM location, and principal moments of inertia [29]. This will be outlined in subsequent sections. It is important to note that due to the confidentiality agreement, limited information is shared regarding the geometric properties of all pitchers involved. External GRF are also unavailable, due to the fact that the data was collected in game, on a sensor-less mound. This means that the developed skeletal models are not entirely dynamically-consistent, which must be considered when assessing the results. All pre-processing of the raw kinematic data used to develop the inverse dynamic model is the same as that outlined in section 3.1.3.

4.1.1 Model Anthropometrics and Inertial Properties

The default model used to develop the inverse dynamic skeletal model is identical to that outlined in section 3.2, and is still pitcher-specific. All updates to the model were applied to each of the 5 pitching models, ensuring consistency when comparing results. Between all 5 pitchers, the key differences come in the segment lengths. When interfacing the KinaTrax kinematic data to V3D, a pre-built inverse kinematic algorithm, which is innate to the KinaTrax data files, estimates the segment lengths. This is done by tracking the distance between the annotated marker-less MoCap data points, used to define the proximal and distal ends of a segment. All subsequent model changes made were generalized and applied identically in all models. This was also done for the inverse kinematic analyses by default, since they were also using KinaTrax source files. It was not mentioned in Ch. 3, since inverse kinematic analyses are not reliant on segmental anthropometry, mass, and geometry, whereas inverse dynamic analyses are.

For a given segment, the mass (represented as a percentage of total mass), COM location, and inertial properties were taken from de Levas modified experimental measures of Zatsiorsky et al.'s 1990 publication [45]. The next parameter that was changed was the subject's height and weight. These were updated to represent the average MLB starting pitcher weight and height [46]. Each model was assigned a height and weight of 192.31 cm and 97.52 kg or around 6'3" and 215 lbs, respectively. An effort was made to check that

the sum of segment lengths was consistent with the prescribed height, where each model was within 0.05 m of the prescribed height.

4.1.2 Ball Model and External Forces

The reliance of inverse dynamic analysis on external forces means that all external forces present in the motion should be captured by the model. Since no GRF are provided, the only external forces present in this model are those due to gravity acting on the body/segments. That is why the correct definitions of the segments' inertial parameters are so important. However, there is an additional source of gravity that is not encapsulated by the skeletal model, which would be the baseball. To address this, an additional solid sphere, connected to the throwing hand was added, to represent the baseball.

To add the baseball, a floating landmark, extending anteriorly by the radius of a regulation MLB baseball, was added from the longitudinal base of the third metacarpal of the throwing hand. In V3D a landmark is a virtual marker, whose position is computed automatically based on references to actual markers, those being the markers of the hand in this case [40]. The ball was rigidly connected to the hand, via the landmark, by prescribing kinematic constraints, which did not permit the ball to have any DOF with respect to the hand. The radius of the ball was set to be 36.44 mm with a weight of 0.145 kg, which is consistent with a regulation MLB baseball [47]. The COM of the ball is located at ball centre and is defined to originate at the floating landmark. The ball was assigned principal moments of inertia, by using the equations for inertia across the centre of a solid sphere (7.68e-05 kg m^2). Finally, the geometry of the ball was visualized as a sphere, using a file that is included in the V3D installation package. The implementation of the ball, which includes all revisions mentioned in section 4.1.1, can be seen in Fig. 4.1.

The addition of the ball may introduce some unexpected behaviours and kinetics. Rigidly connecting the ball to the hand may be problematic, since in reality, the ball is an independent entity after ball release. This is especially exacerbated when using a top-down inverse dynamic analysis, which will be discussed in section 4.2. As such, the effect of the interface of the ball and the hand will be investigated in a sensitivity study in section 4.5, by examining how the kinetics change as the weight of the ball deviates from the regulation mass, in addition to the effects as the position of the ball moves away from the base of the third metacarpal. Not only will this provide insight into the validity of the ball implementation into the model, but it can also express the correlation between grip mechanics/ball placement to elbow kinetics and UCL injuries.

As mentioned in section 3.2.1, the joint radius parameter of all joints was changed from

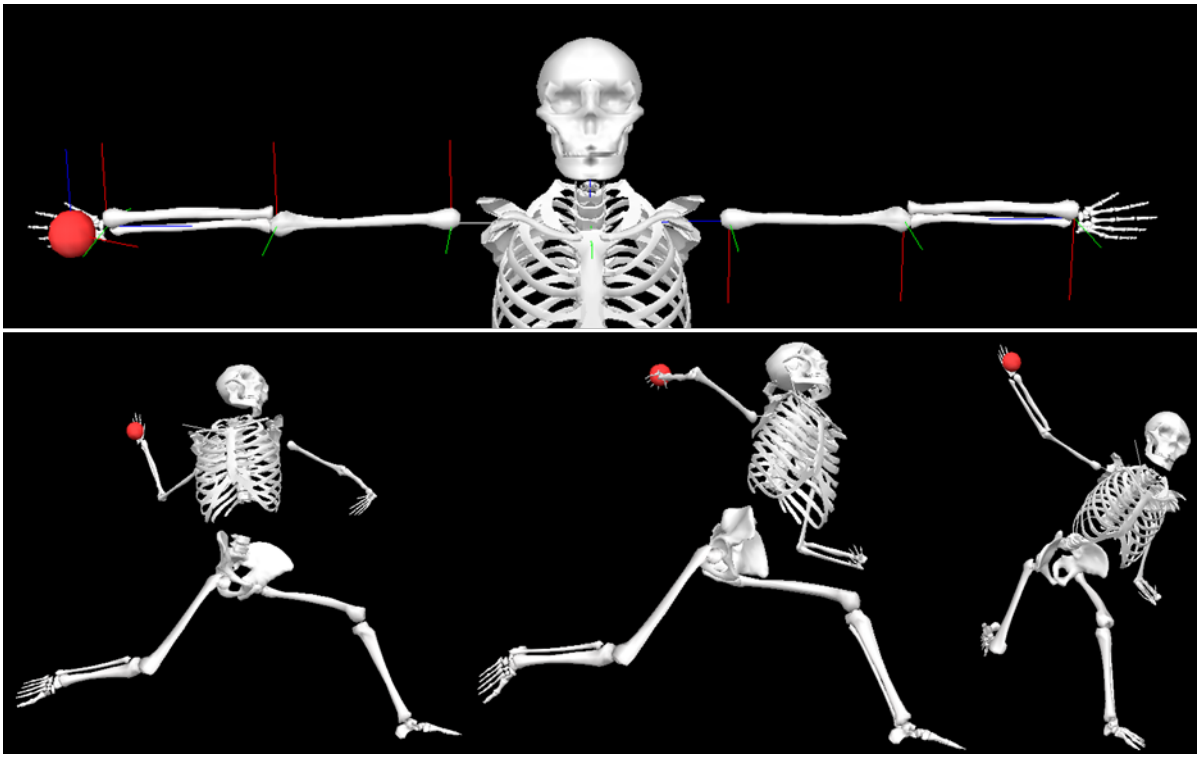


Figure 4.1: Updated Visual3D model that reflects the changes in model anthropometrics and geometry as defined in section 4.1.1. The most significant differences would be the inclusion of the baseball (red). The top image shows the standard model with the newly added baseball, while the bottom sequence depicts the instance of LFC, maximum throwing shoulder external rotation, and ball release, from left to right, respectively.

0.95 cm to 1.1 cm. This was done to account for the addition of the ball to the model, since when the joint radius ratio was 0.95 cm, the articulation of the hand-ball complex was not being recognized as a rigid joint by the software, since the radius was too small to capture the interaction of the hand and ball. Through trial and error, all previously defined joints were recognized, without overlap, in addition to the hand-ball complex, when a joint radius of 1.1 cm was used. This meant that the hand-ball complex was officially recognized by the model as a rigid connection and would be incorporated in all subsequent computations.

4.2 Modelling Approach and Implementation

This section will outline how V3D determines net joint kinetics in their built-in inverse dynamic algorithm, and how the algorithm was set up in a pipeline. Before that, a note must be made on the inverse dynamic methodology used in this research, due to the absence of GRF. Typically, to make accurate conclusions about the kinetics of any movement, the model must be "dynamically-consistent" with external forces, such as the GRF [48]. Recall that inverse dynamics involves the use of kinematic data alongside external forces, to solve for net joint kinetics. GRF provide critical information on the external loads acting on the body and are essential to inverse dynamic analyses. By capturing GRF using force plates, one can quantify the interaction between the foot and the ground. This data is combined with the kinematic information to compute the net forces and moments at each joint through a bottom-up approach, starting from the ground and moving upwards through the body segments. Overall, the measurement of GRF are essential to ensuring that the outputted kinetics are consistent with the measured set of forces experienced between the foot and the ground. This traditional approach to inverse dynamics is called a ground-up methodology, but since no GRF are available in this study, it is difficult to determine the accuracy of the predicted forces, which is a modelling limitation.

Instead, the only external forces in this model are those found from the weight of the segments and ball, as a result of gravity. The forces due to the body segments' gravity were not explicitly measured, putting the kinetic results further into question, since there is no way to determine if the dynamics are consistent with measured external forces throughout the model [48]. This is called a top-down approach, and while it is generally less accurate than the ground-up approach, it is still an invaluable tool in determining net joint kinetics in real-world applications, where force plates cannot be used, such as a pitcher throwing in game on a mound [48]. It is noteworthy that a bottom-up approach also relies on the weight of the segments and the ball as well, but also relies on externally measured forces such as GRF.

A top-down inverse dynamic analysis considers the influence of gravitational forces at each segment. By starting at the more distal segments, which would be the hand-ball complex in this model, the approach ensures that the effects of gravity, which predominantly act on the body's mass, are accurately incorporated into the analysis from the outset. This method helps in determining the joint reaction forces and moments, as the gravitational effects can be systematically propagated from the distal segments to the more proximal ones, ensuring a comprehensive understanding of the biomechanical interactions during human movement. In V3D, if GRF are not specified using the integrated functionality, a top-down approach is taken by default, which relies on gravitational forces to compute net

joint kinetics.

4.2.1 Visual3D Inverse Dynamics Tool

V3D uses a recursive scheme that calculates forces and torques for each joint at a given time step [40]. It relies on standard Newton-Euler equations and principles of multibody system dynamics to estimate joint kinetics. First, the proximal joint reaction force is computed in the global coordinate system while the segments attached distally to any segment are identified. An iterative algorithm for the proximal joint force is used and is just the summation of all external forces acting on the proximal segment, added to the summation of the gravitational forces of all distal segments connected in the chain. There is an additional term, which is a summation of the forces caused by the acceleration of the distal segment masses, where distal segment acceleration is calculated using a finite difference algorithm, as outlined in section 3.3.3. Next, the proximal couple moment, found at the proximal end of a segment, is computed in a segment (local) coordinate system. A transformation then takes place where the inertial torque from the segment coordinate system is transformed to the global (laboratory) coordinate system using a transformation matrix that is computed from the MoCap data. An expression for the couple acting on the proximal segment is then created, which represents the net moment. Expanding the force terms in the coupled moment equations and reducing the resulting terms yields the proximal moment due to the inertial forces and applied moments at the joint. The result is the reactionary kinetics of the proximal joint, and this is done for each segment at each time step, in a recursive fashion. An advantage of this scheme is that the approach requires less bookkeeping to keep track of external forces and torques [40].

4.2.2 Extraction Pipeline for Selected Joint Dynamics

The extraction of the model's kinetics is very similar to the kinematic collection identified in section 3.3. A pipeline was set up so that for a given pitcher, all collected pitches would be opened, and a loop would go through each of the files pertaining to a given pitch. Then, a subroutine called 'Compute Model Based Data' was used to extract joint kinetics. This subroutine will compute a desired signal, which are joint forces and moments in this case, using a model's segments, kinematic, and kinetic data. The biggest difference from kinematic analysis was that the subroutine now specified net joint reaction forces and moments (in separate steps) instead of joint angles. Since joints are automatically detected in the software and named accordingly, the inputs to the pipeline relied on the

selection of the joint, and the resolution coordinate system, which defines the force or moment relative to that coordinate system. The general pattern used for this was to select the proximal or parent segment of the joint as the reference coordinate system. For example, for computation of the kinetics at the elbow joint, the upper-arm was selected as the resolution coordinate system, which is more proximal. This means that the elbow joint kinetics were measured with respect to their reactions against the upper-arm. This was done for all the forces and moments of the throwing elbow and shoulder. The output was a set of reactionary forces and moments at the throwing shoulder and elbow, in all 3 directions, and data existed for each pitch for a given pitcher. The data was exported as a MATLAB file, for post-processing and analysis.

The selected dynamics were that of the throwing shoulder and elbow, and related to their rotational DOF in each direction. For the throwing elbow, the extracted forces were the anterior(+)/posterior(-), medial(+)/lateral(-) and compression(+)/tension(-) forces that exist at the elbow joint's LCS on the y, x, and z axes, respectively. The elbow moments extracted were the flexion(+)/extension(-) and valgus(+)/varus(-) moments, corresponding to rotations about the x and y axes of the elbow joint's LCS. Refer to Fig. 3.3. The positive and negative signs next to a movement indicate the direction of the positive joint rotation relative to the parent segment (upper arm for elbow and glenohumeral socket for shoulder), as defined by the right hand notation, and is outlined in 3.2.3. Similarly, for the throwing shoulder joint, the anterior(+)/posterior(-), superior(+)/inferior(-), compression(+)/tension(-) forces were extracted and exist at the shoulder joint's LCS on the y, z, and x axes, respectively. Moreover, the shoulder abduction(+)/adduction(-), horizontal flexion(+)/extension(-) and internal(+)/external(-) rotation moments were extracted and correspond to y, x, and z rotations along the shoulder joint's LCS, respectively. A visualization of the extracted forces and moments can be seen in Fig. 4.2. Note that the definitions of the kinetics in this figure are not consistent with the positive and negative values associated with the model's local coordinate system presented in Fig. 3.3, since this image was adapted from a different source [49] and was included only as an example. Finally, HOR ABD and HOR ADD are alternative terms used for horizontal extension and horizontal flexion, respectively, which are the descriptions used in this thesis.

4.2.3 Post-Processing and Kinetics Visualization

With the joint kinetics now extracted from V3D, they were uploaded into MATLAB, for post-processing and visualization. The dynamics were already filtered, trimmed, and resampled in the pre-processing steps, so visualization was the next step. The process is identical to that of the kinematic visualization process outlined in section 3.3.4, including

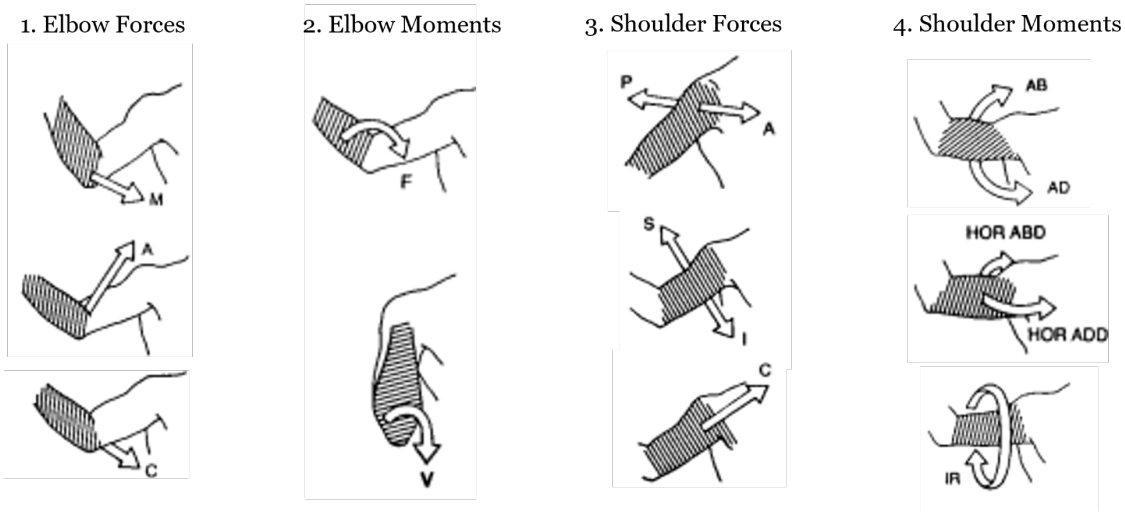


Figure 4.2: Visualization of the movements associated with the extracted kinetics during inverse dynamic analysis. M, A and C represent medial, anterior, and compression forces respectively, while F and V represent flexion and varus moments, respectively. Moreover, P, I, and S represent posterior, inferior and superior forces, respectively, while AB, AD, HOR ABD, HOR ADD, and IR represent abduction, adduction, horizontal abduction, horizontal adduction and internal rotation moments, respectively. Taken with permission from [49].

the determination of means, standard deviations, time normalization, and pitch event inclusion. This was done on a pitcher-specific basis and an example of the elbow varus-valgus moment can be seen in Fig. 4.3. It is important to note that based on the relative definition of joints and segments outlined in section 4.2.2, forces and moments are reactionary and relative to the more proximal or parent segment.

A sample output of the post-processing of the inverse dynamic data can be seen in Fig. 4.3. As expected, the peak moment occurs at the instance of MER, which indicates that the coordinate systems and pitch phase indicators were implemented successfully. However, one may notice that the peak moment is a varus torque, when a valgus torque should be expected at this stage of the pitch (MER). The forces and moments outputted were all defined with respect to the parent segment in V3D. These dynamics are reactionary which means that they create an equal and opposite force on the child segment. All the plots in the inverse dynamic analyses are joint reaction forces and moments, since inverse dynamic studies measure the net forces at a joint in the parent's frame of reference. In the case of Fig. 4.3, the humerus (parent segment) is experiencing a varus moment at MER, meaning

that the forearm (child segment) is under a valgus torque. In the context of the movement, the results make sense considering that the forearm is attempting to externally rotate against the humerus due to the valgus moment on it, subsequently loading the medial elbow (and UCL) under a valgus torque. All dynamics were reported in the parents' frame of reference, so this should be kept in mind in the results and discussion sections. The parent frame was selected since it aligns with ISB standards for inverse dynamics, made the most sense with the defined local joint coordinate systems, and is best practice in V3D inverse dynamics algorithms [40, 41].

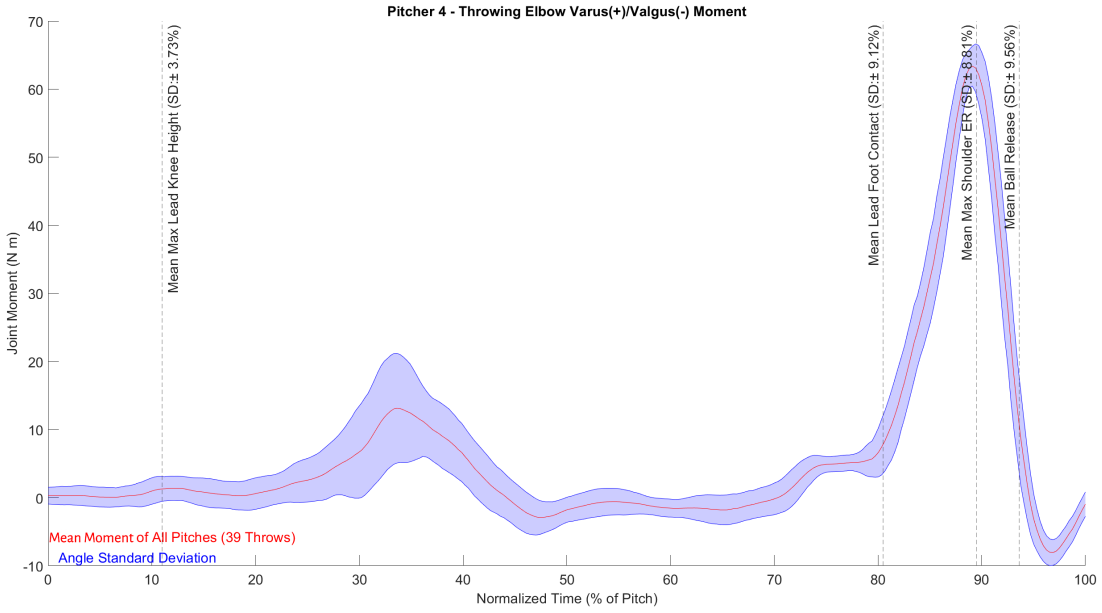


Figure 4.3: Sample kinetic visualization of the throwing elbow varus-valgus moment for Pitcher 4, around 10ms prior to peak lead knee height and 10ms post ball release. The time was normalized as a percentage of the total time. The red line represents the mean value of the kinematic parameter over time, while the blue line and shading represents the standard deviation at that time step. Pitch events are also noted as vertical lines, which includes their standard deviations as well.

4.3 Dynamics Results

This section will review the results of the inverse dynamic analysis, and discuss the major observations. Notably, kinetic variations between the 5 pitchers will be discussed and compared to literature. This chapter will end by highlighting some of the kinetic factors that may contribute to increased performance or injury risk in the subjects analyzed, in addition to a pair of sensitivity studies. The studies can provide further insight into the model's behaviours, and be a useful tool in assessing the model validity. Throughout the analysis, an emphasis on comparing peak loads across pitchers will be made, rather than considering absolute values, due to difficulties in validating the model, as will be discussed in section 4.7. However, efforts will also be made to compare magnitudes to literature, as this is a useful method to reaffirm the efficacy of the model.

This study extracted many dynamic measurements, but will not be elaborating on all of these for the sake of brevity. As such, the kinetics that will be emphasized here are related to those of the throwing (right) shoulder and elbow. These were selected since they are correlated with throwing velocity and can also provide insight into potential injury risks for the UCL. The selected kinetics were the throwing shoulder compression/tension and anterior/posterior forces, throwing elbow anterior/posterior force, compression/tension force and varus/valgus moment. Joint dynamic trajectories for all five pitchers are attached in Appendix C. Unlike the inverse kinematic study, an emphasis on approximate peak values post LFC was made, instead of investigating magnitudes across different phases of the pitch. This was done because the peak values relate to maximum stress on the UCL, and have greater implication of performance, unlike kinematics, where there is a greater interest in patterns and trajectories.

As a reminder, the forces and moments outputted were all defined with respect to the parent segment, and represent net joint dynamics. These kinetics are reactionary, which means that they create an equal and opposite force on the child segment. For example, in the case of the varus/valgus load shown in Appendix C, it is clear that at MER, the elbow is experiencing a varus moment, rather than a valgus load, as one should expect. Considering the coordinate system definitions, the humerus (parent segment) is experiencing a varus moment at MER, meaning that the forearm (child segment) is under a valgus torque. In the context of the movement, the results make sense considering that the forearm is attempting to externally rotate against the humerus due to the valgus moment on it, subsequently loading the medial elbow (and UCL) under a valgus torque.

4.3.1 Net Joint Moments and Forces

The following table highlights the peak values for the joint dynamics of interest across all 5 pitchers from Appendix C, post LFC. Table 4.1 will be used as a reference to investigate and discuss the dynamics in greater detail in the next section. The loads were selected because of their relevance to shoulder and elbow injuries in pitching.

Table 4.1: Post lead foot contact mean peak kinetic values for five pitchers across elbow and shoulder dynamics. Positive values indicate the primary direction of force or moment.

Pitcher	**Dynamics**	**Post Lead Foot Contact Peak Value**
1	Elbow Anterior Force (+)	500 N
	Elbow Compression Force (+)	800 N
	Elbow Varus Moment (+)	61 N·m
	Shoulder Anterior Force (+)	350 N
	Shoulder Compression Force (+)	1000 N
2	Elbow Anterior Force (+)	400 N
	Elbow Compression Force (+)	900 N
	Elbow Varus Moment (+)	62 N·m
	Shoulder Anterior Force (+)	400 N
	Shoulder Compression Force (+)	1050 N
3	Elbow Anterior Force (+)	450 N
	Elbow Compression Force (+)	800 N
	Elbow Varus Moment (+)	63 N·m
	Shoulder Anterior Force (+)	425 N
	Shoulder Compression Force (+)	900 N
4	Elbow Anterior Force (+)	500 N
	Elbow Compression Force (+)	1050 N
	Elbow Varus Moment (+)	62 N·m
	Shoulder Anterior Force (+)	300 N
	Shoulder Compression Force (+)	1000 N
5	Elbow Anterior Force (+)	400 N
	Elbow Compression Force (+)	850 N
	Elbow Varus Moment (+)	65 N·m
	Shoulder Anterior Force (+)	400 N
	Shoulder Compression Force (+)	950 N

The analysis of post-lead foot contact (LFC) peak values for elbow and shoulder forces and moments reveals both similarities and notable differences among the five pitchers. These insights provide understanding of how each athlete manages kinetic loads during the pitching motion, reflecting individual biomechanical strategies, performance priorities, and potential implications for injury risk.

The anterior force at the elbow highlights how pitchers manage loading in the direction of ball propulsion. Pitcher 1 and Pitcher 4 exhibit the highest peak anterior force at 500 N, suggesting a shared strategy to maximize forward energy transfer through the elbow joint. Pitchers 2, 3, and 5 show lower anterior forces, ranging from 400 N to 450 N. The reduced anterior force in Pitcher 5, at 400 N, may indicate a more conservative strategy that relies less on forceful elbow motion, reducing stress on the joint.

Compression forces are essential for joint stability during the high-stress pitching motion, as will be discussed in detail in chapter 5. Pitcher 4 demonstrates the highest elbow compression force at 1050 N, indicating significant joint stabilization during peak loading. In contrast, Pitchers 1 and 3 maintain more moderate compression forces at 800 N, suggesting they prioritize minimizing joint stress while still achieving performance outcomes. Pitcher 2's higher compression force of 900 N may reflect a slightly more conservative stabilization strategy, while Pitcher 5's 850 N reflects a middle-ground approach.

Varus moments are critical for resisting loads to the UCL. The range of varus moments is relatively narrow (61-65 N·m), with Pitcher 5 reaching the highest peak at 65 N·m. This elevated varus moment might indicate increased lateral joint loading, which can place additional strain on the UCL. Pitchers 1, 2, and 4 exhibit similar varus moments, reflecting consistent control strategies across these athletes.

Anterior force at the shoulder reflects the forward-directed load during the pitch. Pitcher 3 exhibits the highest anterior force at 425 N, indicating aggressive forward loading likely aimed at maximizing ball velocity. By contrast, Pitcher 4 demonstrates the lowest anterior force at 300 N, reflecting a more conservative approach that could reduce stress on the shoulder. The remaining pitchers (1, 2, and 5) fall within a middle range (350–400 N), suggesting balanced strategies to manage forward forces.

Compression forces at the shoulder are critical for joint stability and energy transfer. Pitcher 2 demonstrates the highest compression force at 1050 N, reflecting a strong stabilization strategy to manage peak loads. Conversely, Pitcher 3 exhibits the lowest compression force at 900 N, which may reflect a focus on optimizing shoulder mobility and minimizing internal joint loading. Pitchers 1, 4, and 5 show similar values (950–1000 N), suggesting consistent stabilization mechanics across these athletes.

The uniformity in observed elbow varus moments suggests a shared emphasis on controlling lateral joint forces to stabilize the elbow under the high stress of the pitching motion. Similarly, shoulder compression forces are relatively consistent across the group, falling between 900 N and 1050 N. These compression forces reflect a common biomechanical strategy to stabilize the shoulder joint during the rapid energy transfer required for an effective pitch.

Despite these shared characteristics, distinct differences emerge that highlight individual mechanical strategies. Pitcher 1 demonstrates high anterior forces at the elbow (500 N) with moderate compression forces (800 N), suggesting a focus on elbow-driven energy transfer. In contrast, Pitcher 2 exhibits the highest shoulder compression force (1050 N) and a relatively higher elbow compression force (900 N), emphasizing joint stabilization over aggressive forward energy transfer. Pitcher 3 stands out for its highest shoulder anterior force (425 N) and lowest shoulder compression force (900 N), reflecting a strategy that prioritizes mobility and forward-directed energy at the shoulder while relying on moderate elbow forces. Pitcher 4 displays the highest elbow compression force (1050 N) but the lowest shoulder anterior force (300 N), indicating an approach centred on elbow stabilization rather than shoulder-driven propulsion. Finally, Pitcher 5's highest elbow varus moment (65 N·m) suggests increased lateral joint loading, coupled with moderate anterior and compression forces, reflecting a balanced strategy to manage both energy transfer and stabilization.

These findings demonstrate the biomechanical diversity among professional pitchers. While all athletes share fundamental strategies for joint stabilization and force control, their unique force and moment profiles reflect individual adaptations that align with their specific pitching styles and performance goals. These variations underscore the importance of personalized biomechanical analysis for optimizing performance and mitigating injury risk.

4.3.2 Discussion and Comparison of Dynamics Across Pitchers

The analysis of the net joint dynamics across these five pitchers reveals consistent trends in peak values at key pitching events, with notable individual variability that reflects unique mechanical strategies. These findings highlight the dynamic interplay between elbow and shoulder forces and moments throughout the pitch, emphasizing the importance of precise energy transfer, stabilization, and adaptability.

For the majority of metrics, consistent patterns were observed across all pitchers, reinforcing the biomechanical repeatability of elite athletes (See Appendix C for sample plots). Peak varus and valgus loads at the elbow consistently occurred near MER, aligning with the transition from energy storage to transfer in the kinetic chain. Similarly, peak anterior and compression forces at the elbow were observed near BR, underscoring the elbow's role in stabilizing and directing energy during the most dynamic phase of the pitch.

At the shoulder, peak anterior forces occurred earlier in the pitching sequence, typically around LFC. This timing aligns with the abrupt deceleration of the kinetic chain as the

pitcher transitions from single to double support. The resulting shoulder inertia drives a spike in anterior forces, which then transition toward posterior forces near MER and BR. In contrast, shoulder compression forces peaked near BR, reflecting the need for joint stabilization during the rapid transfer of energy to the ball.

The consistent temporal patterns across key events, seen in Appendix C support the validity of the pitch phase extraction algorithm, since peak valgus loads occurred near MER. This is also significant since in chapter 5, a change in the UCL loading equation (section 5.2) is made compared to literature, where shoulder rotation actuation is attributed to loading the UCL. However, individual variations in magnitudes and transitions provide deeper insights into how pitchers adapt their mechanics to optimize performance and mitigate injury risks.

The anterior force at the elbow plays a critical role in loading the joint's medial tissues, given that the direction in which it acts on may add shear forces to mid elbow. This is particularly relevant for assessing UCL stress, as the valgus moment, in combination with anterior force, impact that area of the joint. However, as this analysis only considers net joint moments, muscle contributions are not accounted for, limiting the ability to fully quantify UCL loads. Compression forces at the elbow are vital for resisting valgus loads and maintaining joint stability, as discussed in Chapter 5. Pitchers exhibiting higher compression forces, such as Pitcher 4, likely rely on this mechanism for stabilization during peak loading phases. Conversely, pitchers with lower compression forces, like Pitcher 3, may prioritize mobility and velocity at the expense of increased joint stress.

At the shoulder, anterior forces peaked at LFC, reflecting the abrupt deceleration of the lower body and the inertial response of the shoulder joint. This spike in force highlights the critical role of shoulder stabilization during the early phases of energy transfer. The transition to posterior forces near MER and BR aligns with the internal rotation of the shoulder as the kinetic chain progresses. Compression forces at the shoulder peaked near BR, underscoring the importance of stabilization during the final energy transfer to the ball.

The alignment of peak varus and valgus loads with MER can be attributed to the biomechanical function of the elbow during this phase. MER represents the point of maximal shoulder external rotation, where energy is stored in the shoulder and transferred to the elbow and UCL. This transition generates high forces, which the elbow resists through varus moments and compression forces. The subsequent drop in these loads near BR corresponds with the release of stored energy and the internal rotation of the shoulder.

Peak anterior and compression forces at the elbow occurring near BR reflect the joint's role in stabilizing and directing energy to the ball. This phase demands both high dynamic

stability and precise energy transfer, which is evident in the magnitude of these forces during this temporal stage.

At the shoulder, the early peak in anterior forces at LFC corresponds to the abrupt deceleration of the lower body, which creates a reactive force at the shoulder. As the kinetic chain progresses, the shoulder transitions to posterior forces near MER and BR, reflecting the change in direction of joint loading. Peak compression forces at the shoulder during BR emphasize its stabilizing role as the final energy transfer occurs.

Greater variability was observed in joint dynamics immediately following peak lead knee height, compared to the kinematic results, as seen in Appendix C. This increased standard deviation may be attributed to inconsistencies in pitching mechanics during the transition from single to double foot support, as pitchers manage their COM. Balance issues during this phase could lead to compensatory arm mechanics, introducing variability. Additionally, differentiating error in kinetics and intentional mechanical changes, such as altering cadence to disrupt the batter's timing, as seen in pitchers like Marcus Stroman, may also contribute to this variability.

Fortunately, the variability tightens significantly between LFC and BR, which represent the most critical phases of the pitch, as seen in Appendix C. This tight standard deviation across dynamics during this interval reflects the exceptional repeatability of elite pitchers. Such consistency is critical for optimizing performance, as it ensures reliable energy transfer and minimizes unnecessary joint stress.

To assess the validity of the inverse dynamic model and the subsequent results, it is necessary to evaluate the results against experimental data in literature. Most publications list a mean value across all of their participants, so the same is done here and shown in table 4.2. These values are compared against established findings in the literature, particularly those reported by Fleisig et al. [49], Kaizu et al. [50] and Stodden et al. [15].

Table 4.2: Post lead foot contact mean peak kinetic values for pitcher dynamics across elbow and shoulder forces. Positive values indicate the primary direction of force or moment.

Pitcher	**Dynamics**	**Mean Post Lead Foot Contact Peak Value**
Mean	Elbow Anterior Force (+)	450 N
	Elbow Compression Force (+)	880 N
	Elbow Varus Moment (+)	63 N·m
	Shoulder Anterior Force (+)	370 N
	Shoulder Compression Force (+)	970 N

The findings in this study on mean post-lead foot contact peak joint dynamics align with general trends reported in the literature while demonstrating some differences in magnitude. These discrepancies highlight the unique characteristics of the current elite-level sample, which includes pitchers throwing at velocities consistent with professional standards. The differences in subject population, methodology, and model assumptions likely contribute to the observed variations.

The patterns of load and torque trajectories in this study are consistent with those reported in previous research. Fleisig et al. [49] identified peak varus torque at the elbow near maximum external rotation (MER) and observed that both varus torque and anterior shoulder forces significantly decrease approaching ball release (BR). These trends align with the results of this study (see Appendix C, where peak elbow varus moments and anterior shoulder forces also occur near MER and decrease by BR, reflecting a coordinated energy transfer through the kinetic chain.

Similarly, the timing of peak shoulder compression forces observed in this study corresponds with findings from Fleisig et al. [49] and Stodden et al. [15], where these forces peaked at or near BR. These findings reinforce the notion that shoulder compression forces are critical for joint stabilization during the final stages of energy transfer to the ball.

While the trajectories align, the magnitudes of the forces and moments reported in this study differ slightly from the literature, but are still very comparable. For example, the mean elbow varus moment in this study was 63 N·m, higher than the 26.7 N·m reported by Kaizu et al. [50] in amateur pitchers. Building on these comparisons, Fleisig et al. report a mean elbow varus moment of 64 N·m for his study, which agrees well with the 63 N·m observed in this study. Fleisig et al. [49] analyzed highly-skilled amateur pitchers with a mean fastball velocity of 37.5 m/s (84 mph), whereas the pitchers in the current study likely exceed these velocities. The peak varus/valgus load both occurred during the phase of maximum external rotation (MER). The mean shoulder compression force in this study (970 N) is lower than the 1090 N reported by Fleisig et al. Fleisig et al.'s study reported a shoulder anterior force of 380 N during arm cocking and 400 N near release, which aligns closely with the mean peak value of 370 N observed in this study. Studies including musculature, including the forward dynamic analysis in this thesis, reported peak valgus loads far greater (over 100 N·m) than those outputted by inverse dynamic studies, emphasizing the importance of considering soft tissues when evaluating joint kinetics [11, 51]. This also justifies the need for muscle-based forward dynamic models.

While the results do align closely, differences likely stem from the inclusion of MLB pitchers in this study, who throw at significantly higher velocities with different technique, whereas the other studies focus on amateurs. Previous studies often included youth, high

school, or amateur pitchers, such as Yoichi et al. [50], who examined subjects averaging 25.9 years of age with a ball velocity significantly lower than elite standards. Higher throwing velocities, which are present in this study, inherently increase the kinetic demands on the shoulder and elbow, resulting in larger forces and moments. Moreover, the modelling approaches used in this study may also differ from those used in other studies, further explaining the differences in results. Other reports do not detail their methodology with sufficient details to warrant a fair comparison, but as in any study, differences are bound to occur. Despite the differences, similarities with this study's findings in magnitudes, trajectories, patterns and loading timings were very comparable across all three studies and this study's findings.

4.4 Implications of Dynamics on Injury and Performance

The analysis of joint dynamics in this study provides insights into the relationship between pitching performance and injury risk, particularly concerning the UCL. The interplay between elbow and shoulder forces highlights individual adaptations in mechanics that may prioritize velocity generation, joint stability, or a balance of both. For example, Pitchers 4 and 5 exhibit elevated elbow compression forces (1050 N and 850 N, respectively), reflecting a stabilization strategy that protects the medial elbow and UCL during peak loading phases. However, this comes at a potential cost to velocity generation due to reduced anterior force and energy transfer efficiency. In contrast, Pitchers 1 and 3, with higher anterior elbow forces (500 N and 450 N, respectively), emphasize velocity-driven mechanics, which elevate dynamic loading on the UCL but may contribute to increased throwing speeds. In theory, a pitcher can achieve higher pitching speeds with relatively lower UCL loads, if they optimize their mechanics and seamlessly transfer energy across the kinetic chain. However, this is inconclusive and beyond the scope of this study, given that the pitching speeds were not provided by the collaborators so there was no way to consider speed, but generally, a faster throw will inevitably elevate the loads on the UCL, as the joint velocities and ranges of motions associated with faster throws apply more rapid and intense forces.

The valgus moments observed across all pitchers provide further insight into UCL loading. Pitcher 5 exhibited the highest valgus moment at 65 N·m, which is consistent with the medial joint stress that occurs during the rapid elbow extension phase. While these moments are higher than those reported for amateur pitchers by Kaizu et al. [50], they align closely with Fleisig et al.'s [49] findings for skilled amateur pitchers. These values

underscore the heightened stress placed on the UCL at elite throwing velocities, reinforcing the need for targeted interventions to strengthen the ligament and supporting musculature.

The shoulder dynamics also reveal key strategies for balancing stability and velocity. For instance, Pitcher 3 displayed the highest anterior shoulder force (425 N), a clear indicator of aggressive forward energy transfer aimed at maximizing ball velocity. However, this approach may compromise shoulder stability, as seen in the relatively lower shoulder compression force (900 N). In contrast, Pitcher 2's shoulder compression force peaked at 1050 N, reflecting a stabilization-centric strategy that mitigates joint stress but could limit throwing speed. These variations highlight the trade-offs athletes face in optimizing performance while minimizing the risk of overuse injuries, particularly to the UCL and shoulder structures.

The findings also suggest that the consistency in joint loading across key pitching phases is a hallmark of elite pitchers. The tight standard deviations observed across Appendix C in peak dynamics during critical phases such as LFC and BR indicate mechanical repeatability, which is essential for both performance and injury prevention. However, variability in joint loading immediately following peak lead knee height reflects the challenges pitchers face in managing their COM and transitioning from single to double support. This phase introduces compensatory mechanics, which may contribute to variability in loading and increased injury risk.

The implications for injury prevention are significant. The high valgus moments and anterior forces at the elbow, combined with rapid extension velocities observed in the kinematic analysis, align with known risk factors for UCL injuries. For example, Pitcher 4's transition from maximum external rotation (MER) to BR involved peak extension velocities exceeding -1100°/s, a biomechanical pattern linked to increased UCL strain [52]. Similarly, Pitcher 2 expereinced an elbow extension velocity of -1250°/s.

From a performance perspective, the ability to generate high anterior forces at both the elbow and shoulder is closely linked to ball velocity. However, these forces must be balanced with sufficient joint stabilization, as excessive dynamic loading can lead to chronic injuries or acute ligament failure. Joint stabilization refers to the ability of a joint to maintain its position and resist unwanted movement or dislocation. It involves the coordinated action of various structures, including ligaments, muscles, tendons, and the joint capsule, working together to control movement and provide support. Pitchers like 1 and 3, who prioritize velocity-driven mechanics, may benefit from supplementary stabilization training to mitigate the long-term risk of UCL or shoulder injuries. Conversely, pitchers like 2 and 5, who demonstrate more conservative mechanics, may require interventions to optimize energy transfer and enhance velocity without compromising joint health, such as increased

throwing arm muscular training to provide the elbow with additional stability.

As a whole, the peak valgus moments observed at the elbow consistently occurred near MER, aligning with prior research on the timing of UCL loading during the pitching motion [49]. These valgus moments, averaging 63 N·m, represent the medial elbow stress that the UCL must resist during the rapid energy transfer from the shoulder to the forearm. While these values are much higher than the isolated UCL rupture threshold of 34 N·m reported by Bart et al. [24], it is important to note that the cadaveric findings do not account for the full body dynamic contributions, which contribute to joint loads. However, the consistently high valgus torques observed in this study highlight the cumulative stress placed on the UCL over repeated pitches, a primary factor in the development of chronic UCL injuries among pitchers.

Compression forces at the elbow also exhibited consistent trends, peaking after LFC as the pitcher stabilized their arm during the high-velocity phases of the pitch. The mean compression force of 880 N plays a crucial role in resisting valgus torques and maintaining joint stability under extreme dynamic conditions. This stability is essential for protecting the UCL during the deceleration phase of the pitching motion, where joint loading peaks. The high compression forces observed suggest that professional pitchers rely heavily on this stabilization mechanism to withstand the immense kinetic demands of elite-level pitching. However, the trade-off between stabilizing the joint and allowing for efficient energy transfer to the ball may influence pitching velocity. Higher stabilization forces might reduce the efficiency of forward-directed energy transfer, potentially limiting maximum ball velocity, while lower stabilization forces could compromise joint integrity and increase injury risk. Stabilizing the joint through joint compression is also a key consideration in the forward dynamic determination of UCL loads, which will be discussed in chapter 5.

At the shoulder, consistent peaks in anterior and compression forces near BR reflect the critical role of the shoulder in generating and transferring energy during the final phases of the pitch. Anterior forces, with a mean peak of 370 N, represent the forward-directed loads that contribute to ball propulsion. These forces are closely tied to throwing velocity, as they reflect the ability of the kinetic chain to efficiently transfer energy from the lower body to the throwing arm. However, excessive anterior forces can lead to increased stress on the anterior shoulder structures, including the labrum, which, combined with high valgus elbow moments, can exacerbate injury risk. The mean shoulder compression force of 970 N underscores the stabilization required to manage these dynamic loads, ensuring the joint remains stable during the rapid acceleration and deceleration phases of the pitch.

In conclusion, this study highlights the dynamic interplay between performance optimization and injury risk in elite pitchers. The individual variations observed in joint

dynamics reflect diverse mechanical strategies, each with its own implications for velocity generation and joint health. Personalized biomechanics analyses, combined with targeted training and rehabilitation programs, are essential for balancing these competing demands.

4.5 Sensitivity Study 1: Modelling of the Baseball-Hand Interface and Impact of Ball Variations on Joint Kinetics

The motivation behind this sensitivity study is to assess the validity and accuracy of the inverse dynamic model, under outlier conditions. There is a concern with the top-down inverse dynamic approach used in this research, since the ball is rigidly connected to the hand, which is not the case in reality. This sensitivity study was conducted to examine the reliability of the modified MSK model of a baseball pitcher, specifically assessing the effect of ball weight and position on estimated net joint kinetics. The investigation focused on the hand-ball complex and aimed to provide additional qualitative validation for the top-down inverse dynamics approach commonly used in biomechanics to analyze pitching mechanics. Understanding the influence of these parameters on joint kinetics is critical, as both heavier and lighter baseballs are widely employed in training to improve performance and mitigate injury risk. Additionally, this study sought to explore the effects of traditional fastball grip (ball positioned closer to the thumb) on joint loads, as grip variations have been shown to alter the biomechanical demands on the upper limb during pitching.

The methodology involved systematically modifying the MSK model by altering two key parameters: the weight and the position of the baseball. Three test cases were created to isolate the effects of these modifications. In Test Case 1, the ball was positioned closer to the thumb, simulating the traditional fastball grip. Test Case 2 involved using a heavier ball with a weight of 32 oz, as referenced in prior studies , while Test Case 3 utilized a lighter ball weighing 1 oz [53]. For each scenario, joint kinetics were measured and compared to the original model, which used a standard 5.1 oz (0.145 kg) baseball with a neutral grip position, positioned further further from the thumb than Case 1, at the base of the third metacarpal. The analysis was conducted across multiple pitchers, and joint kinetics were calculated using inverse dynamics to quantify peak magnitudes of joint loading, including valgus torque at the elbow.

4.5.1 Test Case 1 Results: Ball Positioned Closer to the Thumb

The modified model in Test Case 1 showed a slight increase in peak magnitudes across all measured joint kinetics, particularly in valgus torque at the elbow. The peak valgus torque exceeded the values observed with a neutral ball position, with a peak of around 70 N·m. Despite these increased magnitudes, the trajectory patterns remained virtually identical to the original model, indicating that moving the ball towards the thumb affected the magnitude of joint loading without significantly altering the overall kinetic profile.

4.5.2 Test Case 2 Results: Heavier Ball (32 oz)

In Test Case 2, the use of a heavier ball resulted in more pronounced increases in peak kinetic magnitudes across all measured parameters, with peak valgus torques exceeding 90 N·m. The increased weight of the ball consistently produced higher joint loads across all pitchers in the study. Although trajectory patterns remained similar to the original model, there was a slight increase in noise, possibly due to the additional load's impact on the physical stability of the model.

4.5.3 Test Case 3 Results: Lighter Ball (1 oz)

With the lighter ball, Test Case 3 demonstrated a consistent decrease in peak kinetic magnitudes across all measured joint kinetics, with peak valgus torques dropping to approximately 60 N·m. Despite the reduced magnitude of joint loads, the trajectory profiles remained virtually identical to the original model, indicating that a lighter ball reduces joint load without altering the kinetic pattern.

4.5.4 Implications

Overall, these results indicate a strong correlation between ball weight and peak kinetic magnitude, with heavier balls inducing higher load magnitudes and lighter balls resulting in decreased loading. The positional adjustment (closer to the thumb) showed a more moderate impact on load magnitude, although it highlighted the influence of ball placement on joint stress distribution, particularly for valgus torque.

This study's findings have several implications for baseball pitching mechanics and training practices. First, the use of heavier balls in training may increase peak joint loads,

particularly at the elbow, potentially raising injury risk with repetitive use. This suggests that while heavier balls might be beneficial for building strength, their use should be moderated to prevent overloading the throwing arm. Conversely, lighter balls could serve as a safer alternative for refining mechanics, though their reduced weight makes it challenging for pitchers to achieve game-relevant velocity, which may limit their transferability to real pitching scenarios.

Additionally, the results underscore the importance of grip and ball placement. Holding the ball closer to the thumb, as seen with traditional fastball grips, increases joint loads more than holding it centrally. While alternative grips that reduce joint stress could theoretically be explored, they might compromise pitch velocity and accuracy and require a significant adjustment to traditional pitching mechanics.

Finally, it is essential to note that while absolute magnitude values from the model require experimental data for validation, the relative increases and decreases in load magnitudes provide a valuable metric for comparing load effects. This sensitivity study contributes insights into the relationship between pitching mechanics and joint loads, which could inform training protocols, injury prevention strategies, and potential adaptations in pitching techniques through the selective use of ball weights and grips to contribute to the individual athlete's goals. For example, a pitcher recovering from injury could use lighter balls to alleviate some loads during training for a return to play, while a pitcher who aims to throw faster could use the weighted ball, to increase muscle strain, and gain strength. It is also interesting to see the correlation of grip mechanics and the use of heavy training balls as they relate to UCL injury.

The sensitivity study demonstrates promising signs of model validation by aligning with known biomechanical expectations in baseball pitching. This response aligns with prior findings, such as those by Melugin et al., which highlight the heightened stress on a pitcher's arm during weighted ball training programs [53].

In the sensitivity analysis, the model predicts increased valgus torques and joint forces with heavier ball scenarios, while lighter balls correspond to decreased kinetic demands. This observed pattern reinforces the model's reliability, as it mirrors the expected physiological response to load variation. Such responses support the model's accuracy in capturing joint dynamics under varied loading conditions, even though absolute values require further validation. The study's findings suggest that the model can capture relative changes in load, laying the groundwork for further development and refinement towards a fully validated model suitable for analyzing baseball pitching mechanics and injury risk factors.

4.6 Sensitivity Study 2: Pitching Cadence

The second sensitivity study aims to understand how variations in the cadence of a baseball pitcher's motion affect joint kinetics, a consideration that has become increasingly relevant with the introduction of the pitch clock in Major League Baseball (MLB). By mandating a set time within which pitchers must complete their motion, the pitch clock pressures pitchers to speed up, risking disruption in their natural mechanics. Examining the implications of these temporal adjustments on joint loading can offer insights into the potential injury risks associated with a hurried or slowed pitching motion. This analysis holds particular importance for identifying how small modifications in timing may impact the forces exerted on the UCL and other key structures, furthering the understanding of the risks involved in deviating from an athlete's standard cadence.

In this study, the pitching motion cadence was altered by adjusting the time-step values, resulting in two test cases where the cadence was increased and decreased by 15% and 25% from the baseline, for a total of 4 test cases. The modified kinematics were then applied to the musculoskeletal model to evaluate the resulting changes in kinetics for shoulder and elbow joints across multiple pitchers. For each scenario, joint loads were measured, compared, and analyzed against the nominal values obtained from the original pitching motion. By assessing these variations, this study provides a detailed look at how deviations in timing influence peak loading and stress distribution, particularly within the shoulder and elbow.

The study found that peak joint loads changed consistently with alterations in pitch cadence. Specifically, increasing the cadence (simulating a hurried motion) led to a significant rise in peak kinetic values across all measured joint loads, while decreasing the cadence (simulating a slowed-down motion) produced a corresponding reduction in peak joint loads. This monotonic relationship between cadence and joint load was observed uniformly across the shoulder and elbow, indicating that even minor timing adjustments can have substantial effects on the forces exerted on these joints. Notably, while the 25% change scenario exceeds realistic variations, they highlight a critical trend: as pitchers are pressured to speed up their motion, the loads on their joints increase, potentially accelerating the wear and tear on soft tissues over time, particularly the UCL. The results can be seen in Fig. 4.4.

The findings underscore the potential risks associated with rushing a pitching motion due to external pressures, such as the pitch clock. With increased cadence resulting in elevated joint loads, pitchers may face higher risks of injury if forced to deviate from their natural rhythm. This study's results align with expected biomechanical responses, where

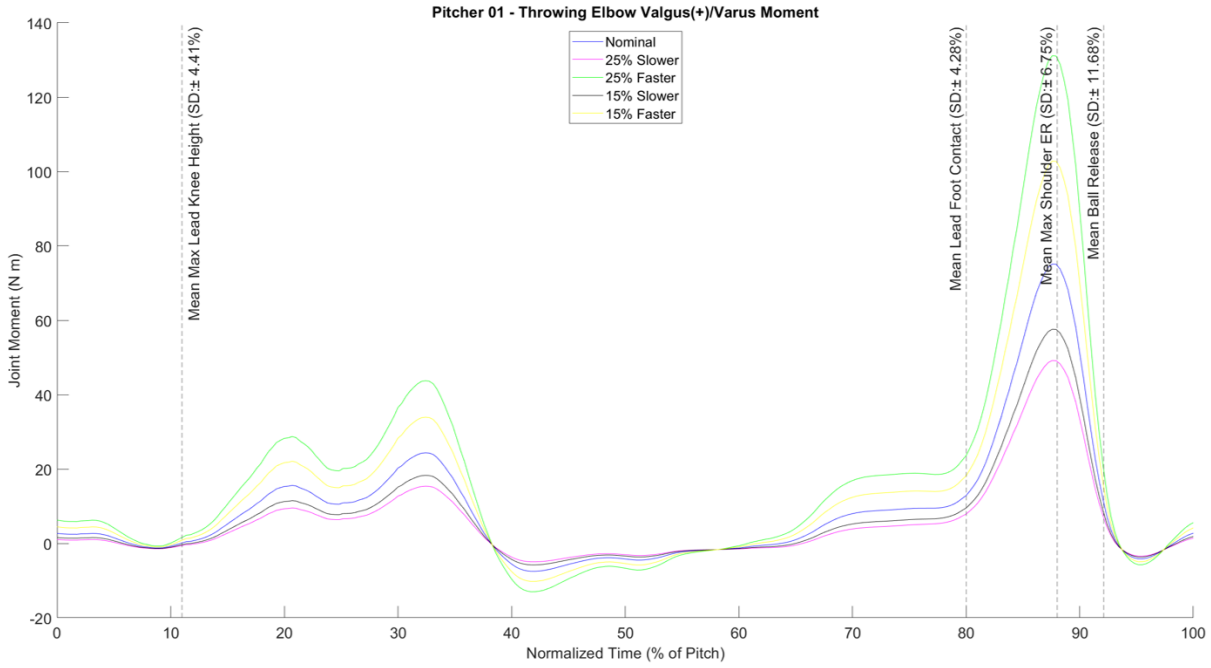


Figure 4.4: Sample kinetic visualization of the throwing elbow varus-valgus moment during the cadence study. Notably, increases in cadence increased peak loads, while decreases in cadence did the opposite. This was consistent for all measured kinetics in the throwing elbow and shoulder, across all pitchers.

faster movements are associated with greater forces, lending support to the model's validity. Such behaviour indicates that the model reflects the mechanical principles governing joint loading under varied temporal conditions, reinforcing its utility in analyzing real-world pitching stresses.

Furthermore, the consistent increase in kinetic demands with elevated cadence, especially at the shoulder and elbow, suggests that even slight accelerations in pitching speed—while seemingly minor—can incrementally elevate injury risk. This highlights the importance of preserving a pitcher's natural cadence and managing pitch timing effectively to mitigate excessive joint loading. The sensitivity study therefore provides insights for coaches, trainers, and athletes, emphasizing the importance of maintaining proper timing and control to reduce the likelihood of overuse injuries, particularly in response to time constraints imposed by new MLB regulations.

In conclusion, this sensitivity study demonstrates that the model is sensitive to biomechanically meaningful changes, with results aligning with expected physiological responses to cadence adjustments. Although further experimental data is necessary validate the model, the model's response to changes in pitch timing supports its reliability and potential application for injury prevention strategies in professional baseball contexts.

4.7 Model Evaluation for Inverse Kinematics and Dynamics

Given that the inverse kinematic and inverse dynamic musculoskeletal MSK models utilized nearly identical frameworks, with the only substantive difference being the inclusion of the baseball, a comprehensive evaluation of these models is warranted. Evaluating such models remains challenging due to their unique construction and specific design decisions. Furthermore, as both models were developed using external KinaTrax data, which, as previously mentioned, integrates directly with the V3D model-building feature, validating externally-built models becomes difficult without accompanying documentation or publications. Nonetheless, efforts were undertaken to ensure that the models used in these analyses were robust and produced reasonable results. Finally, it is important to note that the accuracy of the data collection system itself cannot be independently validated, as KinaTrax has not published its findings.

More specifically, due to the confidentiality agreement underpinning this joint research project, details about validation activities conducted for the KinaTrax modelling algorithm in baseball applications cannot be disclosed. The KinaTrax data were integrated into V3D to develop the MSK models used in the inverse kinematic and inverse dynamic analyses. These models also provided joint positions, which were used to extract joint angles, forces, and torques.

An external agreement was established in 2019 with Driveline Baseball, a well-respected baseball research and development organization that collaborates with MLB teams, to conduct a publicly-available validation study of the KinaTrax system for baseball applications [54]. However, a formal publication from this effort is still pending. Other institutions have also been engaged to validate the system for baseball pitching applications, though these studies have likewise not yet been published.

It is worth mentioning that the KinaTrax system has been validated for other domains, particularly gait analysis [55, 56]. While these gait findings demonstrate the system's accuracy and integrity, the highly dynamic and biomechanically complex nature of baseball

pitching, characterized by rapid joint velocities and accelerations, differs substantially from gait, necessitating caution when extrapolating results. Nonetheless, these studies provide useful context. Two studies conducted by Ripic et al. investigated the validity of artificial intelligence-based markerless MoCap systems, including KinaTrax, for clinical gait analysis [55,56]. The studies assessed spatiotemporal parameters during over-ground gait using both marker-based and markerless tracking methods, with KinaTrax data analyzed using V3D. Both studies concluded that gait speed and select spatiotemporal variables measured using KinaTrax were valid, with biases falling within meaningful clinical thresholds. Specifically, the root mean square error between the marker-based and markerless (KinaTrax) systems was less than 0.03m for all spatial measurements. Additionally, KinaTrax demonstrated the highest tracking accuracy overall when compared to marker-based systems.

These results suggest that the KinaTrax system is accurate in measuring segment trajectories, which is promising for its application in baseball. While gait studies cannot validate the system for baseball pitching due to differences in biomechanical demands, the system's reliability in other applications is encouraging. Consequently, the integration of KinaTrax data with the V3D modelling framework is assumed to be reliable for the purposes of this research. Additionally, the use of V3D software itself is well-documented in the biomechanics community, with numerous studies validating its performance against other biomechanics tools, such as OpenSim [57]. Thus, the application of V3D for both kinematic and kinetic analyses appears reasonable, as these techniques have consistently been shown to yield accurate results in similar research contexts.

With limited ability to evaluate the data, its system and the subsequent model, greater efforts had to be made to demonstrate the accuracy of this research. In the results and discussion sections for both the inverse kinematic and inverse dynamic chapters (chapters 3 and 4, respectively), efforts were made to compare the model output to reviewed publications. In the inverse kinematic chapters, a weaker connection between this research's results and those from the literature was made, but the results from the inverse dynamic study were in good agreement. An attempt to explain why the kinetics were more closely aligned with literature than the kinematics is made below.

The weaker connection between the inverse kinematic results in this research and those reported in the literature, compared to the close alignment observed in the inverse dynamic study, can be attributed to several factors. First, inverse kinematics relies heavily on marker placement, anatomical definitions, and joint constraints, all of which are prone to variability. Small deviations in marker positioning or differences in joint coordinate system definitions can propagate errors through the model, leading to discrepancies with prior studies. In contrast, inverse dynamics directly incorporates external forces, such as GRF, and segment kinematics, making the results less sensitive to such variability and

more robust when compared to established biomechanical patterns. The inverse kinematic results are not necessarily insufficient, but they simply did not line up well with the metrics published in the literature. This is exacerbated by the lack of publications on professional pitchers, which can largely explain the differences. This means the the inverse dynamics, which rely on the kinematics, are well supported as well.

Additionally, inverse kinematic models often simplify joint constraints and assume fixed joint axes, which may reduce the physiological accuracy of the calculated joint angles. These simplifications, combined with the high inter-individual variability in kinematic outputs, particularly in dynamic tasks like baseball pitching, could further weaken their alignment with literature. On the other hand, inverse dynamics relies on Newton-Euler equations to compute joint forces and moments, which are inherently more physics-based and less influenced by individual variability because it avoids modelling how forces are produced and focuses only on what net forces and torques must exist to produce observed motions, as dictated by universal physics laws. This leads to results that are more consistent with existing studies. Moreover, studies in the literature often use different joint coordinate system definitions, particularly for complex joints like the shoulder or elbow, which can lead to discrepancies in kinematic results. Inverse kinematic chapters might be more affected by these differences, while inverse dynamics results (forces and moments) are often less dependent on specific joint coordinate systems. This is because JCS definitions primarily affect how joint motion is described, but not how forces and torques are computed in inverse dynamics. That is, kinematics depend heavily on joint coordinate system definitions due to their descriptive nature, while inverse dynamics is less sensitive to these definitions since it prescribes forces and moments based on observed motion.

The evaluation process may also contribute to these differences. Kinematic data validation often relies on limited or non-standard datasets, whereas inverse dynamics results, such as joint forces and moments, are frequently validated against force plate data and well-established biomechanical principles, ensuring greater comparability. Moreover, the literature may provide fewer consistent or standardized kinematic datasets for comparison, while dynamic variables like joint forces and moments are more widely reported, facilitating stronger alignment. Together, these factors explain the observed divergence in the results between the inverse kinematic and inverse dynamic analyses. Furthermore, given that the models were scaled to averages rather than true anthropometrics measured from the sample population, the kinetic analysis is flawed, given that the moments depend on accurate dimensions of segments.

Finally, the case studies consistently demonstrated expected biomechanical behaviours, highlighting the influence of individual variations on joint kinetics. In the first sensitivity study, the effects of baseball weight and grip position on joint kinetics were systematically

evaluated, revealing predictable trends. Heavier balls resulted in increased joint loads, while lighter balls reduced kinetic demands, consistent with established biomechanical principles linking external load to joint stress. Similarly, grip adjustments, such as positioning the ball closer to the thumb, moderately increased joint torques without altering overall kinematic patterns, reflecting the known influence of grip mechanics on joint loading.

In the second sensitivity study, changes in pitch cadence further validated the model's ability to capture realistic responses. Increasing cadence (hurried motions) led to proportional rises in joint loads, while decreasing cadence reduced these loads, mirroring expected outcomes under altered temporal dynamics. These results align with the fundamental understanding that faster movements generate higher forces due to greater acceleration and velocity.

Across both studies, the model reliably captured the expected biomechanical relationships, reinforcing its robustness. While absolute values require further validation, the consistent trends across all test cases suggest that the model represents joint loading behaviour under varied conditions, providing a valuable tool for understanding individual variations in pitching mechanics and informing injury prevention strategies.

While great efforts were made in the inverse kinematic and dynamic model building to mimic the proportions of MLB pitchers, the lack of information provided by the MLB partner made designing these models difficult. Specifically, the models were scaled to average MLB starting pitcher proportions. Without greater understanding of the actual dimensions of the sample pitchers, the scaled models were either over-scaled or under-scaled to the athlete's nominal proportions. Scaling the model's to values other than the norms can cause complications in the analyses, since the kinematics and kinetics extracted are not designed to be used for that subject. This is a key limitation of this work and can possibly explain the discrepancies observed between the literature and this study in the inverse kinematic analyses, and even the large ranges of standard deviation in the early pitching phases of the inverse dynamic analyses. More notably, joint moments are highly sensitive to the model dimensions, and the use of inaccurate anthropometrics compared to the true values of the sample populations results in inaccurate joint moments.

In summary, the models and results presented in this research demonstrate a reasonable level of validation and alignment with established biomechanical principles, supporting their utility for analyzing baseball pitching mechanics. While challenges remain in independently validating the KinaTrax system and the models due to confidentiality agreements and limited published findings, efforts were made to compare the model outputs to existing literature and expected behaviours. The inverse dynamic results showed strong alignment with prior studies, underscoring the robustness of the model in capturing joint forces and

moments, which are less prone to variability compared to kinematic data.

Chapter 5

Forward Dynamics

This section will outline the modelling, simulation, and interpretation of a forward dynamic analysis of a pitching motion. In contrast to previous literature, this approach will not rely heavily on kinematic/kinetic inputs and it will produce an entirely optimal throwing motion by leveraging optimal control techniques. The goal is to create an optimized motion of pitching, which estimates the contribution of valgus torque resistance/production by the muscles in the throwing arm, to reduce UCL loading without compromising on pitching velocity. The key to maintaining velocity is to constrain pitching velocity to ensure that a reasonable throwing speed is attained. To do so, first the model will be built in OpenSim (OpenSim, Stanford University, USA), with anthropometrics that are comparable to an MLB pitcher. Relevant muscles will be included for the throwing arm, as they relate to the generation/resistance of a varus-valgus torque on the elbow, which is known to cause UCL injuries. These muscles, in addition to the remaining DOF of the model, will be supplemented by reserve actuators to assist in driving the simulation. Next, an optimal control framework will be developed to simulate what should look like a baseball pitch, which will be achieved through the use of boundaries, kinematic constraints, initial conditions, simulation time specifications, cost functions and weights, and convergence and constraint tolerances. Once the model converges, a series of iterative changes will be made to conduct 'what-if' simulations that show how the throwing motion would look while investigating other criteria, without compromising pitching speeds. All of the simulation outputs, including muscle and actuator activations, model states, model controls, muscle forces, and joint reaction forces will be used to compute the moment imposed on the UCL. Finally, tests will be done on the edge cases of the model to see the behaviour of the model under extreme scenarios, which will contribute to the validation of the model. The first step is to develop a MSK model.

5.1 OpenSim Musculoskeletal Model and Revisions

A musculoskeletal model was developed using OpenSim 4.5, an open-source software for creating and analyzing musculoskeletal models of human movement [58]. The model was based on a validated open-source model, which was modified to better represent the anatomy of an MLB pitcher. Key modifications included the removal of kinematic joint coupling constraints, the inclusion of relevant muscles involved in valgus moment production, the addition of reserve actuators to supplement the muscle-generated joint moments, and the use of primary actuators to drive joint coordinates that were not actuated by muscles (i.e. all joints except those of the throwing arm).

The model was designed through a series of pre-processing steps, which used 43 fastball pitches that were recorded using markerless motion capture from a single starting MLB pitcher during a single game, and were anonymized and shared by KinaTrax. Each set of pitching data contained transformation matrices at each time point (300 Hz) for each tracked body segment. All pitches were four-seam fastballs. The pre-processing steps for the forward dynamic analysis relied on inverse kinematic and inverse dynamic analyses of these 43 pitches, which were extracted using custom Visual3D kinematics and kinetics pipelines, respectively. Visual3D was used since it integrates directly with KinaTrax motion capture data to build a custom musculoskeletal model. Consistency across the Visual3D model and forward dynamic model was maintained by extracting the subject–specific anthropometric and inertial properties of the model from Visual3D and using them to design the OpenSim forward dynamic model. Joint trajectories, in the form of Euler angles, from the 43 pitches were averaged from the inverse kinematic analyses and used to define the OpenSim model's initial pose, inform the joint motion limits, and provide joint trajectory initial guesses for the optimization. Peak net joint forces and torques were extracted from the inverse dynamic analyses, averaged over the 43 pitches, and used to define the peak optimal torques of the musculoskeletal model's actuators. The initial pose, joint motion bounds, and actuator peak torque values used in the musculoskeletal model can be found in Appendix D. The inputs from the inverse kinematic and inverse dynamic analyses serve to better approximate the performance capabilities of an elite pitcher, compared to the default model's performance capacity. The model's starting pose was set at the instant of peak lead knee height and simulations proceeded to ball release, as this interval represents the most strenuous portion of the pitching motion [5, 21, 23, 24]. The motion duration, spanning from peak lead knee height to ball release, was calculated as 0.7 s on average from the inverse kinematic analyses; simulation completion bounds were set to between 0.4 s and 1.0 s to align with literature values [7].

The base musculoskeletal model used in this research was adapted to reflect the physical

characteristics and capabilities of a professional pitcher. In OpenSim model development, it is common to adapt existing models for specific use cases [59]. This study required a model with full-body anatomy, including bones and muscles relevant to valgus loading on the UCL of the throwing arm. Since no validated open-source model for dynamic athletic motions like baseball pitching exists, the open-source "Upper and Lower Body Model" was chosen as the base model. This model combines lower limb components from Delp et al. and upper limb components from Holzbaur et al., including bones and most muscles with validated musculoskeletal dynamics [57, 58, 60–64].

The base model was adapted to meet the demands of MLB pitchers, as follows. Muscles not relevant to this study (as they relate to the UCL) were removed, namely those that do not span across the elbow joint. Joint motion coupling constraints were removed to permit the ROM expected in elite pitchers, with the bounds of the ROM informed by inverse kinematic analyses of the pitching motions. Fifteen muscles were identified in the literature as resisting or producing valgus moments at the elbow during pitching and were retained: pronator teres (PT), flexor carpi radialis (FCR), flexor carpi ulnaris (FCU), palmaris longus (PL), four flexor digitorum superficialis muscles (FDSL, FDSR, FDSM, FDSI), biceps (BIClong, BICshort), triceps (TRImed, TRIlat, TRIlong), anconeus (ANC), and brachialis (BRA) [26, 61, 65, 66]. Muscle paths were not changed.

A baseball with appropriate dimensions and inertial properties was rigidly connected to the right (throwing) hand at the base of the second metatarsal, reflecting a fastball grip. The baseball was designed with a mass of 0.145 kg, a radius of 0.0364 m, and principal moments of inertia of 7.68×10^{-5} kg·m^2 (modelled as a solid sphere) with the centre of mass being located at the centre of the ball.

A pre-processing step was conducted to scale the model's dimensions to match those of a typical MLB starting pitcher (height 6'3" or 1.905 m, weight 215 lb or mass 97.5 kg). Scaling was performed using OpenSim's *Scale Tool*, which adjusted the segment lengths and mass properties to match the anthropometry of the pitcher (Table 5.1) [58]. The OpenSim *Scale Tool* updates the dimensions of a model to match a particular individual by minimizing the error between experimental marker position data and markers placed on the musculoskeletal model [58]. Integration between Visual3D and OpenSim permitted direct scaling of body segments using the dimensions of the Visual3D model, which were already scaled to the individual pitcher. Specifically, a set of scale factors (multipliers) representing the relative scale of the Visual3D model's segments to those of the OpenSim model was generated. Inputting the scale factors and the desired height and mass of the model into the *Scale Tool* produced a model with the desired proportions and body segment mass properties.

Table 5.1: Segment scaling factors for the OpenSim scaling tool

Segment	**Scale Factor**
Pelvis	1.020
Thorax	1.117
Skull	1.100
Right Femur	1.210
Right Tibia	1.099
Left Femur	1.210
Left Tibia	1.099
Right Calcaneus	1.210
Right Toes	1.210
Left Calcaneus	1.210
Left Toes	1.210
Right Humerus	1.210
Left Humerus	1.210
Right Radius	1.099
Right Ulna	1.099
Left Radius	1.099
Left Ulna	1.099
Right Hand	1.099
Left Hand	1.099

The muscle models used in this research employed the Millard 2012 Equilibrium Muscle Model, a Hill-type muscle model that estimates muscle force generation assuming that the muscle fibers and tendons remain in equilibrium [67]. Reserve actuators were added to supplement the force-generation capabilities of the muscles, ensuring that the model could generate sufficient joint moments during the pitching motion [61]. The remaining joints, without the support of muscles, were driven by primary actuators, making the elbow the emphasis of this model. Actuator peak torques were extracted from the inverse dynamic analyses conducted in Visual3D (Appendix D).

Some muscle parameters were adjusted to better reflect the athletic capabilities of an elite pitcher; these changes were informed by literature [11, 61, 68, 69]. Muscle maximum isometric forces were increased by 30% from their default values in the base model. Reserve actuator maximum torques were also increased by 30%, but with respect to the mean peak torques extracted from the inverse dynamic analyses in Visual3D. Namely, peak throwing shoulder rotation actuation was set to 450 N·m, shoulder abduction/adduction and horizontal flexion/extension actuation were also set to 450 N·m, elbow flexion/extension and

pronation/supination actuation were set to 350 N·m, and wrist flexion/extension and deviation were set to 300 N·m and 120 N·m, respectively. Primary actuator maximum torques were doubled with respect to the mean peak torques for their respective joints determined from the inverse dynamic analyses in Visual3D. Primary actuators were assigned higher peak torques than reserve actuators because the joints that they actuate do not have any modelled muscles to support the generation of motion. These changes were informed by Hortobágyi and Katch [68] and Buffi et al. [11]. Optimal fiber lengths and tendon slack lengths were scaled using the multipliers identified from the model scaling process for their respective body segments. The muscle activation time constant was reduced from 0.01 s to 0.005 s and the maximum normalized force achievable during eccentric contraction (force–velocity multiplier) was increased from 1.4 to 1.8, as outlined by Buffi et al. [11].

The final model included 34 degrees of freedom (DOF), with each joint actuated by either muscles with reserve actuators or by primary actuators. The pelvis served as the root segment of the model with 6 DOFs relative to the ground (3 translations, 3 rotations). The joint limits were modified to allow for a full ROM that is typically seen in elite pitchers, which surpasses the bounds of average joint ranges included in the default model [57]. The ROM bounds were relaxed by ±10% on each end based on mean joint angle trajectories from Visual3D. The joint DOF and ROM are tabulated in Appendix D.

Ground reaction forces were modelled using contact spheres in OpenSim, which were placed on the leading (left) foot to simulate interactions with the ground during pitching [58,60,70]. Two contact spheres were used: one was fixed to the calcaneus at the heel and one was fixed to the toes at the ball of the foot, with radii 0.03 m and 0.015 m, respectively (Fig. 5.2). The stiffness, damping, and friction properties of these contact spheres were based on those used in previously validated gait models [58]. The lagging (right) foot was pinned to the ground using a revolute joint that permitted rotation about the vertical axis (using contact spheres on the right foot caused the model to pass through the ground and increased computation time, so this approach was abandoned). This model simplification is mechanically consistent with the pivoting seen in professional pitching during the pitching phases that were simulated. The original and revised models are shown in Fig. 5.1.

5.2 Post-Processing and UCL Loading Calculations

Simulation outputs included kinematic states (joint positions and speeds) and control inputs (muscle and actuator controls), along with joint and actuator forces and moments. To analyze UCL loading, post-processing followed Buffi et al.'s framework, employing OpenSim's *Joint Reaction Analysis* to compute forces and moments responsible for maintaining

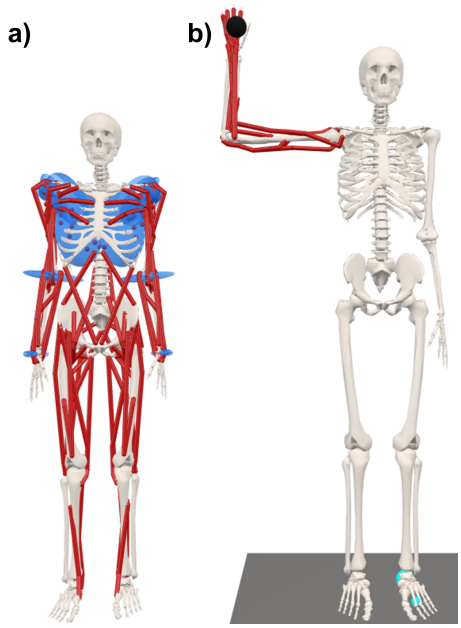


Figure 5.1: (a) Base OpenSim musculoskeletal model developed by combining the models from Delp et al. and Holzbaur et al., and assembled by Andrea Menegolo [57, 58, 60–64]. (b) Revised OpenSim musculoskeletal model for use in forward dynamic simulations of pitching. The revised model was scaled to the proportions of an MLB starting pitcher, includes a baseball, contains the 15 essential muscles for the study of UCL loads, and includes the ground. Ground contact was modelled with contact spheres (left foot) and a vertically oriented revolute joint (right foot). Developed in OpenSim.

elbow joint stability [11]. The analysis assumes that there is a force and moment balance at the varus–valgus centre of rotation of the elbow. This approach identifies the contributors to valgus loading as the indirect valgus torque at the elbow due to the arm's inertia and shoulder rotation, while the key resistor to a valgus load was shown to be the osseous articulation (joint compression) moment [11, 12]. The compression force of the elbow joint was necessary to calculate the osseous articulation moment. This moment was found by isolating the component of the compression force vector aligned with the radius's longitudinal axis and orthogonal to the varus–valgus axis of the elbow. This component of the osseous articulation moment represents the compressive load experienced by the elbow joint over time and is denoted by $F_{\mathrm{JC}}(t)$. To calculate the UCL load, $M_{\mathrm{UCL}}(t)$, where $M_{\mathrm{UCL}}(t)$ is defined as the net elbow valgus moment being resisted by the UCL, a method following the work of Buffi et al. was implemented [11]:

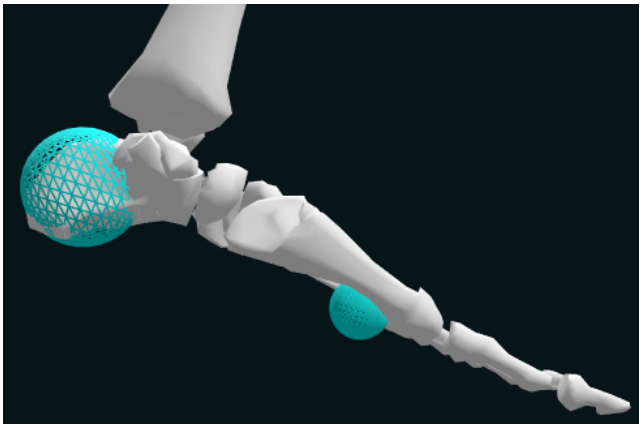


Figure 5.2: Contact spheres placed on the heel and ball of the foot in the OpenSim model, to define an interaction with the ground contact half-space.

$$M_{\mathrm{UCL}}(t) = T(t) - M_{\mathrm{Art}}(t) = T(t) - (F_{\mathrm{JC}}(t) \cdot d_{\mathrm{Art}}) \tag{2}$$

where $T(t)$ is a valgus torque–generating actuator that uses results from the predictive simulation (according to Buffi et al., this torque is generated by actuation of a varus–valgus DOF), and $M_{\mathrm{Art}}(t)$ is a valgus-resisting moment, known as the osseous articulation or joint compression moment. In the work of Buffi et al., d_{Art} was half the length of the vector from the joint centre to the medial edge of the elbow (radius), perpendicular to the varus–valgus axis of rotation, and functioned as a moment arm. Based on measurements in the scaled musculoskeletal model, d_{Art} was found to be 18.6 mm.

For each simulation, the joint compression force profile in the elbow and the corresponding UCL load were calculated. Equation (1) shows that the valgus load on the UCL is driven by torque from the reserve actuator at the varus–valgus DOF, $T(t)$, while the joint compression force provides an opposing varus moment for stability. The model of Buffi et al. included an additional varus–valgus DOF at the elbow, which was actuated and appears as $T(t)$ in Eq. (1) [11]. Their decision to add and actuate an additional varus–valgus DOF at the elbow may not be physiologically justifiable, as valgus loading at the medial elbow is an inertial byproduct of shoulder external rotation during pitching [10,20,21,71,72]. Instead, this torque was attributed to the shoulder rotation actuator, which is more consistent with anatomy while maintaining the dynamic consistency of Eq. (1) [20,72]. This adjustment shifts the rotational driver, $T(t)$, found in the throwing arm

from the distal end of the humerus (elbow) to the proximal end (shoulder). Consistency is maintained given that the shoulder's axis of rotation remained parallel to the elbow's varus–valgus axis of rotation because of the definitions of the model's local joint coordinate systems.

Post-processing of the simulations extracted key metrics from the Moco output. Metrics of interest included inputs for UCL loading equations, muscle forces, and actuator contributions to UCL torque. Additionally, joint states and reaction forces, particularly elbow compression forces, were analyzed to assess their role in resisting moments on the UCL. UCL loading patterns were visualized during the critical arm cocking and acceleration pitching phases using Python. The study employed MATLAB algorithms and OpenSim tools to analyze UCL loading, focusing on shoulder rotation actuator control and elbow joint compression forces. The magnitude of shoulder rotation actuator torque was derived as a function of its control signal. The control values (ranging from -1 to 1) were multiplied by the maximum shoulder rotation torque of 450 N·m, which was determined from the inverse dynamic analyses in Visual3D.

5.3 Optimal Control of the Pitching Motion

Optimal control of the model was used to determine the pitching motion that minimized UCL loading while maintaining pitching speed. The OpenSim Moco software was used to solve the optimal control problem, which involved minimizing actuation effort while achieving a competitive pitch speed [73]. Constraints were imposed on joint angles and speeds, muscle activations, and ball speed to reflect realistic bounds for elite athletes. The final cost function of the optimal control problem rewarded reaching a desired pitch speed threshold, achieving a lead foot speed of zero at ball release (to maintain balance and prevent slipping), and minimizing the actuation of the shoulder rotation actuator, which tends to load the UCL [10, 11, 21]. All actuator outputs were minimized to reduce oscillations in the actuator controls that are products of the time discretization used by the Moco optimization [73]. Each actuator was assigned a relatively low cost weight (0.001), with the exception of the shoulder rotation actuator (1). The ultimate goal of the optimizer was to minimize actuation effort (with particular attention to the throwing shoulder rotation DOF), subject to endpoint constraints of zero lead foot speed and achieving the desired ball speed at release.

Actuation effort represented the absolute values of torque (for actuators) and force (for muscles) as a function of their control input, integrated over the motion duration. Controls were parameterized as piecewise linear functions of time that represented the amplitude of

control signals (for actuators) and excitations (for muscles). The controls vector sampled the value of actuator controls/muscle excitations at 1 ms intervals, where the vector size was equal to the combined number of muscles (15) and actuators (34) in this model (49 total) times the number of time points (variable simulation time that depended on the optimization goal).

Cost functions and equality constraints were not defined directly in Moco's optimization framework. They were implemented using Moco's custom optimization functions, which can be tailored to different problems. Actuation minimization was achieved using the *MocoControlGoal*, where muscle and actuator effort were specified, while *MocoFinalOutputGoal* was used to assign the endpoint constraints on foot and ball speed. *MocoFinalOutputGoal* provides functionality to assign weights to the endpoint constraints, which was done in this model to penalize deviations from the desired final values. Considering the weighted endpoint constraint terms as penalties (soft constraints), the cost function was as follows:

$$J = W_1 \left(\frac{v_{\text{ball, final}} - v_{\text{ball, desired}}}{v_{\text{ball, desired}}} \right)^2 + W_2 \left(\frac{v_{\text{foot, final}}}{v_{\text{foot, maximum}}} \right)^2 + \sum_{i=1}^{n_{\text{actuators}}} C_i \left(\frac{\text{actuation effort}_i}{\text{maximum effort}_i} \right)^2 \tag{2}$$

$$\text{subject to} \quad \begin{aligned} &|v_{\text{ball, final}} - v_{\text{ball, desired}}| \leq 0.0001 \text{ m/s} \\ &|v_{\text{foot, final}}| \leq 0.0001 \text{ m/s} \\ &-1 \leq \text{controls}_{\text{ actuators}} \leq 1 \\ &0 \leq \text{controls}_{\text{ muscles}} \leq 1 \end{aligned}$$

$$\text{where} \quad W_1 = 15, \quad W_2 = 5$$

$$C_i = \begin{cases} 1, & \text{for the shoulder rotation actuator} \\ 0.001, & \text{otherwise} \end{cases} \qquad i = 1 \ldots n_{\text{actuators}}$$

The absolute magnitudes of the cost function weights were less important than their relative magnitudes, which was shown during validation. The hierarchy used reflects the prioritization of a pitcher's performance when pitching, where the magnitudes were identified through trial and error. Each cost function term was squared to ensure that the terms

were positive and the function was smooth and differentiable, which simplifies the search space and derivative calculations for the direct collocation optimal control method used in OpenSim Moco [73]. Additionally, the cost function terms were all normalized to ensure a unitless output.

A two-step optimization approach, commonly used in Moco-based optimal control, was employed to enhance robustness and ensure convergence [74]. The first step utilized a tracking optimal control simulation (*MocoTrackingGoal*) which used the mean joint angle trajectories from the inverse kinematic analyses extracted from Visual3D as input, and minimized the sum of squared errors between the experimental and simulated joint trajectories. The output of this simulation provided joint trajectories for each DOF in addition to the actuator controls and muscle excitations responsible for producing this motion, as was done by Buffi et al. [11]. This step provided a good initial guess for muscle excitations and joint angle trajectories, given that the excitations and joint angles were fit to an observed pitching motion. The second step minimized UCL load while maintaining the desired pitch speed, using the joint trajectory and control outputs of the first simulation as an initial guess. This two-step approach resulted in feasible pitching motions while addressing both performance and safety. This approach also ensured that the final solution was unique and did not simply track the kinematics of the initial guess.

5.4 Case Studies

Three case studies were evaluated to study the effects of the optimization process on the simulated motion: (1) a 93 MPH (41.6 m/s) pitch, (2) a 110 MPH (49.2 m/s) pitch, and (3) a pitch optimized to minimize valgus moment at the elbow [75]. Each simulation produced unique pitching techniques and kinematic variations, with Case 3 incorporating an additional cost function term for directly minimizing valgus moment, $M_{\mathrm{UCL}}(t)$, at the elbow. All case studies used the previously described optimization framework, with some noted adjustments.

5.4.1 Case 1: Average MLB Fastball

The first case study simulates the pitching motion to produce a ball velocity of 93 MPH, at release. This is the average MLB velocity over the years, which serves as a solid foundation for the first study [75]. To achieve this, the cost function related to pitch velocity was given a threshold of 93 MPH (41.5747 m/s), and the rest of the optimizer was left unchanged. The

solution converged after over 70 iterations, meeting the cost function and error tolerance of 10^{-4}. The simulated motion took 0.44 seconds to complete the motion, which was consistent with the expected range from inverse kinematics. The throw also looked most similar to the kinematic tracking data used for step 1 of the optimization, but had some key differences which will be discussed (See Fig. 5.6). Fig. 5.3a illustrates the resultant motion of this study.

5.4.2 Case 2: Excessively Fast Throw

The second case study simulates the pitching motion to produce a ball velocity of 110 MPH at release. This is 5 MPH greater than any pitch ever recorded in the MLB [75]. To achieve this, the cost function related to pitch velocity was given a threshold of 110 MPH (49.1744 m/s), and the rest of the optimizer was left unchanged. The solution converged after 85 iterations, meeting the cost function and error tolerance of 10^{-4}. The simulated motion took 0.47 seconds to complete the motion, which was consistent with the expected range from inverse kinematics. This speed was selected to assess the edge case behaviour to see how the model reacts under extreme scenarios.

Despite converging and producing a velocity of 110 MPH at release, the simulated motion did not resemble a traditional pitch, and more closely resembled a cricket throw. During the motion, the model appeared to be losing balance, almost falling down away from the arm during the arm cocking and acceleration phases. There is extreme contralateral tilt of the trunk and the arm slot is very overhead. This was likely due for the need for the model to generate additional torque in the arm to generate the extreme velocity, which was achieved by seemingly falling over to the side while the arm is in motion. The reason the model did not fall over is due to the stabilizing contributions of the lower body. Unlike a traditional throw, the feet remain shoulder width apart during the stance phase, whereas this simulation has them crossed over. This is likely done to maintain a centre of balance, although if the simulation were to continue, the model would likely fall over. This is visualized in Fig. 5.3b.

5.4.3 Case 3: Minimizing the Valgus Load

The third case study simulates the pitching motion while directly minimizing the valgus torque at the elbow. To achieve this, the cost function related to pitch velocity was again given a threshold of 93 MPH, and the rest of the parameters were left unchanged. However, an additional cost function, which aimed to minimize the moment of the elbow about the

y-axis, also known as the valgus torque, was added, and given a weight of 5. To implement this, the cost function was updated to minimize the reaction moment from the motion of the forearm against the humerus (parent segment), about the varus-valgus axis. The main idea of this study was to reduce the load on the UCL, by directly minimizing the valgus load on the elbow. After numerous attempts, the solution would not converge, since the motion failed to produce the necessary ball velocity under the optimizers current configuration. The optimizer was updated by iterating over ball speeds, until the simulation converged. Ultimately, convergence was reached when the throwing velocity was changed to 75 MPH (49.1744 m/s), which is well below a competitive fastball pitch in the MLB [75]. The solution converged after over 110 iterations, meeting the cost function and error tolerance of 10^{-4}. The simulated motion took 0.65 seconds to complete the motion, which was consistent with the expected range from inverse kinematics.

The simulated motion differed greatly from the tracking kinematics of the first step of the optimization. In contrast to the second case study, this throw had excessive ipsilateral trunk tilt, a low sidearm arm-slot, and virtually no external rotation of the shoulder throughout the entire duration of the throw, which is most likely why the model was incapable of generating high throwing speeds. However, the fact that a simulation focused on minimizing the valgus torque of the elbow did not exhibit significant shoulder rotation was very reassuring, given that both literature and the UCL loading calculation implemented correlate moments on the ligament to shoulder rotation (See section 5.2) [20, 24, 25, 31]. Similar to the 110 MPH simulation, the stabilizing contributions of the lower body prevented the model from falling over due to excessive trunk tilt (ipsilateral in this case) by crossing the feet to maintain a centre of balance.

Interestingly, this sort of throwing motion is not entirely absent in the MLB. Plenty of pitchers rely on a sidearm slot. Notably, pitcher Tyler Rogers has a similar degree of ipsilateral tilt as the simulation, compared to many pitchers who are taught to keep straight up or slightly contralaterally tilt. Of even greater importance is that Tyler Rogers has a notoriously low average fastball velocity (around 82 MPH, lowest in the MLB), has an extremely low sidearm arm slot, has excessive ipsilateral tilt at his trunk and has also never torn his UCL, highlighting some striking similarities to the predictions of the simulation [75]. The output of the simulation compared to Tyler Rogers' form can be seen in Fig. 5.3c.

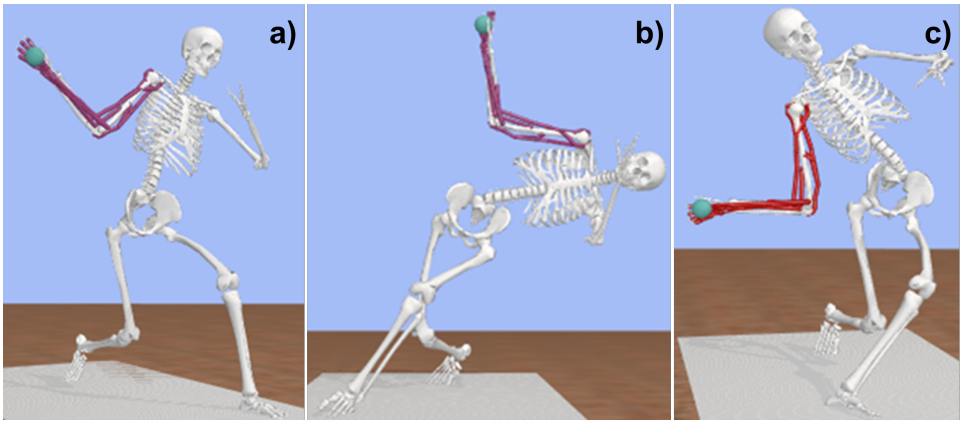


Figure 5.3: Simulated pose of the forward dynamic model at ball release for the a) 93 MPH and b) 110 MPH pitches, and c) for the pitch that minimizes valgus torque at the elbow. Developed in OpenSim.

5.5 Results and Discussion

The first case study simulated a 93 MPH (41.6 m/s) pitch, the MLB average speed, by solving an optimization problem that constrained solutions to this threshold. The simulated motion, completed in 0.44 s, resembled traditional pitching mechanics, with some notable differences, but compared favourably with the inverse kinematics data. The optimized solution produced adjustments in trunk tilt and arm slot position that have been correlated with elevated UCL loads and increased ball speeds in the literature [43]. Notably, adopting kinematics with slight contralateral trunk tilt and an arm slot not aligned with the shoulder (Fig. 5.3a) produced a competitive pitch speed with expected UCL loads (Fig. 5.4) [11, 43]. However, the level of shoulder abduction was inconsistent with what one would expect from a competitive pitcher [43].

The second case study simulated a 110 MPH (49.2 m/s) pitch, exceeding the fastest in-game MLB pitch by 5 MPH [75]. The motion, completed in 0.47 s, prioritized ball speed but deviated from typical pitching mechanics, resembling a cricket bowl (Fig. 5.3b). Extreme contralateral trunk tilt and an overhead arm slot were observed, alongside destabilizing lower-body mechanics, such as crossed-over feet during the stance phase. Adopting these extreme kinematics produced greater loads on the UCL, aligning with the claims in the literature that an overhead arm slot and contralateral trunk tilt increase loads on the UCL (Fig. 5.4) [43]. However, the overhead arm slot observed was a result of the extreme contralateral trunk tilt instead of expected shoulder abduction.

The third case study introduced an additional term in the cost function that minimized valgus torque to directly reduce UCL load (in addition to the default minimization of shoulder rotation actuation), targeting a pitch speed of 93 MPH (41.6 m/s). However, the simulation failed to converge at 93 MPH and only succeeded at 75 MPH (33.5m/s), producing a complete motion in 0.65 s. This pitch featured a sidearm slot, severe ipsilateral trunk tilt, and low shoulder rotation, characteristics of low UCL loads but also slow ball speed (Fig. 5.3c). The limited shoulder rotation observed when directly minimizing valgus loads at the elbow demonstrates the impact that shoulder rotation has on the UCL and validates its use in the UCL loading equation (Eq. (2)) as $T(t)$. These results may explain why MLB pitcher Tyler Rogers, who exhibits similar mechanics, has avoided UCL injuries with similar fastball velocities [75]. Historically, pitchers with low arm slots as exhibited in this simulation also have slower-than-average fastball speeds [75]. These pitchers often rely on deception and change of speeds rather than top-end pitch speeds, so the fact that this simulation failed to produce competitive speeds supports the idea that these mechanics limit speed generation.

Comparisons between the case studies highlighted the trade-offs between performance and injury mitigation. The analysis of varus–valgus torque at the elbow provides insights into UCL loading as the simulated kinematics change across the case studies, particularly at ball release (Fig. 5.4). The muscle force profiles for all case studies are shown in Fig. 5.5.

5.5.1 Validation of Predictive Simulations

The model was validated by comparing to literature, performing sensitivity studies, and evaluating simulation consistency. Although direct experimental validation was constrained by a lack of comparable data, the simulation framework demonstrated robustness in producing plausible pitching motions.

The model's ability to estimate valgus loading and muscle coordination was assessed by comparing to findings from Buffi et al. [11] and Anz et al. [51]. Simulated peak UCL loads of 117 N·m (Case 1) were similar to the values reported in the literature, where Buffi et al. and Anz et al. reported loads of 115 N·m and 100 N·m, respectively. Furthermore, the UCL load profile from the inverse kinematic initial guess (Fig. 5.4) closely resembled the UCL load profile reported by Buffi et al. (both results relied on measured kinematics). Both the literature [11] and this work identified the three triceps compartments as primary contributors to elbow stabilization during peak valgus loading, based on their force profiles (Fig. 5.5). Furthermore, the inverse kinematic and experimental observations in Case 1

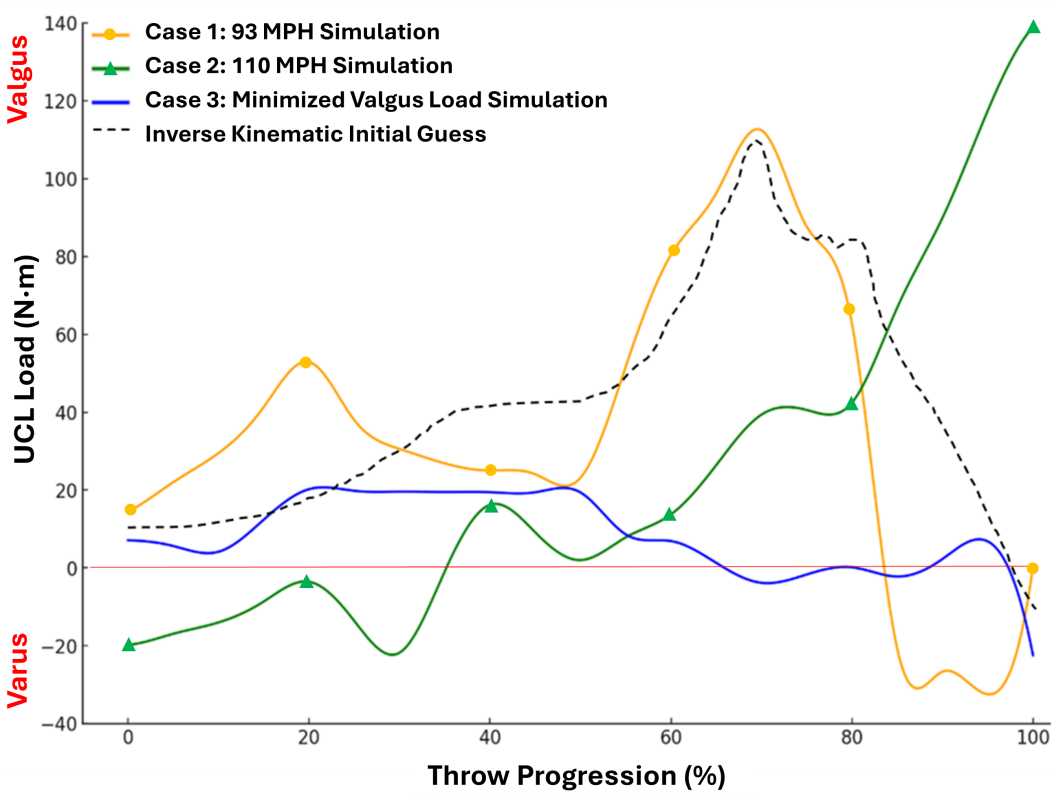


Figure 5.4: UCL load for three case studies during arm cocking and acceleration phases to release. 0% corresponds to initiation of arm cocking; 100% represents the instant of ball release. Developed in Python.

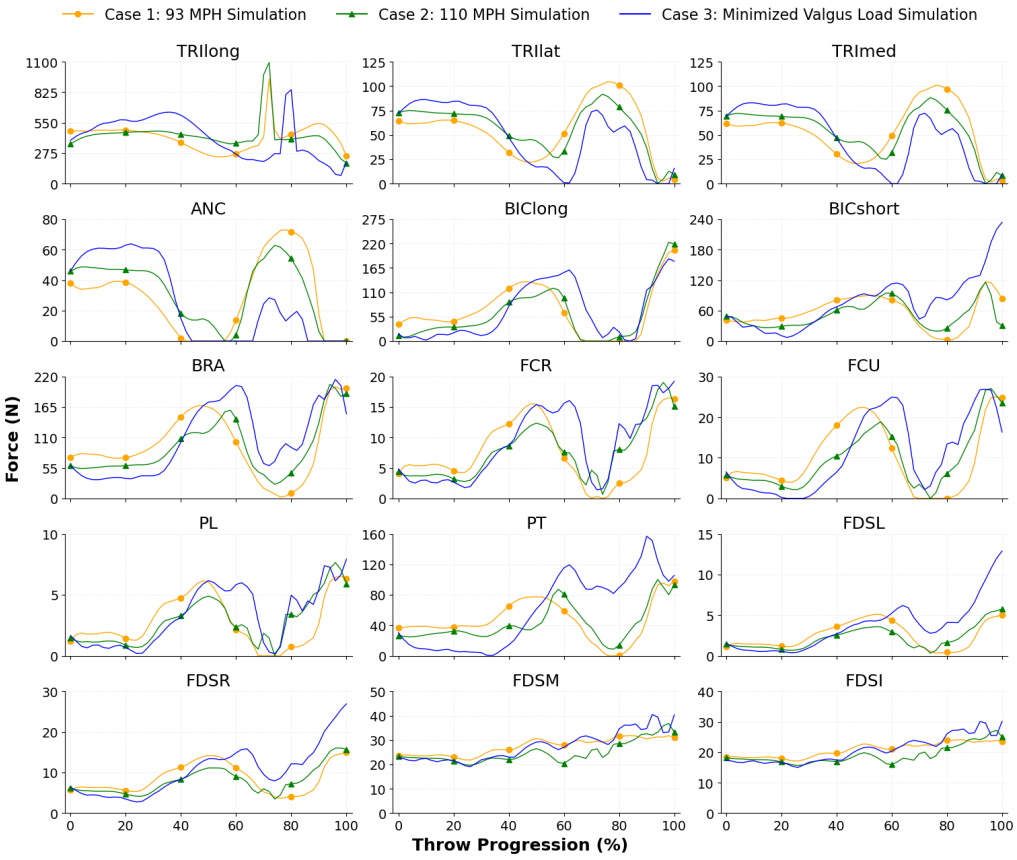


Figure 5.5: Muscle forces across three case studies during arm cocking and acceleration phases to release. 0% corresponds to initiation of arm cocking; 100% represents the instant of ball release. 70% to 90% represents the arm acceleration phase. The muscle abbreviations are as follows: triceps (TRIlong, TRIlat, TRImed), anconeus (ANC), biceps (BIClong, BICshort), brachialis (BRA), flexor carpi radialis (FCR), flexor carpi ulnaris (FCU), palmaris longus (PL), pronator teres (PT), and the four flexor digitorum superficialis muscles (FDSL, FDSR, FDSM, FDSI). Developed in Python.

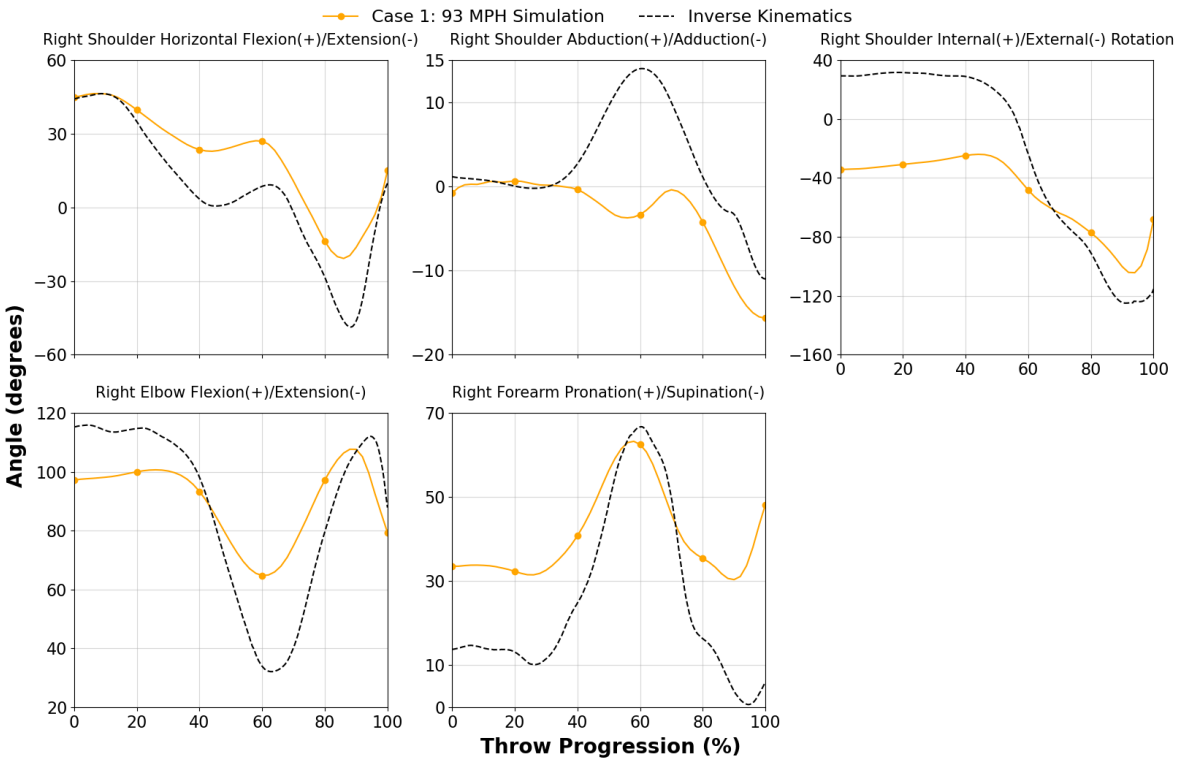


Figure 5.6: Comparison of arm kinematics between experimental (Inverse Kinematics) and simulated (Case 1: 93 MPH Simulation) joint trajectories during arm cocking/acceleration initiation (0%) to release (100%). Neutral position is defined as a T-pose with the palms facing downwards. Developed in Python.

showed some similarities, but also some notable differences, specifically in shoulder abduction/adduction, which will be discussed in Section 5.5.4 (Fig. 5.6). However, discrepancies in the motion compared to Buffi et al. were noted in elbow flexion and forearm pronation trajectories, which may stem from differences in optimization methodologies and the scope of analysis. For example, Buffi et al. considered follow-through dynamics while the present model focused on pre-release phases. Moreover, differences in elbow flexion and pronation trajectories between this model and that of Buffi et al. may have occurred as a result of the absence of the varus–valgus DOF in this model, which was instead relocated to the shoulder in this model.

Sensitivity studies were conducted to assess the simulation framework's robustness. First, adjustments to initial guesses were considered, including kinematics from other pitchers and trials. Although the model was developed using data from a single pitcher (Pitcher 1), data from five pitchers were available. Mean joint angles from Pitchers 2 through 5, as well as ten randomly selected pitching trials for each pitcher, were selected as initial guesses for use in the sensitivity studies. The simulation of these initial guesses produced consistent within-pitcher results, reflecting the model's ability to adapt to natural variability in a single pitcher's motion. Specifically, the model consistently produced similar joint angles, quantified through root mean square error calculations on joint trajectories (which were always less than 5 degrees), and a similar total motion time for a given pitcher. Variability was observed between pitchers, particularly in arm slot and shoulder abduction, highlighting the influence of individualized kinematics on optimization outcomes. While these differences underscore inter-individual variability, all motions remained biomechanically plausible, as demonstrated through the observed ROM for all simulations, which remained within the anatomical boundaries [57].

Next, sensitivity to cost function weights in the optimization problem was studied. Arbitrary changes to the cost function weights (W_1, W_2, and C_i in Eq. (2)) were made, reflecting different orders of importance among the objectives. The sets of weights were chosen to disrupt the initial hierarchy and evaluate the model behaviour when foot speed or actuation effort were prioritized over ball speed. The implementation of these simulations followed the procedure for Case 1. Simulations consistently converged to plausible motions when the weights prioritized ball speed over final foot speed with actuator torque weighted lowest (Table 5.2), which aligns with the procedure used in the case studies. Failures to converge occurred when deviations from this hierarchy were introduced. For example, prioritizing actuator torque minimization yielded insufficient pitching speed, while reducing the weight of the lead foot final speed caused the model to slip and fall.

In each study that converged, similar outcomes were achieved with respect to the baseline simulation, reaching the desired ball speed outlined in Case 1/Study 1 (93 MPH), in

Table 5.2: Sensitivity Study Results While Varying Cost Function Weights ($C_i = 0.001$ for all other actuators in all cases).

Study	**Ball Speed (W_1)**	**Foot Speed (W_2)**	**Shoulder Rotation Actuation Effort (C_i)**	**Outcome**
1	15	5	1	Baseline
2	8	10	15	Failed
3	10	15	2	Failed
4	15	5	3	Converged
5	15	5	10	Failed
6	15	7	1	Converged
7	15	10	2	Converged
8	17	7	1	Converged
9	18	4	2	Converged
10	18	6	1	Converged
11	20	5	1	Converged
12	20	8	2	Converged
13	22	6	2	Converged
14	25	7	3	Converged
15	30	10	1	Converged

addition to producing consistent joint angles (as quantified by Study 1). Three unique failure modes were observed when the hierarchy of cost function terms was disrupted. In Study 5, where the actuation effort weight exceeded the final foot speed weight, the simulation failed due to the front foot slipping. In Study 3, prioritizing final foot speed over ball speed resulted in decreased ROM in all joints of the lower body, which may have led to the observed decrease in ball speed that prevented convergence [76]. Moreover, in Study 2, prioritizing actuation effort minimization led to insufficient shoulder rotation ROM, resulting in slow ball speed and subsequent failures to converge. These findings align with the biomechanics of real-life pitching scenarios, where performance (i.e. maximizing ball speed and lead-foot stability/balance) is prioritized over conscious injury mitigation (i.e. minimizing UCL load).

The results are consistent with literature, consistent across simulations with different inputs, and adaptable to varying initial conditions and cost function weights, collectively providing confidence in the simulation framework in analyzing MLB pitches [11, 12, 51]. While some discrepancies were observed, particularly in follow-through dynamics and inter-individual variability, the results demonstrate the simulation framework's robustness and reliability in replicating key aspects of pitching motions. Moreover, the differences observed between the simulated UCL load of the initial guess simulation and the three case studies (Fig. 5.4) are due to the optimization framework's ability to produce unique motions, not merely tracking kinematic inputs. Despite these differences, the subtle similarities

across simulations, experimental data, and literature demonstrate the ability of the forward dynamics approach to produce plausible novel kinematics in a unique pitching motion.

5.5.2 Varus-Valgus Torque Balance at the Elbow: UCL Loading

Case 1 (93 MPH) simulated a traditional pitching motion (Fig. 5.3a) and torque profile (Fig. 5.4), showing a peak valgus torque of approximately 117 N·m, which was consistent with values observed in literature (see Section 5.5.1) [11,51]. However, early motion phases in Case 1 deviated from Buffi et al.'s arm kinematics, which may have stemmed from actuation minimization in the arm, potentially yielding more subtle movements in shoulder abduction and elbow flexion. Despite these early-phase differences, the critical late phases (e.g. the instant of maximum external shoulder rotation, where the peak UCL load was observed) show similarities in UCL loading patterns.

Case 2 (110 MPH) exhibited the highest valgus torque (140 N·m) and an atypical torque profile (Fig. 5.4), driven by extreme contralateral trunk tilt and an overhead arm slot (Fig. 5.3b). These kinematic adjustments suggest that extreme contralateral tilt impacts valgus torque by increasing the moment arm and mechanical demand on the elbow, supporting the findings of Hakanson et al. [77].

Case 3 (75 MPH), designed to minimize valgus torque, reduced peak UCL load to 20 N·m (Fig. 5.4) through extreme sidearm delivery and ipsilateral trunk tilt (Fig. 5.3c). These adjustments shortened the valgus moment arm and reduced shoulder external rotation, kinematic patterns that are consistent with reduced UCL loads [10, 20, 21, 71, 77]. However, these changes reduced ball speed, demonstrating a trade-off between performance and injury prevention.

Further simulations examining pitches with ball speed between 75 and 110 MPH revealed an approximately linear increase in valgus torque as ball speed increased, with a shallower slope beyond 93 MPH (Fig. 5.7). This result suggests that UCL loading does not increase proportionally with higher ball speeds. The results shown in Fig. 5.7 provide insight into the biomechanical demands of pitching, suggesting a trade-off between ball speed and injury risk, offering a basis for future explorations of performance optimization and injury prevention in baseball pitching.

5.5.3 Muscle Behaviours

The muscle activations in the 93 MPH simulation highlighted critical phases of the pitching motion (Table 5.3). Identifying peak muscle activations, which are typically spiky and

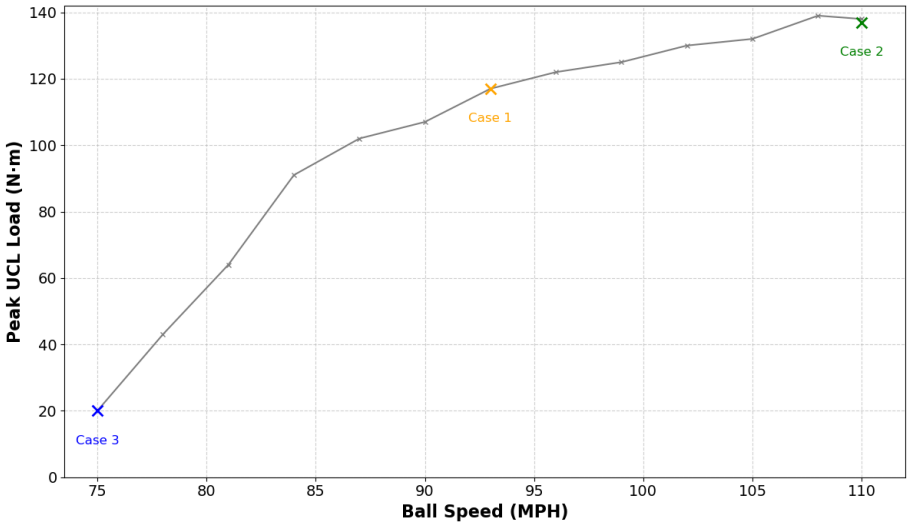


Figure 5.7: Peak UCL load vs. ball speed for the three case studies and additional simulations. Case 1: a 93 MPH (41.6 m/s) pitch, Case 2: a 110 MPH (49.2 m/s) pitch, and Case 3: a pitch optimized to minimize valgus moment at the elbow. Developed in Python.

variable, is difficult to do, given the variability in the EMG signals. However, given that particular attention is made to identify the peak activation during the most dynamic arm acceleration phase of the pitch, which is less than 50 ms in duration, clear peaks were identified and tabulated in Table 5.3. For additional details on complete EMG signals, see Appendix E.

Muscle activations peaked during the arm acceleration phase (70% to 90% of the complete motion), with the three triceps compartments exceeding activation levels of 0.8. These muscles may be key contributors to rapid elbow extension, crucial for generating high velocity at the elbow, as evident by the steep onset of peak activation of the triceps observed during the arm acceleration phase. This result supports the findings of Acosta et al. [52], who showed that the three triceps compartments are the largest contributors to elbow extension velocity during pitching, and strengthening these muscles leads to increased pitching performance. Furthermore, a study by McCutcheon et al. [78] showed that pitchers with higher ball speeds also demonstrated greater elbow extension velocities. The PT, BRA, and biceps also exhibited high activations, with PT peaking at 0.73 and BRA at 0.68, supporting previous findings that these muscles are important for stabilizing the forearm and protecting the elbow during pitching [11, 79]. The FCR and FCU showed moderate peak activations (0.5–0.6), supporting existing studies that identify their role in

counteracting valgus forces and stabilizing the medial elbow [79]. Finally, both heads of the biceps showed spikes in activation during the arm acceleration phase, suggesting their importance in resisting the rapid elbow extension during pitches.

Table 5.3: Peak Muscle Activation During Arm Acceleration and Corresponding Throw Progression for the 93 MPH Simulation

Muscle	**Peak Activation (% Maximum)**	**Throw Progression at Peak (%)**
Anconeus (ANC)	57	90
Biceps Brachii Long Head (BIClong)	58	71
Biceps Brachii Short Head (BICshort)	59	82
Brachialis (BRA)	68	81
Flexor Carpi Radialis (FCR)	58	71
Flexor Carpi Ulnaris (FCU)	55	80
Flexor Digitorum Superficialis Index (FDSI)	58	72
Flexor Digitorum Superficialis Long (FDSL)	51	87
Flexor Digitorum Superficialis Middle (FDSM)	60	72
Flexor Digitorum Superficialis Ring (FDSR)	53	72
Palmaris Longus (PL)	53	79
Pronator Teres (PT)	73	82
Triceps Brachii Lateral Head (TRIlat)	81	83
Triceps Brachii Long Head (TRIlong)	92	73
Triceps Brachii Medial Head (TRImed)	80	84

Comparisons of muscle forces (Fig. 5.5) across the three case studies reveal consistent patterns in timing and magnitude, with the triceps (TRIlong, TRIlat, and TRImed) consistently generating the greatest forces during the arm acceleration phase (70% to 90%). The valgus torque minimization case showed lower overall muscle forces, reflecting reduced valgus load, while flexor–pronator muscles (e.g., FCU, FCR, and PT) exhibited greater forces during acceleration, aiding elbow stabilization and counteracting valgus torque. Despite differences in pitching speed and kinematics, muscle force trajectories were similar across case studies. The triceps compartments and flexor–pronator group consistently peaked during arm acceleration, suggesting their importance in elbow stabilization and dynamic protection [79].

Variations in ball speed may be attributed to differences in the kinematic contributions of the trunk, pelvis, and lower extremities, given the similarity of muscle force production across case studies. This result may suggest that, in an optimized throwing motion, the trajectory of the arm relative to the thorax should be similar even if the full-body mechanics differ. The similarity in arm trajectories despite different full–body mechanics is demonstrated in Fig. 5.6. For example, the 110 MPH simulation (Case 2) involved exaggerated contralateral trunk tilt and greater angular velocity of the throwing arm than Cases 1 and 3, increasing the speed of the ball but altering arm kinematics and dynamic

demands on the elbow. In contrast, the valgus torque minimization case (Case 3) utilized a sidearm motion with ipsilateral trunk tilt, reducing muscle forces yet maintaining consistent muscle force patterns. These findings underscore the interconnected nature of the pitching motion, where deviations in trunk mechanics affect elbow loads even if throwing arm trajectory remains relatively consistent (Fig. 5.6) [76]. The ability to maintain arm stability across varying pitching velocities and mechanics, despite changes in the kinetic chain due to altered trunk contributions, underscores the importance of integrated full-body optimization in analyses of pitching strategies [80].

Results of the muscle behaviour analysis align with the study by Seiber et al. [79], which highlighted the stabilizing role of the triceps, biceps, and brachialis in reducing varus–valgus laxity during dynamic elbow motion. Furthermore, comparisons to Buffi et al. [11] revealed similarities in muscle behaviour, where the triceps, biceps, and flexor–pronator groups demonstrated similar activation peaks and patterns during arm acceleration. Both studies identified the triceps compartments as primary contributors to the net varus moment at the elbow during peak valgus loading. This agreement demonstrates the biomechanical advantages of eccentric contractions during elbow flexion, which enable the triceps to generate high forces [67]. Furthermore, the dynamic interplay between the biceps and flexor–pronator groups, acting synergistically to protect the UCL, was consistent across the results of Buffi et al. [11], van der Pijl [12], and this model.

5.5.4 Simulated Kinematics

Comparison of simulated pitching kinematics revealed unique characteristics across the three case studies, emphasizing the optimizer's ability to generate solutions independently of input kinematics. Case 1 (93 MPH), which had plausible kinematics, was compared against the inverse kinematics data from motion capture and literature, since it most closely resembled the inverse kinematics solution (i.e. a traditional pitch). While joint trajectories for shoulder horizontal flexion/extension, elbow flexion/extension, and forearm pronation/supination were within plausible ROM, differences in magnitudes between experimental and simulated data were observed (Fig. 5.6). For example, the optimized Case 1 pitch simulation predicted lower elbow flexion during the late cocking phase and less angular displacement in forearm pronation. These discrepancies likely reflect the optimizer's minimization of actuation (C_i in Eq. (1)). Furthermore, notable differences were identified in the degree of elbow extension during the dynamic phases of the motion (Fig. 5.6). Rapid elbow extension is a key contributor to ball speed but also increases UCL loads, as supported by McCutcheon et al.'s study where they identified that faster pitchers consistently produced greater elbow extension velocity and greater UCL loads [78].

The differences in elbow extension at ball-release may stem from minimization of joint actuation, but also potentially from the bound on elbow angular velocity, which was set to 3000 °/s in this model. Fleisig [7] cites elbow extension angular velocities up to 2400 °/s in collegiate pitchers, which are likely greater in an MLB population. Despite never reaching the bound on elbow extension angular velocity, the optimizer was still able to achieve competitive ball speeds, which may be attributed to contributions from the trunk and shoulder. If true, the optimizer's ability to consistently achieve desired ball speeds suggests that pitchers can pitch competitively without the need for the elbow extension velocities that tend to increase loads on the UCL, through the adoption of altered trunk and shoulder mechanics. However, while the adoption of minimal shoulder abduction at ball release (seen in all simulated Cases) may have some benefits on reducing UCL load, it may increase the risk of injury elsewhere, such as the shoulders, which is also common and punishing to a pitcher's career [7, 10].

Notable differences in joint angle magnitudes were observed in shoulder abduction/adduction, where the optimized motion maintained a relatively static abduction angle, diverging from the trajectory observed in the inverse kinematic data. This difference may be a result of the optimizer's emphasis on minimizing full-body actuation (C_i in Eq. 2), which can reduce the observed ROM if actuation of that joint does not contribute to the optimization goal. Given that shoulder abduction/adduction actuation remained relatively constant (around 0.5), the minimized actuation primarily functioned to keep the arm statically abducted.

Comparison of kinematics between Buffi et al. [11] and Case 1 revealed both similarities and differences. Both studies captured consistent patterns in shoulder internal/external rotation and shoulder horizontal flexion/extension, validating the simulation's ability to model shoulder dynamics during arm cocking and acceleration phases. However, discrepancies in elbow flexion and forearm pronation were noted. For instance, Buffi et al. reported a sharper decrease in elbow flexion during acceleration compared to the smoother transition predicted by the optimizations. These differences likely stem from differences in modelling assumptions and optimization methodologies. The comparison of these optimization results with inverse kinematic data and the results of Buffi et al. [11] underscores the strengths and limitations of these results. While the agreement in shoulder dynamics validates the simulation's plausibility in achieving the observed mechanics in a pitcher, the discrepancies in elbow and forearm kinematics reveal areas for refinement, such as the addition of elbow and wrist joint coupling constraints.

5.6 Limitations of Forward Dynamic Work

The forward dynamics model presented in this study offers novel insights into pitching biomechanics but is not without limitations, which are critical to address for further refinement and validation. First and foremost, there is a significant challenge in comparing the results to existing literature. The lack of directly comparable studies or datasets makes it difficult to validate the simulated movements, particularly when the model produces unique or novel pitching motions that have no established precedent.

One specific assumption that warrants scrutiny is the contribution of the four compartments of the flexor digitorum superficialis (FDS). The model assumes that the force generated by each compartment directly contributes to a joint moment about the varus-valgus axis of the elbow. While this assumption is grounded in biomechanics, it requires further examination and experimental validation to ensure accuracy, particularly given the complexity of elbow joint dynamics. This is consistent with a limitation stated by Buffie et al [11].

Another limitation lies in the anatomical parameters of the model, which were obtained from multiple sources rather than a unified dataset. This approach, as noted by Goislard De Monsabert et al., can introduce biases in predicted muscle forces [81]. A model based on a single, comprehensive dataset would likely yield more accurate muscle force predictions. Unfortunately, no existing dataset includes all the anatomical parameters required for this model, making this an inherent limitation of the current study.

Additionally, the coupling of muscles and joint movements was ignored in this model. Some joints in the original muscles were designed to be coupled with other joint motions. For example, the scapulothoracic joint was removed entirely from the MSK model used in this research. Initially, the movement of this joint was coupled with that of the shoulder, meaning that movements in one of these joints would create reactionary movements in the other, due to their proximity and shared musculature (known as the shoulder rhythm). While this provides some simplicity to the model, it does not comprehensively account for all aspects of muscle function and interaction during pitching. These omissions may have reduced the fidelity of shoulder dynamics and affected the overall accuracy of the model.

The use of mean values from inverse kinematics for the initial guess, combined with a model scaled to the proportions of Pitcher 1, could also have introduced bias in the sensitivity studies. These factors may have limited the generalizability of the findings, as the model's structure inherently favours the biomechanics of a single individual, potentially influencing the outcomes when testing kinematics from other pitchers.

In summary, while the model provides insights into pitching biomechanics, several lim-

itations—including assumptions about joint moments, reliance on multi-source anatomical parameters, absence of a scapulothoracic joint, and challenges in validation highlight the need for refinement and integration of comprehensive datasets. These steps will be essential to improving the model's accuracy, reliability, and applicability in future studies.

Chapter 6

Conclusions

In this conclusive chapter, the research undertaken in this thesis is summarized and recommendations are made based on the results of the simulation experiments and analyses. The chapter concludes with suggestions for future research to help improve the models presented. This thesis presents a thorough biomechanical investigation of baseball pitching, focusing on optimizing performance while minimizing injury risks, particularly UCL injuries. The research is divided into three interconnected methodologies: Inverse Kinematics, Inverse Dynamics, and Forward Dynamics, each contributing unique insights into the complex mechanics of MLB-level pitching.

6.1 Project Summary

This research aimed to develop a detailed forward dynamic model of elite baseball pitchers to evaluate the impact that pitching mechanics have on the risk of UCL injuries, with the goal of balancing performance and injury mitigation. Leveraging advanced musculoskeletal modelling and optimal control methodologies, the study addressed gaps in understanding pitching mechanics by integrating data from professional athletes into an in-depth simulation framework.

Key contributions include a novel muscle-driven forward dynamic elbow model, scaled and tuned to replicate in-game mechanics, and detailed analyses of kinematic and kinetic factors influencing elbow valgus torque and UCL loading. The forward dynamic simulations provided insights into the individual biomechanical strategies pitchers employ to achieve competitive ball velocities, highlighting the variability in UCL loading across different mechanics.

Inverse dynamic analyses quantified the joint moments and forces during pitching, while forward dynamic simulations evaluated hypothetical scenarios, elucidating the physiological and biomechanical factors most critical to injury prevention and performance enhancement. These findings contribute to the development of personalized training protocols and equipment designs that could support long-term athlete health and performance sustainability.

6.1.1 Inverse Kinematics

The inverse kinematics phase reconstructed joint trajectories from high-resolution MoCap data. This analysis utilized V3D software to process segment transformation matrices, enabling calculation of joint angles and velocities. A carefully selected Cardan sequence (XYZ rotation) was employed to ensure consistency and alignment with the anatomical conventions used in the literature.

The analysis focused on key phases of the pitching motion, particularly the arm cocking and acceleration phases, where the greatest biomechanical loads on the elbow are experienced. These phases are critical as they coincide with peak valgus torque—a primary contributor to UCL stress and injury. Validation and evaluation efforts compared reconstructed kinematics to existing datasets from elite pitchers, demonstrating some accuracy and consistency with established biomechanical patterns. Namely, in comparison to the works of Fortenbaugh et al. [43] and Fleisig et al. [44], the average root mean square error between comparable joint kinematics at the various discrete pitching phases was around 20°. The differences between this work and that of the literature comes from the sample populations, where the references publications used amateur/collegiate level players whereas this work relied on professional kinematics.

Key findings from the inverse kinematics analysis underscored the importance of trunk rotation and shoulder external rotation in generating ball velocity, while also highlighting their role in the pitching motion. The results provided essential inputs for the subsequent inverse dynamics and forward dynamics analyses.

6.1.2 Inverse Dynamics

Building on the kinematic data, inverse dynamics quantified the forces and moments acting on key joints, with a particular focus on the shoulder and elbow. A detailed skeletal model was developed and scaled to match the anthropometric characteristics of each pitcher, incorporating a ball-hand complex to simulate realistic grip dynamics. The absence of

ground reaction force data was mitigated through a top-down approach to calculate joint kinetics.

The analysis revealed patterns in joint loading, particularly the prominence of valgus torque during the acceleration phase. This torque was identified as the primary mechanical contributor to UCL stress, aligning with known injury mechanisms in baseball pitching. Additionally, the study explored the influence of external factors, such as ball weight and grip position, on joint kinetics. Heavier balls were shown to significantly increase joint loads, while lighter balls reduced them. Similarly, an increased pitching cadence resulted in elevated forces, whereas a slower cadence alleviated joint forces. These findings emphasized the mechanical demands placed on the upper extremities during pitching.

Evaluation of the inverse dynamics was achieved by comparing calculated joint moments and forces with benchmarks from biomechanical studies on elite pitchers. The results demonstrated some alignment with expected kinetic patterns.

6.1.3 Forward Dynamics

The forward dynamic analysis offers a novel approach to understanding and optimizing the mechanics of baseball pitching, with a focus on minimizing the risk of UCL injuries while maintaining or enhancing performance. This study is the first predictive dynamic simulation of baseball pitching: we adopt a two-step approach that does not strictly track input kinematics and estimate muscle activations based on observed motions, as was done in previous studies [11, 12, 64]. The optimizer's ability to produce novel motions is evident from the unique simulation outputs of Cases 2 and 3, and emphasized by the differences in kinematics compared to experimental measurements and results reported in the literature. The cost functions, which were informed by documented performance and injury markers, were able to reasonably drive motion, mimicking the expected trade-offs of an elite pitcher's throws.

Simulation results highlighted the strategies pitchers use to achieve competitive pitch velocities. The model demonstrated that while aggressive mechanics, such as increased shoulder external rotation and excessive trunk tilt, are effective at generating greater ball velocities, they also increase UCL loads. The analysis underscored the critical role of the shoulder and elbow musculature, specifically the triceps and flexor–pronator group, in counteracting valgus torque during high-stress phases like arm cocking and acceleration. The results emphasize the importance of incorporating full-body dynamics and standardized musculoskeletal modelling methodologies to capture the complex interplay between pitching mechanics and injury risk.

The forward dynamics model has several limitations. The lack of directly comparable datasets or computational studies poses challenges for validation, particularly when novel pitching motions are simulated (Cases 2 and 3). Assumptions about the contributions of the flexor digitorum superficialis (FDS) compartments to joint moments, while biomechanically plausible, also require experimental validation [11]. The model's reliance on anatomical parameters from multiple sources introduces potential biases, as noted in prior studies, and the omission of the scapular motion relative to the thorax limits the accuracy of shoulder dynamics [81]. Finally, the use of mean inverse kinematic joint trajectories to inform the design of the model's DOF and scaling the anthropometry to a single pitcher may reduce the model's generalizability across diverse populations.

In summary, the results of this study bridge gaps in the understanding of pitching biomechanics. We present a thorough framework for simulating and optimizing pitching motions, emphasizing the importance of balancing performance objectives with injury prevention. The findings hold significant implications for personalized training programs, biomechanical interventions, and the development of advanced tools for real-time assessment of pitching mechanics.

6.2 Recommendations

The findings of this research offer actionable insights into optimizing pitching performance while minimizing the risk of UCL injuries, particularly through individualized training strategies and biomechanical interventions.

First, the inverse kinematics analysis emphasizes the importance of consistent and efficient mechanics during critical phases of the pitching motion, particularly the arm cocking and acceleration phases. Coaches and trainers should focus on refining shoulder external rotation and trunk rotation mechanics, as these were found to significantly influence ball velocity and UCL loading. Real-time MoCap tools can provide feedback to ensure pitchers maintain these optimal movement patterns during training.

Second, insights from the inverse dynamics analysis underscore the necessity of balancing pitching cadence and grip mechanics. Slower pitching cadences and lighter ball weights were shown to reduce joint forces, particularly valgus torque on the elbow, while heavier balls and faster cadences increased joint forces and torques. Training programs can incorporate drills with increased cadence or heavier balls to strain the muscles beyond their nominal use in games to further develop strength and stability in the shoulder and elbow joints. In contrast, slower cadence drills and the use of lighter balls can be used in

a rehabilitative environment or to refine pitching mechanics due to the reduced stresses observed using these techniques.

The forward dynamics simulations demonstrate the potential for muscle-driven optimization in reducing UCL loads. Conditioning programs should prioritize strengthening the shoulder and elbow musculature, particularly the flexor-pronator mass, which plays a critical role in stabilizing valgus torque. Exercises that enhance these muscles' capacity to resist excessive loads without compromising throwing velocity are highly recommended.

Additionally, the sensitivity analyses highlight the importance of individualized biomechanical profiles for pitchers. Every pitcher's unique mechanics result in different loading patterns, indicating that one-size-fits-all training programs may not effectively mitigate injury risks. Teams should leverage musculoskeletal modelling tools, as used in this research, to tailor training and recovery protocols to the specific needs of each athlete.

Finally, technological adoption is essential. Using markerless MoCap systems and integrating them with biomechanical simulation tools like OpenSim can offer real-time evaluations of pitching mechanics, enabling timely interventions. Moreover, advanced wearable technology that monitors elbow workload in-game can help identify risky mechanics before injuries occur. An examples of this technology includes the PULSE Throw Workload Monitor by Driveline Baseball.

By adopting these strategies, coaches and practitioners can not only enhance the performance of elite pitchers but also extend their careers by mitigating the risk of debilitating injuries like UCL tears. These recommendations bridge the gap between theoretical biomechanical insights and practical applications in professional baseball settings.

6.3 Future Research Opportunities

Several future directions can enhance the understanding of baseball pitching biomechanics while addressing areas for improvement. First, refining the anatomical accuracy of the model is critical. Developing a unified dataset of anatomical parameters can minimize biases introduced by varying sources, while including the scapulothoracic joint could better capture shoulder dynamics and the role of the scapula in stabilizing the pitching motion. Improved model validation is another key area. Collecting experimental data from elite pitchers, joint torque measurements, and muscle activation patterns, would provide direct validation of the model's predictions. On-mound force plates and similar technologies could further support these efforts by capturing dynamic interactions between the lower body and the pitching surface in the form of ground reaction forces, which can be used

to validate predicted joint kinetics. By collecting athlete-specific measurements such as anthropometrics, torque outputs (via dynamometers), and muscle activation patterns, the MSK model's proportions and the muscle models' dynamics used during the predictive forward dynamic simulations can be designed to the exact specification of the athletes, yielding more accurate results. Overall, the model as currently constructed cannot be truly validated, but efforts made to evaluate its efficacy show strong alignment with expected results.

Expanding the model to include coupled joint motions would allow for a deeper understanding of interdependencies during pitching motions. For example, the scapulothoracic joint was removed entirely from the MSK model used in this research. Initially, the movement of this joint was coupled with that of the shoulder, meaning that movements in one of these joints would create reactionary movements in the other, due to their proximity and shared musculature (known as the shoulder rhythm). The inclusion of this joint motion coupling in future work, in addition to others (i.e. lumbar and hip joints), would provide additional insight into the pitching mechanics and provide more realistic simulations. Investigating the specific contributions of individual muscle groups to joint torques and loads could also refine current assumptions about muscle function.

Additionally, future work should explore the contributions of the kinetic chain, particularly the lower body and trunk mechanics, to energy transfer and their effects on joint loading and pitch velocity. Simulating hypothetical scenarios, such as variations in pitching cadence, arm slot adjustments, or ball weight, could identify safer and more effective pitching strategies.

Optimization frameworks used in forward dynamics simulations could also be refined. Alternative cost functions that prioritize injury prevention while balancing performance optimization could improve the utility of the model. Robustness checks should be included to ensure that solutions generalize across a broader range of pitcher anthropometrics and mechanics. Longitudinal studies are another promising area, focusing on the progression of joint health and performance metrics in pitchers adhering to the model's recommendations. Observing the cumulative effects of repetitive pitching motions over a full season or career would provide valuable insights into injury prevention.

Environmental factors, such as weather conditions, mound consistency, and game scenarios, could also be integrated into future analyses to assess their impact on pitching biomechanics. Advanced data integration techniques, including machine learning, could further enhance predictive capabilities by dynamically adjusting pitching mechanics in response to real-time biomechanical data. Incorporating a dynamic baseball trajectory model would also assist in the adoption of this model as a more valuable tool, to see whether the

predicted motions can truly achieve the expected performance metrics. The physics-based trajectory model could highlight whether the predicted throwing conditions truly achieve desired fastball velocity, but also if the throws were a strike. Finally, a focused investigation into the ball-release phase would improve the accuracy of modelling release dynamics, particularly the forces and moments during this critical phase, offering deeper insights into pitch effectiveness.

By addressing these opportunities, future research can bridge existing gaps, improve the practical applicability of biomechanical models, and further the dual objectives of optimizing performance and preventing injuries in elite baseball pitchers. These directions hold significant potential for advancing the field and providing actionable insights for athletes, coaches, and sports scientists.

References

[1] C. Gough, "Major league baseball (MLB) - statistics and facts," Statista, February 2024, accessed 6 June 2024. [Online]. Available: https://www.statista.com/topics/968/major-league-baseball/#topicOverview

[2] "Roster Resource - 40-man Roster Breakdown," FanGraphs, June 2024, accessed 6 June 2024. [Online]. Available: https://www.fangraphs.com/roster-resource/breakdowns/40-man-roster

[3] "MLB team salary payroll tracker," Sportrac, 2024. [Online]. Available: https://www.spotrac.com/mlb/payroll/_/year/2024/sort/cap_maximum_space2

[4] S. F. DeFroda, P. K. Kriz, A. M. Hall, D. Zurakowski, and P. D. Fadale, "Risk stratification for ulnar collateral ligament injury in major league baseball players: A retrospective study from 2007 to 2014," *Orthop. J. Sports Med.*, vol. 4, no. 2, p. 2325967115627126, 2016. [Online]. Available: https://doi.org/10.1177/2325967115627126

[5] P. N. Chalmers, B. J. Erickson, B. Ball, A. A. Romeo, and N. N. Verma, "Fastball pitch velocity helps predict ulnar collateral ligament reconstruction in Major League Baseball pitchers," *Am. J. Sports Med.*, vol. 44, no. 8, pp. 2130–2135, 2016.

[6] G. Lacques. (2023, August) Velocity at what cost? MLB's hardest throwers keep succumbing to Tommy John surgery. USA Today. [Online]. Available: https://www.usatoday.com/story/sports/mlb/columnist/gabe-lacques/2023/08/31/tommy-john-surgery-mlb-hardest-throwers-shohei-ohtani/70721548007/

[7] G. Fleisig, "Biomechanics of baseball pitching: Implications for injury and performance," in *Proc. 28th Int. Conf. Biomech. Sports, Marquette, MI, USA, July 19–23*, July 2010, pp. 46–50.

[8] A. M. Pappas, R. M. Zawacki, and T. J. Sullivan, "Biomechanics of baseball pitching: A preliminary report," *Am. J.Sports Med.*, vol. 13, no. 4, 1985.

[9] A. Z. Diffendaffer, M. S. Bagwell, G. S. Fleisig, Y. Yanagita, M. Stewart, E. L. Cain, J. R. Dugas, and K. E. Wilk, "The clinician's guide to baseball pitching biomechanics," *Sports Health*, vol. 15, no. 2, pp. 274–281, March 2023, PMID: 35465789. [Online]. Available: https://doi.org/10.1177/19417381221078537

[10] A. L. Aguinaldo and H. Chambers, "Correlation of throwing mechanics with elbow valgus load in adult baseball pitchers," *Am. J. Sports Med.*, vol. 37, no. 10, pp. 2043–2048, 2009.

[11] J. H. Buffi, K. Werner, T. Kepple, and W. M. Murray, "Computing muscle, ligament, and osseous contributions to the elbow varus moment during baseball pitching," *Ann. Biomed. Eng.*, vol. 43, no. 2, pp. 404–415, 2015.

[12] L. D. van der Pijl, "Identification of muscles (un)loading the UCL during baseball pitching," Master's thesis, Delft University of Technology, Delft, Netherlands, 2022.

[13] N. Fujii and M. Hubbard, "Validation of a three-dimensional baseball pitching model," *J. Appl. Biomech.*, vol. 18, pp. 135–154, 2002. [Online]. Available: https://api.semanticscholar.org/CorpusID:110387497

[14] G. S. Fleisig, R. F. Escamilla, J. R. Andrews, T. Matsuo, Y. Satterwhite, and S. W. Barrentine, "Kinematic and kinetic comparison between baseball pitching and football passing," *J. Appl. Biomech.*, vol. 12, no. 2, pp. 207 – 224, 1996. [Online]. Available: https://doi.org/10.1123/jab.12.2.207

[15] D. F. Stodden, G. S. Fleisig, S. P. McLean, and J. R. Andrews, "Relationship of biomechanical factors to baseball pitching velocity: Within pitcher variation," *J. Appl. Biomech.*, vol. 21, no. 1, pp. 44 – 56, 2005. [Online]. Available: https://doi.org/10.1123/jab.21.1.44

[16] A. Hazari, A. G. Maiya, and T. V. Nagda, *Conceptual Biomechanics and Kinesiology*. Springer, 2022, ch. 1, pp. 2–10.

[17] G. S. Fleisig, A. Z. Diffendaffer, B. Ivey, K. T. Aune, W. A. Laughlin, and D. Fortenbaugh, "Comparison of marker-less and marker-based motion capture for baseball pitching kinematics," *Sports Biomech.*, pp. 1–10, 2022. [Online]. Available: https://doi.org/10.1080/14763141.2022.2076608

[18] K. Das, T. de Paula Oliveira, and J. Newell, "Comparison of markerless and marker-based motion capture systems using 95% functional limits of agreement in a linear mixed-effects modelling framework," *Nature Scientif. Rep.*, vol. 13, p. 22880, 2023. [Online]. Available: https://doi.org/10.1038/s41598-023-49360-2

[19] L. Wade, L. Needham, P. McGuigan, and J. Bilzon, "Applications and limitations of current markerless motion capture methods for clinical gait biomechanics," *PeerJ*, vol. 10, p. e12995, Feb 2022. [Online]. Available: https://doi.org/10.7717/peerj.12995

[20] G. J. Calabrese, "Pitching mechanics, revisited," *Int. J. Sports Phys. Ther.*, vol. 8, no. 5, pp. 652–660, Oct 2013.

[21] M. E. Feltner and J. Dapena, "Three-dimensional interactions in a two-segment kinetic chain. part i: General model," *Int. J Sports Biomech.*, vol. 5, no. 4, pp. 403 – 419, 1989. [Online]. Available: https://doi.org/10.1123/ijsb.5.4.403

[22] R. Alexander, "Optimum timing of muscle activation for simple models of throwing," *J. Theoret. Bio.*, vol. 150, no. 3, pp. 349–372, 1991. [Online]. Available: https://doi.org/10.1016/S0022-5193(05)80434-5

[23] D. P. Leland, S. Conte, N. Flynn, N. Conte, K. Crenshaw, K. E. Wilk, and C. L. Camp, "Prevalence of medial ulnar collateral ligament surgery in 6135 current professional baseball players: A 2018 update," *Orthop. J. Sports Med.*, vol. 7, no. 9, p. 2325967119871442, 2019.

[24] B. Van-Trigt, L. W. Vliegen, T. Leenen, and D. H. Veeger, "The ulnar collateral ligament loading paradox between in-vitro and in-vivo studies on baseball pitching (narrative review)," *Int. Biomech.*, vol. 8, no. 1, pp. 19–29, 2021, PMID: 33998377. [Online]. Available: https://doi.org/10.1080/23335432.2021.1916405

[25] A. L. Aguinaldo and H. Chambers, "Correlation of throwing mechanics with elbow valgus load in adult baseball pitchers," *Am. J. Sports. Med.*, vol. 37, no. 10, pp. 2043–2048, 2009, PMID: 19633230. [Online]. Available: https://doi.org/10.1177/0363546509336721

[26] T. Yanai, K. Onuma, R. L. Crotin, and D. Monda, "A novel method intersecting three-dimensional motion capture and medial elbow strength dynamometry to assess elbow injury risk in baseball pitchers," *Sci. Rep.*, vol. 13, no. 1, p. 12253, 2023.

[27] UBC Wiki contributors. (2020) Ulnar collateral ligament (ucl) injuries in baseball. Accessed: 2025-06-02. [Online]. Available: https://wiki.ubc.ca/Documentation:FIB_book/Ulnar_Collateral_Ligament_(UCL)_Injuries_in_Baseball

[28] S. L. Werner, G. S. Fleisig, C. J. Dillman, and J. R. Andrews, "Relationship between throwing mechanics and elbow valgus in professional baseball pitchers," *J. Shoulder Elbow Surg.*, vol. 11, no. 2, pp. 151–155, 2002.

[29] E. Otten, "Inverse and forward dynamics: Models of multi-body systems," *Phil. Trans. Roy. Soc. Lond. Series B, Biol. Sci.*, vol. 358, no. 1437, pp. 1493–1500, 2003. [Online]. Available: https://doi.org/10.1098/rstb.2003.1354

[30] M. Shourijeh and J. McPhee, "Optimal control and forward dynamics of human periodic motions using fourier series for muscle excitation patterns," *J. Comp. Nonlin. Dyn.*, vol. 9, pp. 1–7, Published 2013.

[31] M. E. Feltner, "Three-dimensional interactions in a two-segment kinetic chain. Part II: Application to the throwing arm in baseball pitching," *J. Appl. Biomech.*, vol. 5, no. 4, pp. 420–450, 1989.

[32] T. Matsuo, G. S. Fleisig, N. Zheng, and J. R. Andrews, "Fluence of shoulder abduction and lateral trunk tilt on peak elbow varus torque for college baseball pitchers during simulated pitching," *J. Appl. Biomech.*, vol. 22, no. 2, pp. 93–102, 2006. [Online]. Available: https://doi.or/10.1123/jab.22.2.93

[33] K. Naito, T. Takagi, H. Kubota, and T. Maruyama, "Multi-body dynamic coupling mechanism for generating throwing arm velocity during baseball pitching," *Hum. Mov. Sci.*, vol. 54, pp. 363–376, 2017. [Online]. Available: https://doi.org/10.1016/j.humov.2017.05.013

[34] G. J. Alderink, S. R. Ely, B. D. H. Bliven, B. G. Rettig, and C. A. LaBella, "Upper body contributions to pitched ball velocity in elite high school pitchers using an induced velocity analysis," *J. Biomech.*, vol. 120, p. 110360, 2021.

[35] S. A. McErlain-Naylor, M. A. King, and P. J. Felton, "A review of forward-dynamics simulation models for predicting optimal technique in maximal effort sporting movements," *Appl. Sci.*, vol. 11, no. 4, 2021. [Online]. Available: https://doi.org/10.3390/app11041450

[36] "Kinatrax motion capture," KinaTrax, accessed 14 June 2024. [Online]. Available: https://www.kinatrax.com/kinatrax-motion-capture/#in-game

[37] X. Zhao, G. Ross, B. Dowling, and R. B. Graham, "Three-dimensional motion capture data of a movement screen from 183 athletes," *Sci. Data*, vol. 10, no. 1, p. 235, apr 2023. [Online]. Available: https://doi.org/10.1038/s41597-023-02082-6

[38] The MathWorks Inc, "Matlab version: R2023b," Natick, Massachusetts, United States, 2024. [Online]. Available: https://www.mathworks.com

[39] C. I. Dillman, G. S. Fleisig, and J. R. Andrews, "Biomechanics of pitching with emphasis upon shoulder kinematics," *Journal of Orthopaedic and Sports Physical Therapy*, vol. 18, no. 2, pp. 402–408, 1993. [Online]. Available: https://www.jospt.org/doi/10.2519/jospt.1993.18.2.402

[40] HAS-Motion, "Visual3d documentation," Kingston, Ontario, Canada, 2024. [Online]. Available: https://wiki.has-motion.com/Visual3D_Documentation

[41] G. Wu, F. C. van der Helm, H. (DirkJan) Veeger, M. Makhsous, P. Van Roy, C. Anglin, J. Nagels, A. R. Karduna, K. McQuade, X. Wang, F. W. Werner, and B. Buchholz, "Isb recommendation on definitions of joint coordinate systems of various joints for the reporting of human joint motion—part ii: shoulder, elbow, wrist and hand," *J. Biomech.*, vol. 38, no. 5, pp. 981–992, 2005. [Online]. Available: https://doi.org/10.1016/j.jbiomech.2004.05.042

[42] R. F. Escamilla, J. S. Slowik, A. Z. Diffendaffer, and G. S. Fleisig, "Differences among overhand, three-quarter, and sidearm pitching biomechanics in professional baseball players," *Journal of Applied Biomechanics*, 2018, published online April 13, 2018.

[43] D. Fortenbaugh, G. S. Fleisig, and J. R. Andrews, "Baseball pitching biomechanics in relation to injury risk and performance," *Sports Health*, vol. 1, no. 4, pp. 314–320, 2009.

[44] G. S. Fleisig, B. Bolt, D. Fortenbaugh, K. E. Wilk, and J. R. Andrews, "Biomechanical comparison of baseball pitching and long-toss: implications for training and rehabilitation," *J. Orthop. Sports Phys. Ther.*, vol. 41, no. 5, pp. 296–303, 2011.

[45] P. de Leva, "Adjustments to Zatsiorsky-Seluyanov's segment inertia parameters," *J. Biomech.*, vol. 29, no. 9, pp. 1223–1230, 1996. [Online]. Available: https://doi.org/10.1016/0021-9290(95)00178-6

[46] P. T. Donahue, E. Beiser, S. J. Wilson, and J. C. Garner, "Comparison of anthropometrics and physical performance in professional baseball pitchers,"

J. Trainology, vol. 9, no. 2, pp. 39–42, 2020. [Online]. Available: https://doi.org/10.17338/trainology.9.2_39

[47] A. M. Nathan, J. Hopkins, L. Chong, and H. Kaczmarski, "The effect of spin on the flight of a baseball," in *The Engineering of Sport 6*. New York, NY: Springer New York, May 2006, pp. 23–28. [Online]. Available: https://doi.org/10.1007/978-0-387-46050-5_5

[48] K. Werling, N. A. Bianco, M. Raitor, J. Stingel, J. L. Hicks, S. H. Collins, S. L. Delp, and C. K. Liu, "Addbiomechanics: Automating model scaling, inverse kinematics, and inverse dynamics from human motion data through sequential optimization," *bioRxiv*, September 2023. [Online]. Available: https://doi.org/10.1101/2023.06.15.545116

[49] G. S. Fleisig, J. R. Andrews, R. F. Dillman, and N. H. Escamilla, "Kinetics of baseball pitching with implications about injury mechanisms," *Am. J. Sports Med.*, vol. 23, no. 2, pp. 233–239, 1995.

[50] Y. Kaizu, H. Watanabe, and T. Yamaji, "Correlation of upper limb joint load with simultaneous throwing mechanics including acceleration parameters in amateur baseball pitchers," *J. Phys. Ther. Sci.*, vol. 30, no. 2, pp. 223–230, 2018.

[51] A. W. Anz, B. D. Bushnell, L. P. Griffin, T. J. Noonan, M. R. Torry, and R. J. Hawkins, "Correlation of torque and elbow injury in professional baseball pitchers," *Am. J. Sports Med.*, vol. 38, no. 7, pp. 1368–1374, 2010.

[52] M. R. Acosta, J. M. Van Ness, W. P. Lydon, B. G. Graham, A. C. King, and C. D. Jensen, "Biceps and triceps contribute to pitching performance in college baseball," June 2019, med. Sci. Sports Exerc. **51**(6S), p.65.

[53] B. R. K. H. T. Melugin and s. Falsone, "The evidence behind weighted ball throwing programs for the baseball player: Do they work and are they safe?" *Sports Heal. Multidisc. Appr.*, vol. 13, no. 1, pp. 49–55, 2021.

[54] J. Lemire, "Driveline baseball, kinatrax partner on joint research validation study," Sports Bus. J., January 2019. [Online]. Available: https://www.sportsbusinessjournal.com/Daily/Issues/2019/01/16/Technology/driveline-baseball-kinatrax-pitching-biomechanics-research.aspx

[55] Z. Ripic, J. F. Signorile, C. Kuenze, and M. Eltoukhy, "Concurrent validity of artificial intelligence-based markerless motion capture for over-ground gait analysis:

A study of spatiotemporal parameters," *J. Biomech.*, vol. 143, 2022. [Online]. Available: https://doi.org/10.1016/j.jbiomech.2022.111278

[56] Z. Ripic, J. F. Signorile, T. M. Best, K. A. Jacobs, M. Nienhuis, C. Whitelaw, C. Moenning, and M. Eltoukhy, "Validity of artificial intelligence-based markerless motion capture system for clinical gait analysis: Spatiotemporal results in healthy adults and adults with parkinson's disease," *J. Biomech.*, vol. 155, 2023. [Online]. Available: https://doi.org/10.1016/j.jbiomech.2023.111645

[57] B. E. W. Xuan, S. S. Chan, H. Johan, L. S. Lim, B. Zuo, and W. T. Ang, "Investigation of modeling differences between OpenSim and Visual3D for gait analysis of healthy gait," in *Proc. 16th Int. Conv. Rehabil. Eng. Assist. Tech.* New York, NY, USA: Asssoc. Comp. Mach., 2023, pp. 42–46.

[58] S. L. Delp, F. C. Anderson, A. S. Arnold, P. Loan, A. Habib, C. T. John, E. Guendelman, and D. G. Thelen, "OpenSim: Open-source software to create and analyze dynamic simulations of movement," *IEEE Trans. Biomed. Eng.*, vol. 54, no. 11, pp. 1940–1950, 2007.

[59] S. D. Uhlrich, T. K. Uchida, M. R. Lee, and S. L. Delp, "Ten steps to becoming a musculoskeletal simulation expert: A half-century of progress and outlook for the future," *J. Biomech.*, vol. 154, p. 111623, 2023. [Online]. Available: https://www.sciencedirect.com/science/article/pii/S0021929023001926

[60] S. L. Delp, J. P. Loan, M. G. Hoy, F. E. Zajac, E. L. Topp, and J. M. Rosen, "An interactive graphics-based model of the lower extremity to study orthopaedic surgical procedures," *IEEE Transac. Biomed. Eng.*, vol. 37, pp. 757–767, 1990.

[61] F. C. Anderson and M. G. Pandy, "Dynamic optimization of human walking," *J. Biomech. Eng.*, vol. 123, no. 5, pp. 381–390, 2001.

[62] K. R. Holzbaur, W. M. Murray, and S. L. Delp, "A model of the upper extremity for simulating musculoskeletal surgery and analyzing neuromuscular control," *Ann. Biomed. Eng.*, vol. 33, no. 6, pp. 829–840, Jun 2005.

[63] G. T. Yamaguchi and F. E. Zajac, "A planar model of the knee joint to characterize the knee extensor mechanism," *J. Biomech.*, vol. 22, no. 1, pp. 1–10, 1989.

[64] F. C. Anderson and M. G. Pandy, "A dynamic optimization solution for vertical jumping in three dimensions," *Comput. Method. Biomech. Biomed. Eng.*, vol. 2, no. 3, pp. 201–231, 1999.

[65] W. T. Dempster and G. R. L. Gaughran, "Properties of body segments based on size and weight," *Am. J. Anat.*, vol. 120, no. 1, pp. 33–54, 1967.

[66] K. E. Wilk, C. A. Arrigo, M. S. Bagwell, M. A. Rothermich, and J. R. Dugas, "Repair of the ulnar collateral ligament of the elbow: Rehabilitation following internal brace surgery," *J. Orthop. Sports Phys. Ther.*, vol. 49, no. 4, pp. 253–261, Apr 2019.

[67] M. Millard, T. Uchida, A. Seth, and S. L. Delp, "Flexing computational muscle: Modeling and simulation of musculotendon dynamics," *J. Biomech. Eng.*, vol. 135, no. 2, p. 021005, 2013.

[68] T. Hortobágyi and F. I. Katch, "Eccentric and concentric torque–velocity relationships during arm flexion and extension—influence of strength level," *Eur. J. Appl. Physiol.*, vol. 60, pp. 395–401, 1990.

[69] D. Cazzola, T. P. Holsgrove, E. Preatoni, H. S. Gill, and G. Trewartha, "Cervical spine injuries: A whole-body musculoskeletal model for the analysis of spinal loading," pp. –, Jan 2017, pLoS ONE **12**(1), e0169329.

[70] D. K. Ramsey and R. L. Crotin, "Stride length impacts on sagittal knee biomechanics in flat ground baseball pitching," *Appl. Sci.*, vol. 12, no. 3, p. 995, 2022.

[71] S. L. Werner, G. S. Fleisig, C. J. Dillman, and J. R. Andrews, "Biomechanics of the elbow during baseball pitching," *J. Orthop. Sports Phys. Ther.*, vol. 17, no. 6, pp. 274–278, Jun 1993.

[72] B. Van Trigt, L. W. Vliegen, T. Leenen, and D. H. Veeger, "The ulnar collateral ligament loading paradox between in-vitro and in-vivo studies on baseball pitching (narrative review)," *Int. Biomech.*, vol. 8, no. 1, pp. 19–29, 2021.

[73] C. L. Dembia, N. A. Bianco, A. Falisse, J. L. Hicks, and S. L. Delp, "OpenSim Moco: Musculoskeletal optimal control," 12 2020, PLoS Comp. Biol. **16**(12), e1008493.

[74] A. N. Denton and B. R. Umberger, "Computational performance of musculoskeletal simulation in OpenSim Moco using parallel computing," 2023, int. J. Numer. Method. Biomed. Eng. **39**(12), e3777.

[75] Major League Baseball, "Baseball savant - pitch arsenals leaderboard," 2024, accessed: 2024-11-08. [Online]. Available: https://baseballsavant.mlb.com/leaderboard/pitch-arsenals

[76] M. Kageyama, T. Sugiyama, Y. Takai, H. Kanehisa, and A. Maeda, "Kinematic and kinetic profiles of trunk and lower limbs during baseball pitching in collegiate pitchers," *J. Sports Sci. Med.*, vol. 13, no. 4, pp. 742–750, Dec 2014.

[77] S. Hakanson, S. T. Johnson, E. C. Norcross, and C. N. Brown, "The effects of contralateral trunk tilt on elbow varus torque in baseball pitchers: A critically appraised topic," *J. Sport. Rehabil.*, vol. 30, no. 8, pp. 1214–1219, 2021.

[78] T. W. McCutcheon, J. S. Slowik, and G. S. Fleisig, "Kinematic parameters associated with elbow varus torque in elite adult baseball pitchers," *Orthop. J. Sports Med.*, vol. 13, no. 2, 2025.

[79] K. Seiber, R. Gupta, M. H. McGarry, M. R. Safran, and T. Q. Lee, "The role of the elbow musculature, forearm rotation, and elbow flexion in elbow stability: An in vitro study," *J. Shoulder Elbow Surg.*, vol. 18, no. 2, pp. 260–268, 2009.

[80] G. S. Fleisig, J. R. Andrews, C. J. Dillman, and R. F. Escamilla, "Kinetics of baseball pitching with implications about injury mechanisms," *Am. J. Sports Med.*, vol. 23, no. 2, pp. 233–239, 1995.

[81] B. Goislard de Monsabert, G. Rao, A. Gay, E. Berton, and L. Vigouroux, "A scaling method to individualise muscle force capacities in musculoskeletal models of the hand and wrist using isometric strength measurements," *Med. Biol. Eng. Comput.*, vol. 55, no. 12, pp. 2227–2244, 2017.

APPENDICES

Appendix A

Selected Angular Kinematics and Joint Movement Definitions for Inverse Kinematic Analysis

Table A.1: Joint definitions and degrees of freedom for inverse kinematic analysis

	Joints	Child Segment	Parent Segment	DOF	Axis	Positive Agonist	Negative Antagonist
Lead	Elbow	Forearm	Upper Arm	1	x	Flexion	Extension
	Shoulder	Upper Arm	Thorax/Abdomen	2	x	Horizontal Flexion	Horizontal Extension
					y	Abduction	Adduction
	Knee	Shank	Thigh	1	x	Extension	Flexion
	Hip	Thigh	Pelvis	2	x	Flexion	Extension
					y	Abduction	Adduction
Throwing	Wrist	Hand	Forearm	2	x	Flexion	Extension
					y	Ulnar Deviation	Radial Deviation
	Elbow	Forearm	Upper Arm	2	x	Flexion	Extension
					z	Pronation	Supination
	Shoulder	Upper Arm	Thorax/Abdomen	3	x	Horizontal Flexion	Horizontal Extension
					y	Adduction	Abduction
					z	Internal Rotation	External Rotation
	Knee	Shank	Thigh	1	x	Extension	Flexion
	Hip	Thigh	Pelvis	1	x	Flexion	Extension
Chest	Trunk	Thorax/Abdomen	Pelvis	3	x	Posterior Tilt	Anterior Tilt
					y	Contralateral Tilt	Ipsilateral Tilt
					z	Contralateral Rotation	Ipsilateral Rotation

The joint movements are defined based on the definitions of the LCS as seen in Fig. 3.3. A few things to note are that while pronation and supination are initiated at the wrist joint in the human body, they are defined as an elbow DOF, since it is considered to be the relative rotation of the forearm, against the upper arm, where those two segments span the elbow joint. Furthermore, ipsilateral movements in this case are defined as the movements that trend towards the throwing arm, which is right for all subjects, and contralateral pertains to trending away from the throwing arm.

Appendix B

Inverse Kinematic Results of Interest

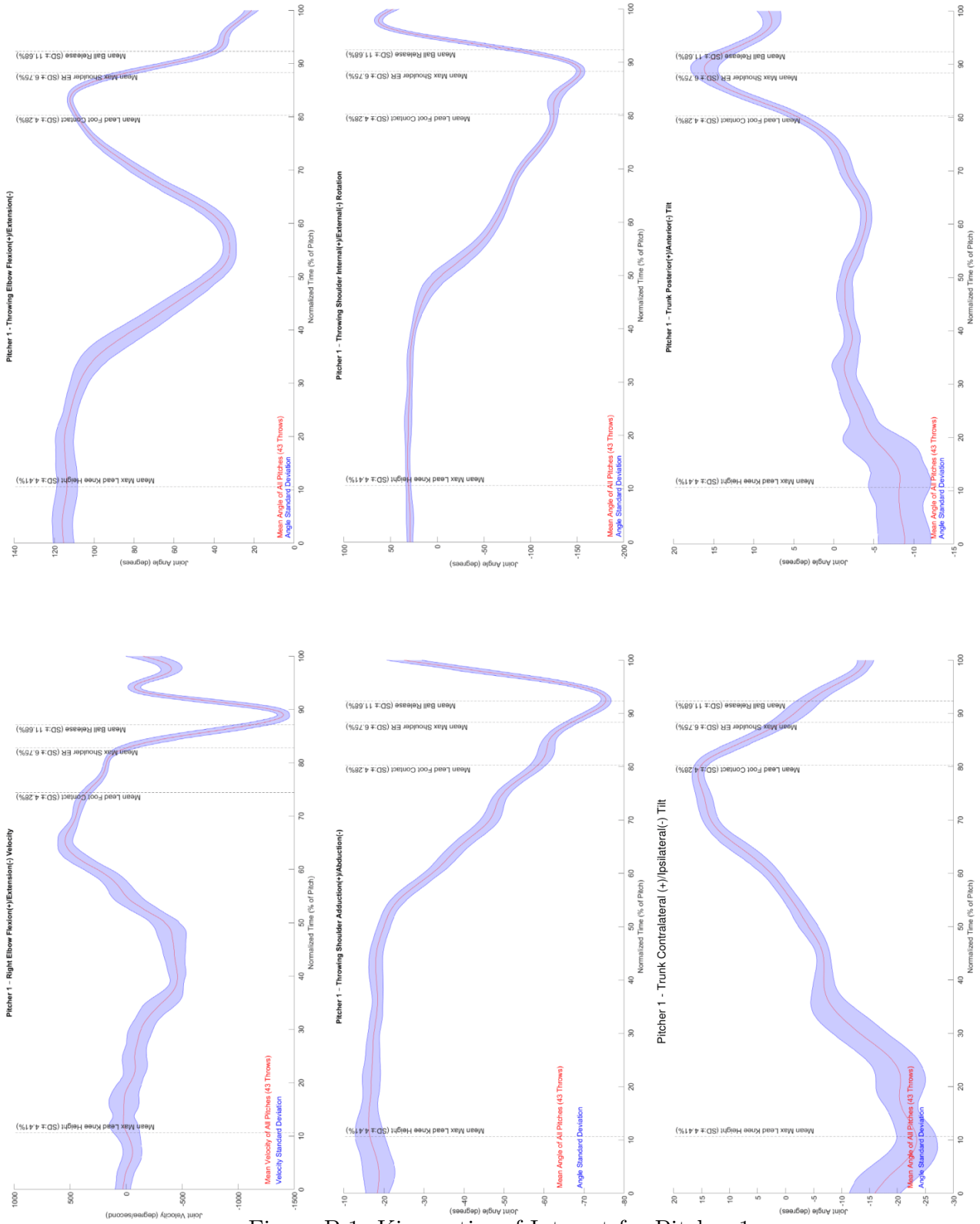


Figure B.1: Kinematics of Interest for Pitcher 1

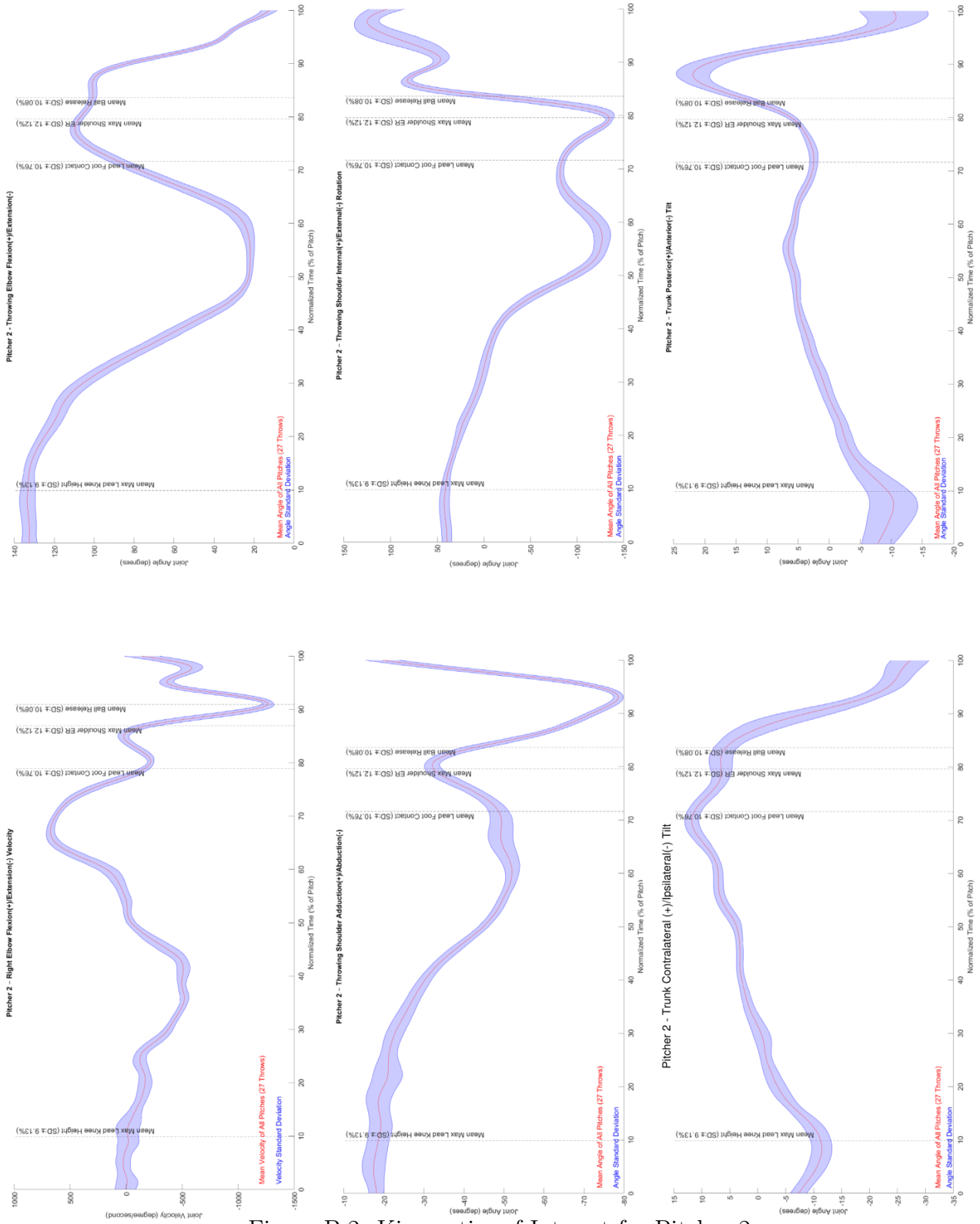


Figure B.2: Kinematics of Interest for Pitcher 2

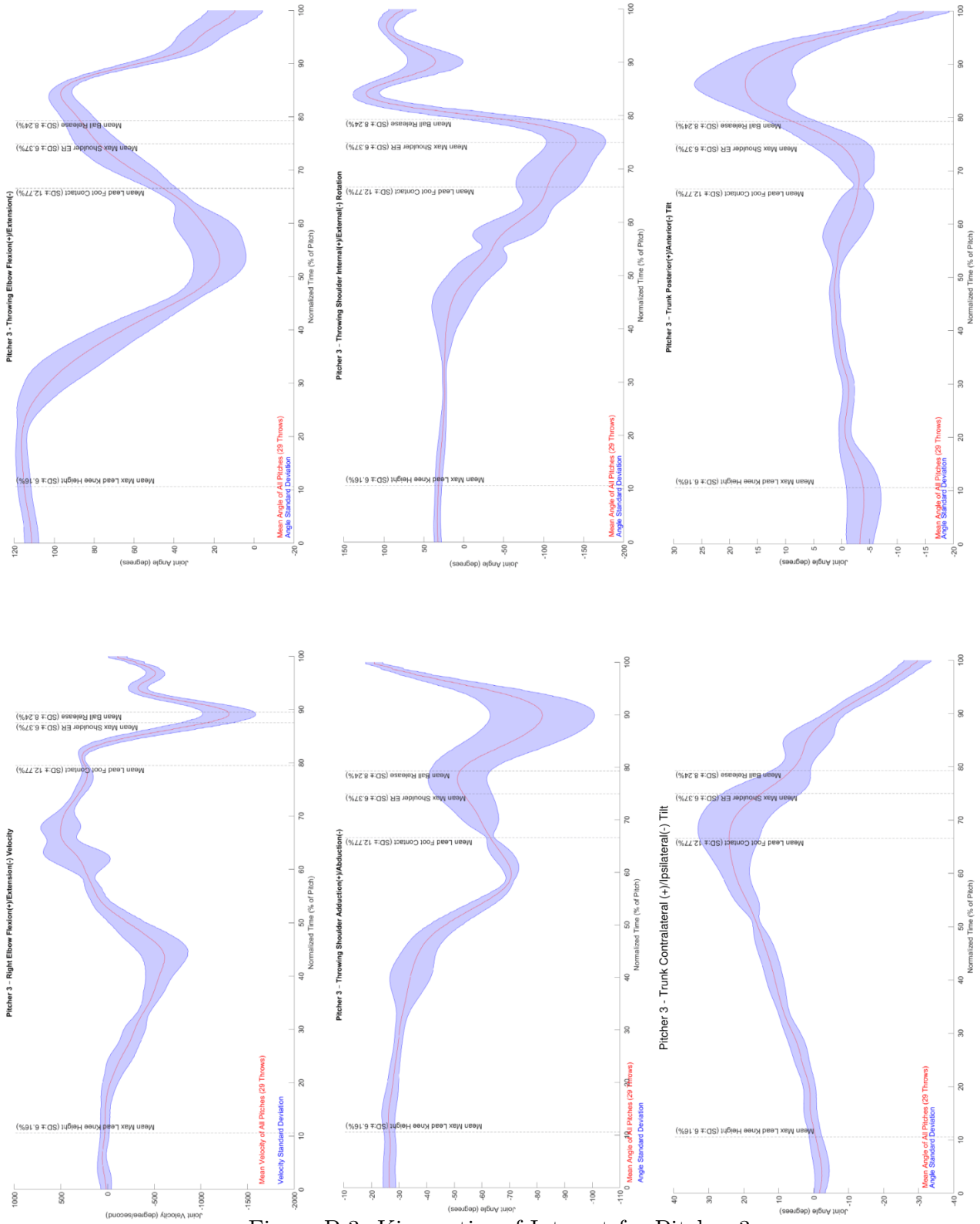


Figure B.3: Kinematics of Interest for Pitcher 3

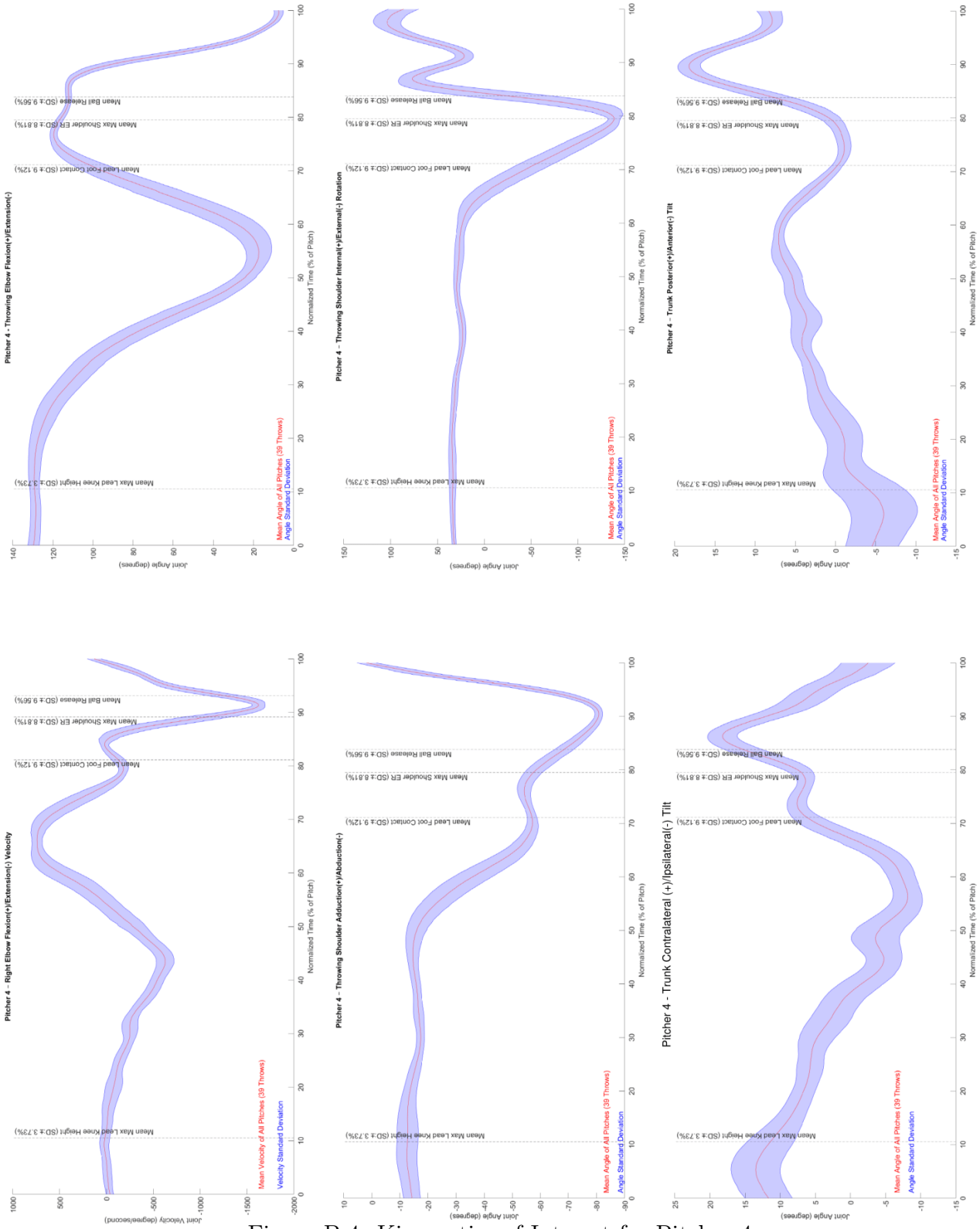


Figure B.4: Kinematics of Interest for Pitcher 4

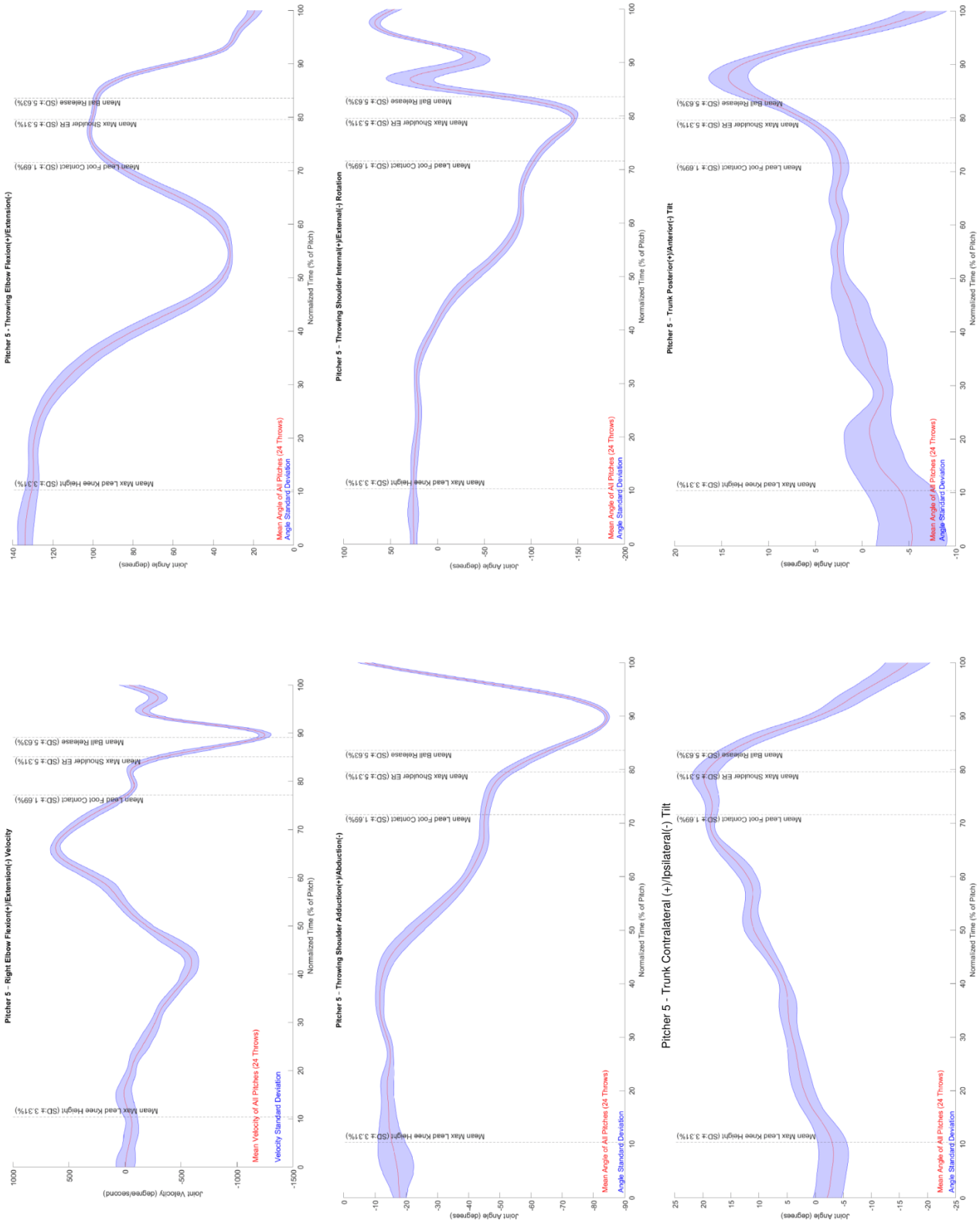


Figure B.5: Kinematics of Interest for Pitcher 5

Appendix C

Inverse Dynamic Results of Interest

The forces and moments outputted were all defined with respect to the parent segment in V3D. These dynamics are reactionary which means that they create an equal and opposite force on the child segment. For example, the humerus (parent segment), is experiencing a varus moment at MER, meaning that the forearm (child segment) is under a valgus torque, which is expected during this stage of the pitch. All shoulder dynamics presented are the forces and moments that the thorax (glenohumeral socket) experience, while the elbow dynamics shown are with respect to the humerus. The parent frame was selected since it aligns with ISB standards for inverse dynamics, made the most sense with the defined local join coordinate systems and is best practice in V3D inverse dynamics [40,41].

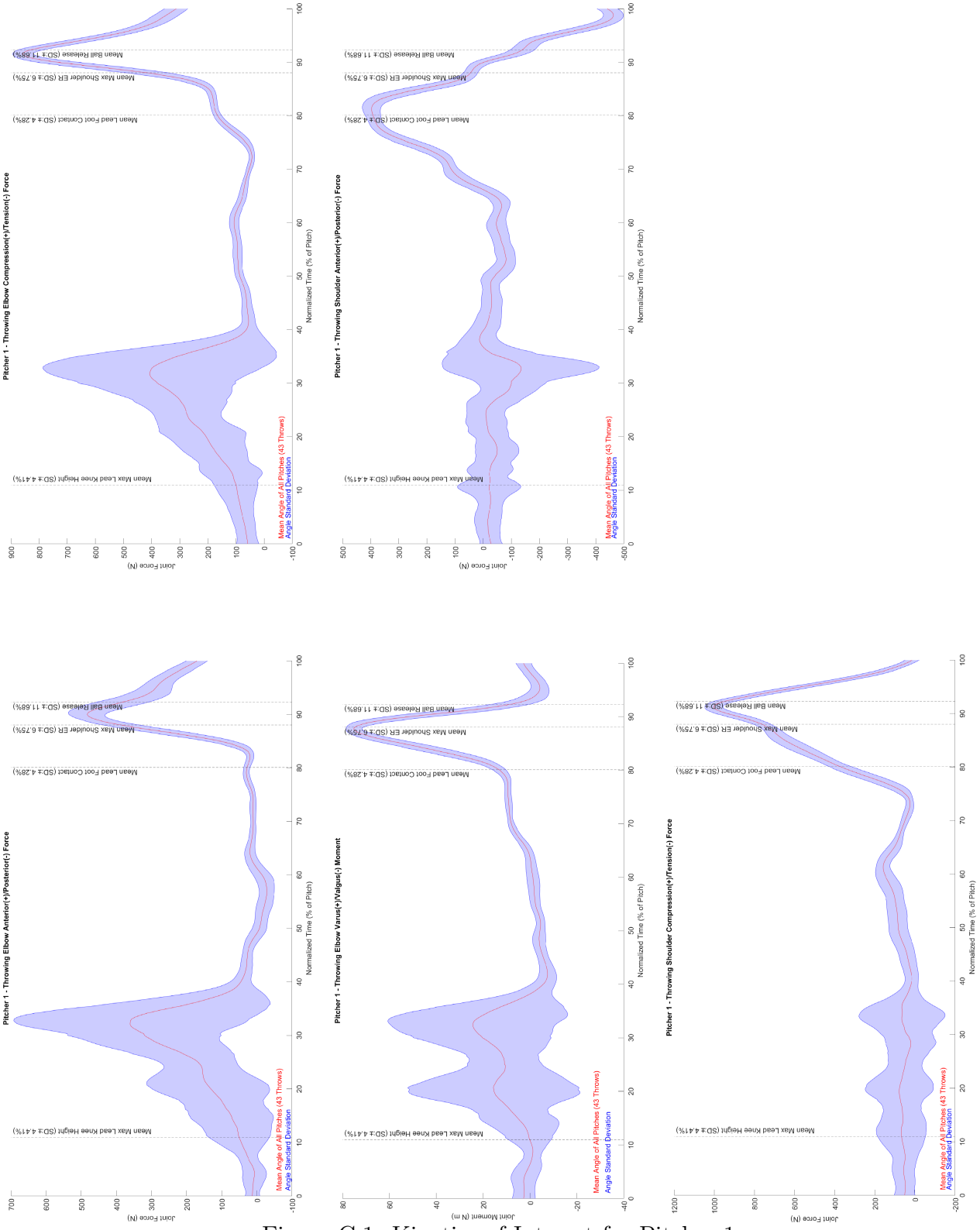


Figure C.1: Kinetics of Interest for Pitcher 1

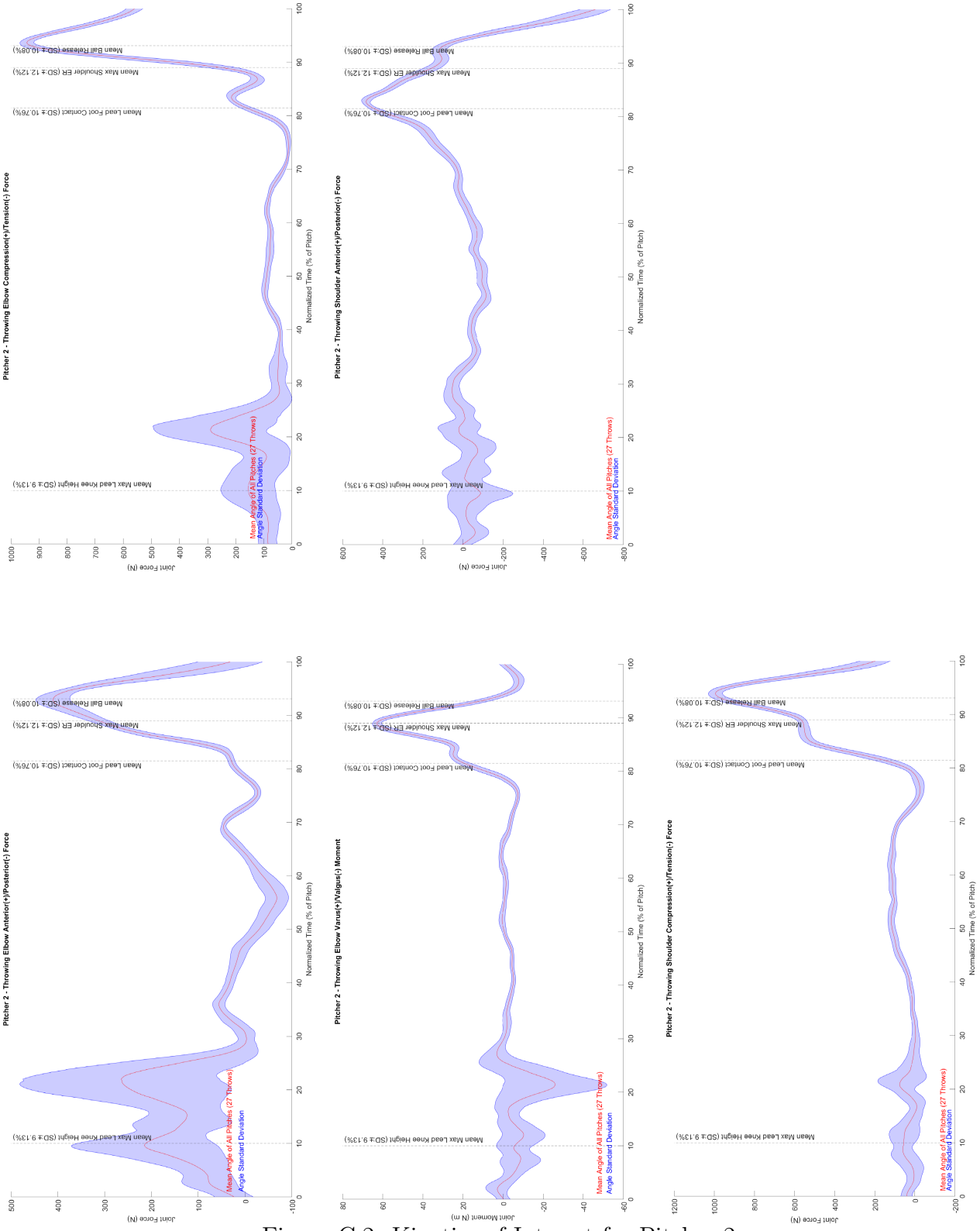


Figure C.2: Kinetics of Interest for Pitcher 2

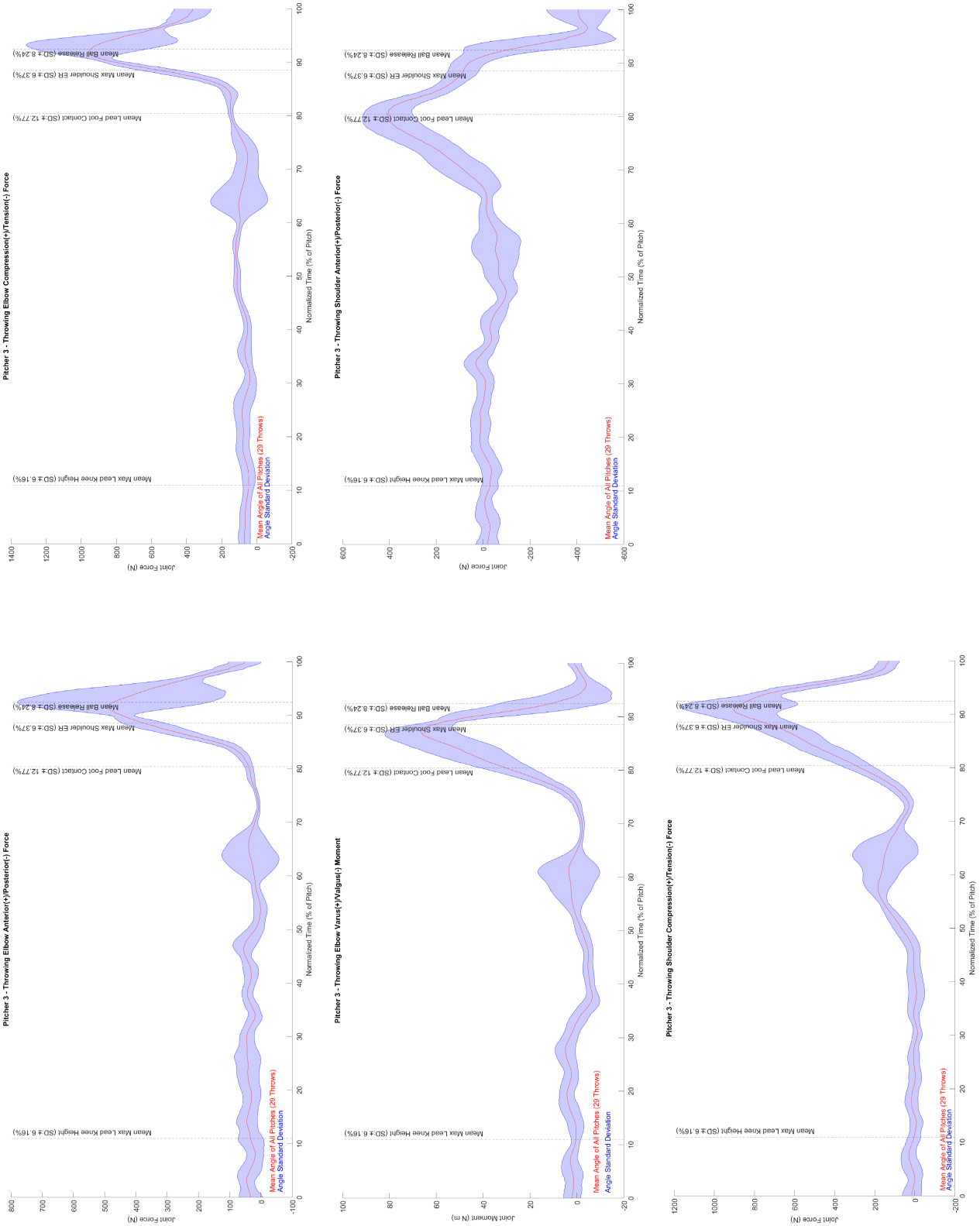


Figure C.3: Kinetics of Interest for Pitcher 3

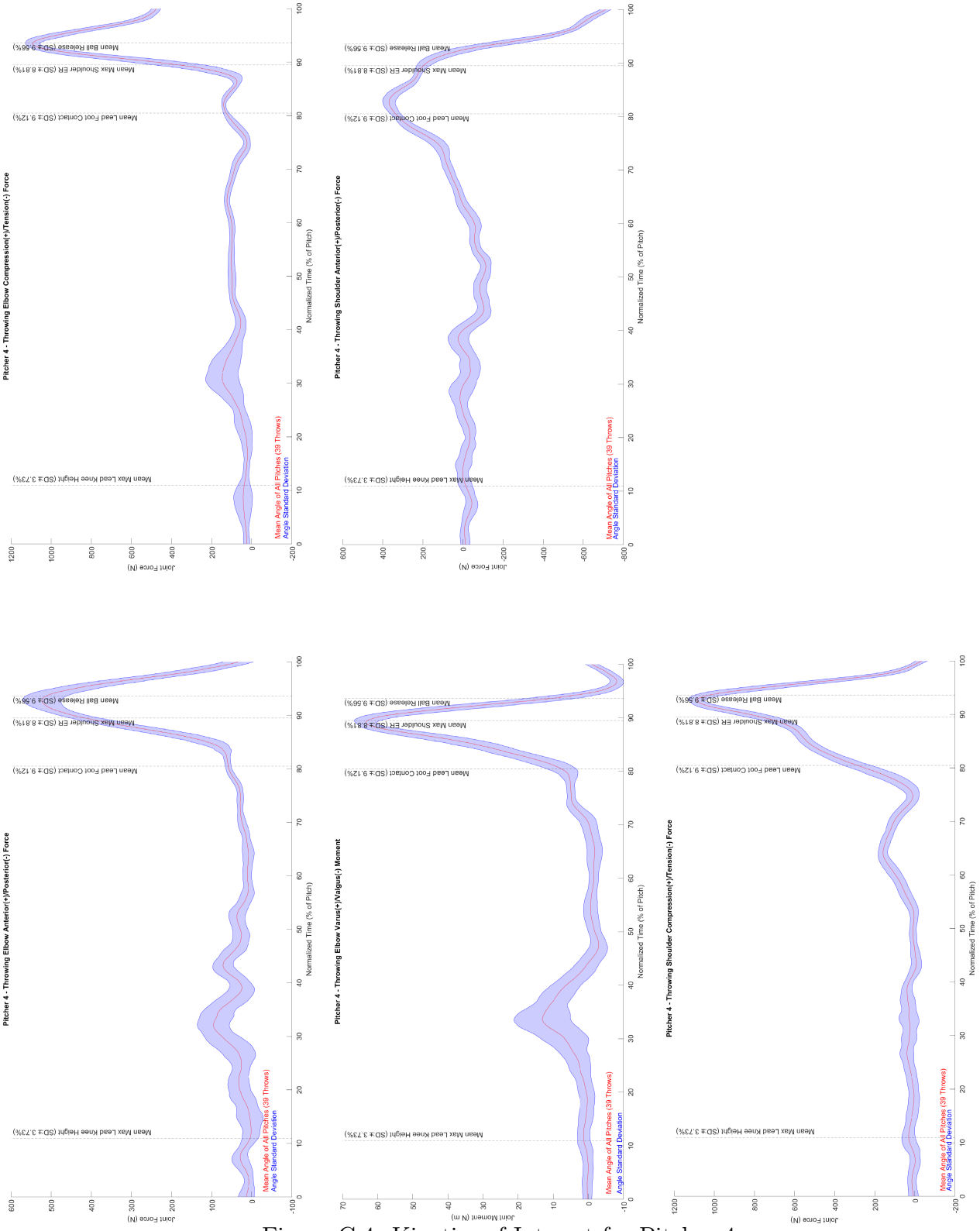


Figure C.4: Kinetics of Interest for Pitcher 4

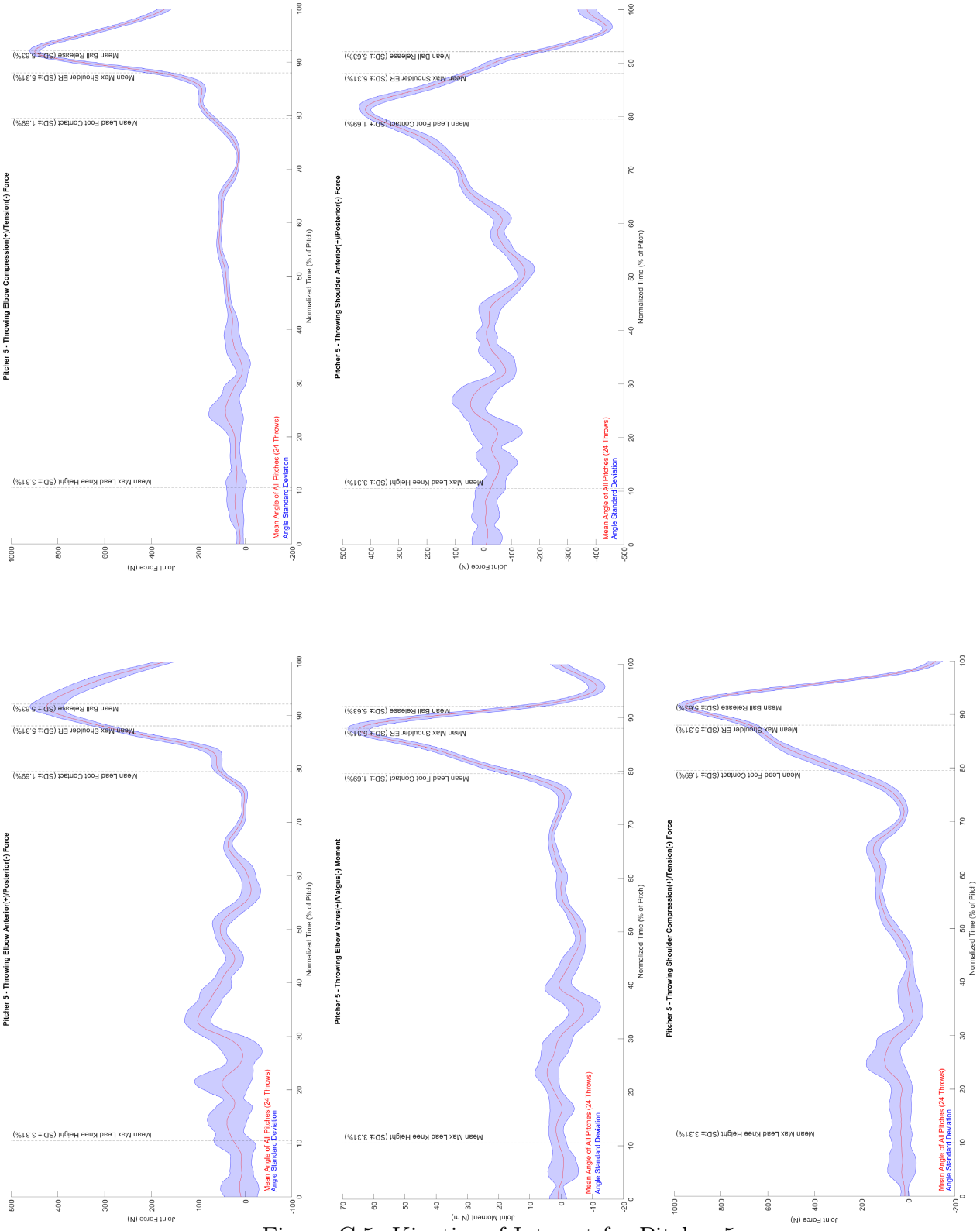


Figure C.5: Kinetics of Interest for Pitcher 5

Appendix D

Forward Dynamic Model Degrees of Freedom and Ranges of Motion

Table D.1: Musculoskeletal parameters for the OpenSim forward dynamic model

Degree of Freedom	Lower Bound (-)	Upper Bound (+)	Actuator Optimal Torque (N·m)	Initial Position
Pelvis Ipsilateral(+)/Contralateral(-) Tilt	-75	75	600	-11.1
Pelvis Clockwise(+)/Counterclockwise(-) Rotation	-90	90	600	-90.0
Pelvis Posterior(+)/Anterior(-) Tilt	-90	90	600	-6.6
Pelvis Posterior(+)/Anterior(-) Translation	0 m	1.1 m	650	0 m
Pelvis Superior(+)/Inferior(-) Translation	0.5 m	1.5 m	650	1.0 m
Pelvis Ipsilateral(+)/Contralateral(-) Translation	-0.3 m	0.3 m	650	0 m
Lumbar Ipsilateral(+)/Contralateral(-) Tilt	-75	75	500	-15
Lumbar Clockwise(+)/Counterclockwise(-) Rotation	-90	90	500	20
Lumbar Posterior(+)/Anterior(-) Flexion	-90	40	500	10
Right Hip Flexion(+)/Extension(-)	-45	120	750	28
Right Hip Adduction(+)/Abduction(-)	-60	40	750	4
Right Hip Internal(+)/External(-) Rotation	-90	90	750	14
Right Knee Extension(+)/Flexion(-)	-130	10	500	-30
Right Ankle Dorsiflexion(+)/Plantar Flexion(-)	-75	75	175	20
Right Ankle Inversion(+)/Eversion(-)	-50	50	150	0.6
Left Hip Flexion(+)/Extension(-)	-45	120	750	120
Left Hip Adduction(+)/Abduction(-)	-60	40	750	10
Left Hip Internal(+)/External(-) Rotation	-90	90	750	0
Left Knee Extension(+)/Flexion(-)	-130	10	500	-120
Left Ankle Dorsiflexion(+)/Plantar Flexion(-)	-75	75	175	0
Right Shoulder Horizontal Flexion(+)/Extension(-)	-40	90	450	40
Right Shoulder Abduction(+)/Adduction(-)	0	180	450	20
Right Shoulder Internal(+)/External(-) Rotation	-180	20	450	10
Right Elbow Flexion(+)/Extension(-)	0	130	350	120
Right Forearm Pronation(+)/Supination(-)	-90	90	350	90
Right Wrist Ulnar(+)/Radial(-) Deviation	-10	10	120	0
Right Wrist Flexion(+)/Extension(-)	-70	70	300	10
Left Shoulder Horizontal Flexion(+)/Extension(-)	-40	90	450	10
Left Shoulder Abduction(+)/Adduction(-)	0	180	450	10
Left Shoulder Internal(+)/External(-) Rotation	-180	20	450	10
Left Elbow Flexion(+)/Extension(-)	0	130	350	105
Left Forearm Pronation(+)/Supination(-)	-90	90	350	0
Left Wrist Ulnar(+)/Radial(-) Deviation	-10	10	300	0
Left Wrist Flexion(+)/Extension(-)	-70	70	120	0

NOTE: All units are in degrees unless otherwise indicated. In this model, contralateral refers to motion towards the opposite side of the throwing (right) arm (i.e. to the left), while ipsilateral refers to motion towards the throwing side (i.e. to the right). Neutral position is defined as a T-pose with the palms facing downwards.

Appendix E

Muscle Behaviour During Forward Dynamic Simulations

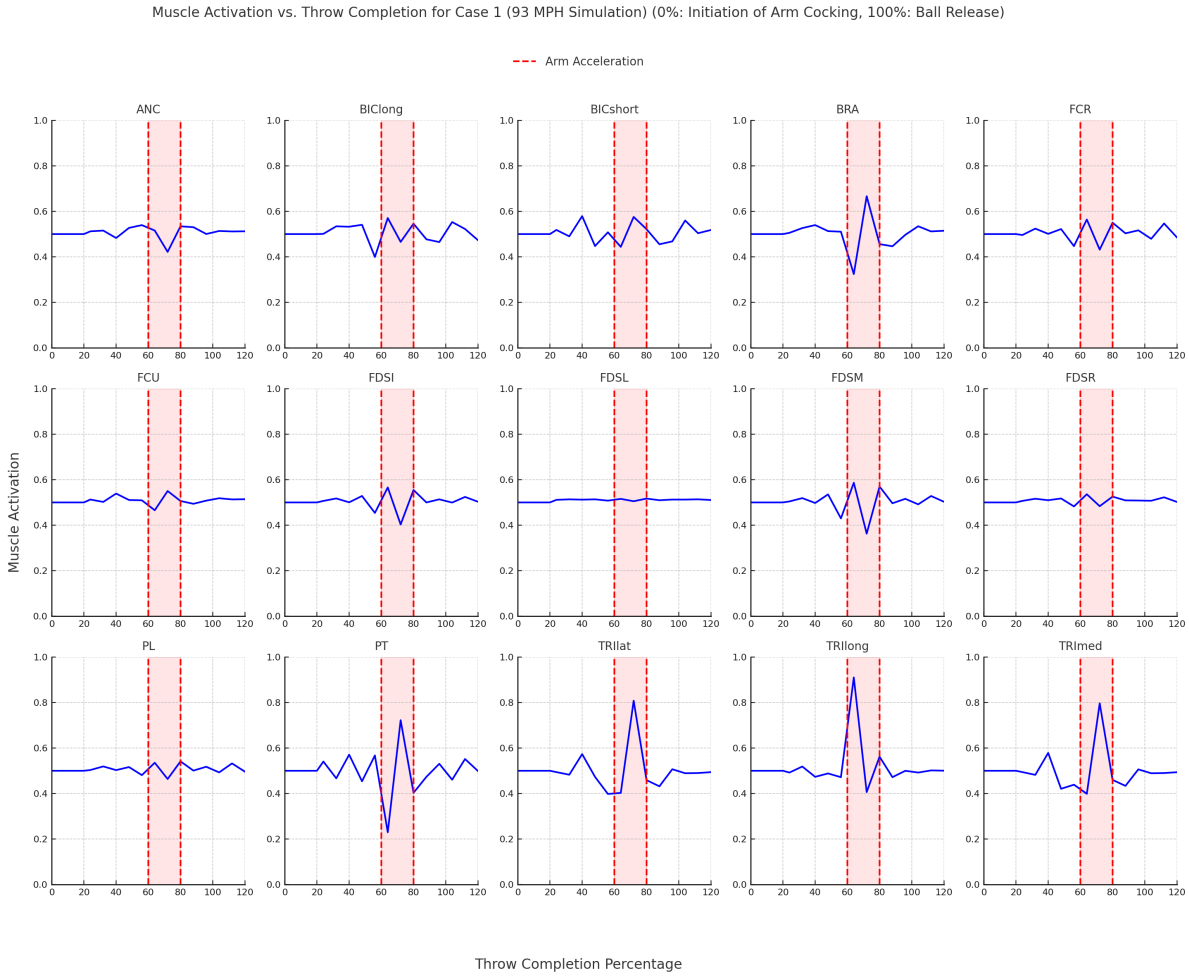


Figure E.1: Muscle activations for the 93 MPH simulation during late arm cocking phase (0%) to ball release (100%), which peaked predominantly during the arm acceleration phase (70-90%), marked by the red dashed lines, as the arm transitioned into rapid motion for ball release. This covers approximately 100 ms of time. with an emphasis on the 50 ms during arm acceleration. An extra 20% of data was interpolated post ball release (100% to 120%), to gain insight into the stabilizing characteristics of the arm's muscles, and their effects on minimizing UCL loads.